Multi-sensor mooring development and its use to characterise physical processes relevant to Harmful Algal Bloom dynamics in the St Helena Bay area, South Africa

Alexandra Fawcett

Thesis submitted in fulfillment of the requirements of the degree of
MASTER OF SCIENCE

in the Department of Oceanography
UNIVERSITY OF CAPE TOWN

August 2006

Abstract

Harmful algal blooms (HABs), typically attributed to dinoflagellate species, occur along the west coast of South Africa, particularly during the latter part of the upwelling season. As part of the Benguela Current Large Marine Ecosystem (BCLME) programme, a buoy has been developed locally for monitoring the development and occurrence of HABs. The mooring is situated three and a half kilometres offshore from Lambert's Bay, downstream from the Cape Columbine upwelling cell, on the west coast of South Africa, and collects high frequency time series data, available in real-time. The instrument package on the buoy provides bio-optical data analogous to remote sensing reflectance, temperature and current profile data, and fluorescence. The locally developed mooring and observing system is the only real-time, bio-optical mooring in southern Africa. Its development, and configuration of the instruments, data collection and telecommunications systems, are fully documented in this thesis.

HABs in the southern Benguela are closely linked to synoptic weather patterns and cycles of upwelling. The potential for predicting these events requires an improved understanding of the processes underlying the introduction of blooms to an area, and their subsequent transport and dissipation. In the second part of this thesis time scales of variability in local winds, the response of currents and water column structure to these, and their effect on local phytoplankton dynamics, are characterised. Time series of local wind data and current and temperature profile data from the mooring are described for three periods, which are representative of the latter part of the upwelling season, winter conditions and the early part of the upwelling season in 2005. CTD, chlorophyll profile and surface phytoplankton count data from a field study conducted off Lambert's Bay in March 2005 are reported, along with concurrent wind and mooring data.

There are two scales of current variability within the data sets: local diurnal wind forcing drives strong inertial oscillations, while north-south wind reversals at periods of two to five days drive sub-inertial current variability. Sub-inertial currents were found to lag wind reversals by approximately 12 hours, with relaxation of upwelling-favourable winds leading to poleward advection of warm water, creating stratification and conditions conducive to bloom formation. Differences observed in mean wind strength and direction between data sets are indicative of seasonal changes in synoptic meteorological

conditions. These quasi-seasonal variations in wind forcing affect the nearshore current flow and water column structure, despite the shorter time scales of variability detected within different data sets being similar throughout the year. An increase in periods of relaxation from upwelling-favourable winds and levels of stratification observed in the latter part of the upwelling season is consistent with the increased reported HAB incidence at that time of year.

Variations in alongshore currents, forced by changes in the local wind field, are observed to affect the introduction, transport and dispersion of high biomass blooms. Differing levels of mixing and stratification driven by local winds, insolation and advection alter water column structure and determine phytoplankton life-form selection. The close relationship observed between alongshore currents, levels of stratification and local winds may allow a degree of predictability of these parameters to be achieved, based on wind observations and forecasts.

Acknowledgements

My supervisors Grant Pitcher and Frank Shillington for their support, advice and guidance.

Trevor Probyn, Desiree Calder, Tarron Lamont, Pieter Truter, Paul Hanekom and Howard Waldron for data, advice and assistance.

Andre Du Randt for all the boat skippering and buoy handling.

Stewart Bernard for much assistance and putting up with the scamps.

My parents for all the opportunities, all those who have made Cape Town and Lambert's Bay enjoyable places to be, and Dan for the incentive to finish.

The South African Weather Service for wind data.

The Benguela Current Large Marine Ecosystem programme and the Department of Science and Technology's Frontier programme for direct funding.

Contents

1 Introduction 1

1.1 Background 3

1.1.1 Winds 3

1.1.2 St Helena Bay circulation and characteristics 4

1.1.3 Phytoplankton dynamics and harmful algal blooms 5

1.2 Rationale 7

1.3 Objectives 8

1.4 Thesis Organisation 8

2 System Development 11

2.1 Instrument Package 12

2.1.1 Radiometers 12

2.1.2 Fluorometer 12

2.1.2.1 Limitations of Fluorescence Data 13

2.1.3 Thermistor Chain 13

2.1.4 Acoustic Doppler Current Profiler 13

2.1.5 GPS 15

2.1.6 Modifications 15

2.2 Mooring Design 16

2.2.1 Demonstration Mooring 16

2.2.1.1 Modifications 18

2.2.2 Second Phase Mooring 18

2.2.2.1 Modifications 21

2.3 Control System 22

2.3.1 Modifications 23

2.4 Power 24

2.4.1 Modifications 27

2.5 Sampling Routine 28

2.5.1 SCUFA 30

2.5.2 GPS 30

2.5.3 ADCP 31

2.5.4 Thermistors 31

2.5.5 Other Schedule Considerations 32

2.5.6 Modifications 32

2.6 Data Storage 33
2.7 Buoy Servicing and Calibration 34
2.8 Data Transmission 35
2.9 Data Collection and Processing 36
2.10 System Deployment 37
2.10.1 Mooring Location 37
2.10.2 Deployment Dates 37
2.11 Recommendations 38
2.12 Example Data: Buoy Diagnostics and Performance 39
3 Variability and time scales of physical processes: February 2005 43
3.1 Data Analysis 43
3.2 Results 45
3.2.1 Wind 45
3.2.2 Currents 47
3.2.2.1 Low Frequency Currents 48
3.2.2.2 High Frequency Currents 51
3.2.3 Temperature and water column structure 53
3.3 Discussion 58
3.3.1 Low frequency currents 58
3.3.2 High Frequency Currents 60
3.3.3 Water column structure 61
3.3.4 Summary 65
4 Comparison between winds, currents and water column structure in three data sets from different periods 67
4.1 Results 67
4.1.1 Winds 67
4.1.2 Currents 69
4.1.3 Temperature and water column structure 71
4.2 Discussion 73
4.2.1 Differences in winds and current response to wind forcing 73
4.2.2 Differences in water column structure 76
4.2.3 Implications for HABs 77
5 Phytoplankton response to physical forcing: March 2005 79
5.1 Results 79

List of Figures

Figure 1-1 Maps depicting the location of the mooring off Lambert's Bay, and the Nortier weather station, in the greater St Helena Bay region on the west coast of South Africa 2

Figure 2-1 Schematics (courtesy of S. Bernard) and photograph of demonstration mooring and buoy (Bokkom) 17

Figure 2-2 Schematics (courtesy of S. Bernard) and photograph of second phase mooring and buoy design (BOB) 20

Figure 2-3 Photographs of BOB removed from mooring for monthly servicing, illustrating levels of bio-fouling on buoy and instruments. The SCUFA and radiance sensor can be seen wrapped in copper sheet which helps to reduce local fouling (left) 35

Figure 2-4 Half hourly diagnostic data from the mooring illustrating variations in tilt and roll (top), the depth of the radiance sensor (middle) and battery voltage (bottom) for a week in January/ February 2005 40

Figure 2-5 Half hourly median (top) and standard deviation (bottom) tilt and roll measurements from the mooring for a week in January/ February 2005 40

Figure 2-6 Half hourly median (top) and standard deviation (bottom) radiance sensor depths from the mooring for a week in January/ February 2005 41

Figure 3-1 Progressive vector diagram of wind data from the Lambert's Bay Nortier weather station between the 27th January and 22nd February 2005. Red dots and dates are positioned at midnight, green dots are positioned at midday. Data starts at the origin (0,0) 46

Figure 3-2 Wavelet analysis of alongshore wind data from Nortier weather station. Top: time series of the alongshore with the linear trend removed. Middle: amplitude of the signal over the time period of the data set. Bottom: integrated power of the signal over the data set period. 46

Figure 3-3 Progressive vector diagram of ADCP current data for the 5 m bin (left) and the 45 m bin (right) from the mooring (BOB) between the 27th January and 22nd February 2005. 48

Figure 3-4 Wavelet analysis of alongshore current data from the ADCP bin at 5m. Top: time series of the alongshore current with the linear trend removed. Middle: amplitude of the signal over the time period of the data set. Bottom: integrated power of the signal over the data set period. 49

Figure 3-5 Wavelet analysis of across-shelf current data from the ADCP bin at 5m. Top: time series of the across-shelf current with the linear trend removed. Middle: amplitude of the signal over the time period of the data set. Bottom: integrated power of the signal over the data set period. 49
Figure 3-6 Low pass filtered alongshore ADCP current from 5 m bin and alongshore wind from Lambert's Bay Nortier weather station between 27th January and 22nd February 2005. In the bottom diagram the alongshore wind has been shifted by 12 hours illustrating the correlation between alongshore current and wind reversals at this phase lag. 50
Figure 3-7 Low pass filtered alongshore and across-shelf ADCP current from 5 m bin between 27th January and 22nd February 2005 51
Figure 3-8 Low pass filtered current velocities [cm s^{-1}] for ADCP bins between 5 m and 45 m for alongshore component (top) and across-shelf component (bottom) between the 27th January and 22nd February 2005 51
Figure 3-9 High frequency current velocities [cm s^{-1}] for ADCP bins between 5 m and 45 m for alongshore component (top diagram) and across-shelf component (bottom diagram) between the 27th January and 22nd February 2005. 52
Figure 3-10 Progressive vector diagram of high frequency ADCP current from 5 m bin between 12th and 22nd February 2005. Red dots are positioned at midnight, green dots at midday. 53
Figure 3-11 Time series of temperature profile data between 0 and 30 m depth and current profile data for alongshore and across-shelf ADCP bins between 5 and 45 m depth from the mooring (BOB) between the 27th January and 22nd February 2005 54
Figure 3-12 Wavelet analysis of surface temperature data from mooring. Top: time series of surface temperature with the linear trend removed. Middle: amplitude of the signal over the time period of the data set. Bottom: integrated power of the signal over the data set period. 55
Figure 3-13 Low pass filtered ADCP current vectors from 5 m bin and surface temperature from thermistor chain on mooring between 27th January and 22nd February 2005 56
Figure 3-14 Temperature profiles from thermistor chain deployed on mooring for the 3rd and 4th February 2005 (left) and the 5th and 6th February 2005 (right). 57
Figure 3-15 Time series of alongshore ADCP current [cm s^{-1}] from 5 m bin. The depth of the top of the thermocline is plotted in grey. 62

Figure 3-16 One day composite satellite sea surface temperature images from NOAA AVHRR satellite and temperature profile data (°C) from thermistor chain deployed on mooring for 4th to 7th February 2005 64
Figure 4-1 Wind vectors from Lambert's Bay Nortier weather station from the late upwelling season (top), winter conditions (middle) and the early upwelling season (bottom) in 2005. 68
Figure 4-2 Current vectors from ADCP bin at 5 m from the late upwelling season (top), winter conditions (middle) and the early upwelling season (bottom) in 2005. 70
Figure 4-3 Low pass filtered alongshore current from ADCP bin at 5 m and alongshore wind from Lambert's Bay Nortier weather station from the late upwelling season (top), winter conditions (middle) and the early upwelling season (bottom) in 2005. 71
Figure 4-4 Temperature profiles [°C] from thermistor chain deployed on mooring from the late upwelling season (top), winter conditions (middle) and the early upwelling season (bottom) in 2005. 73
Figure 4-5 Mean current profiles from ADCP bins between 5 and 45 m (top) and mean temperature profiles from thermistor chains deployed on mooring (bottom) for late in the upwelling season, early in the upwelling season and winter conditions in 2005. 75
Figure 5-1: Progressive vector plot of wind data from Lambert's Bay Nortier weather station between the 8th March and 5th April 2005. The plot commences seven days prior to the study period. Red dots and dates are positioned at midnight, green dots are positioned at midday. Data starts at the origin (0,0). 80
Figure 5-2: Progressive vector plot of ADCP current vectors for the bin at 5m from the mooring (BOB) between the 19th March and 5th April 2005 80
Figure 5-3: Low pass filtered alongshore ADCP current from 5 m bin and alongshore wind from Lambert's Bay Nortier weather station between 19th March and 5th April 2005 82
Figure 5-4 Current velocity [cm s^{-1}] for ADCP bins between 5m and 45m for alongshore component (top) and across-shelf component (bottom) between 19th March and 5th April 2005 82
Figure 5-5 Temperature [°C] from mooring thermistor chain (colour plot) and daily CTD casts at mooring location (contour plot) (top), daily chlorophyll [mg m^{-3}] profiles from fluorometer (middle) and daily surface phytoplankton counts with surface fluorescence from mooring (bottom) 84

Figure 5-6 Low-pass filtered ADCP current vectors for bin at 5m and surface temperature from mooring thermistor chain between 19th March and 5th April 2005. 85
Figure 5-7 MERIS chlorophyll a images of St Helena Bay region illustrating movement of areas of high biomass – chlorophyll levels [mg m^{-3}]are calculated using an experimental algorithm 90
Figure I-1 Schematic of Start Acquisition process in Ocean-i unit software 111
Figure II-2 Schematic of Update Files process in Ocean-i unit software 112

List of Tables

Table 2-1: Daily power requirements of instruments on demonstration mooring (reproduced from BP Solar spreadsheet). 26
Table 2-2: Solar array sizing calculations given power requirements from Table 2-1 (reproduced from BP Solar spreadsheet). 26
Table 2-3: Daily power requirements of instruments on second mooring (reproduced from BP Solar spreadsheet). 27
Table 3-1 Characteristics of alongshore and across-shelf current data gathered from the ADCP deployed on the mooring (BOB) between the 27th January and 22nd February 2005. Positive values are directed to the north and east. 48
Table 3-2 Characteristics of temperature data gathered from the thermistor chain deployed on the mooring (BOB) between the 27th January and 22nd February 2005. All temperatures are in degrees Celsius. 55
Table 4-1 Characteristics of alongshore wind data from Lambert's Bay Nortier weather station for the three data sets from the late upwelling season, winter conditions and early in the upwelling season in 2005. 68
Table 4-2 Periods at which the three highest powered peaks are found using wavelet analysis for various data for the three data sets 69
Table 4-3 Characteristics of near-surface currents from ADCP bin at 5 m from the late upwelling season (top), winter conditions (middle) and the early upwelling season (bottom) in 2005. 70
Table 4-4 Characteristics of water column temperatures from mooring thermistor chains for the three data sets from February, May and November/ December 2005. 72
Table 5-1 Periods at which the three highest powered peaks are found using wavelet analysis for various data 81
Table 5-2 Components of heat budget calculations for the surface mixed layer for specified dates 86

1 Introduction

Whilst the majority of the phytoplankton in the southern Benguela make a useful contribution to the productivity of the region, supporting a large fishery, harmful algal blooms (HABs) are a regular feature of the west coast of South Africa, particularly during the latter part of the upwelling season (Pitcher *et al.* 1998, Pitcher & Calder 2000), and are usually attributed to species of dinoflagellate. Blooms of harmful algae may affect commercial and recreational activities in the area, with harmful effects attributed to the toxicity of some species leading to faunal mortalities and illness due to contaminated shellfish, or to the collapse of high biomass blooms leading to anoxia (Pitcher *et al.* 1998).

Effective coastal management requires HAB monitoring programmes to be in place, accompanied by scientific programmes aimed at increasing the understanding of processes underlying the dynamics and impacts of HABs (Pitcher & Calder 2000). As part of the Benguela Current Large Marine Ecosystem (BCLME) programme, a project was established to develop an operational capacity for the real-time observation and forecasting of harmful algal blooms in the BCLME region through the deployment of bio-optical moorings. This project led to the development of a demonstration mooring, deployed off Lambert's Bay, in the greater St Helena Bay region (Figure 1-1), from February to June 2004, and a second phase mooring, deployed in January 2005, which is still in use. These moorings, equipped with radiometers providing data analogous to remote sensing reflectance, a fluorometer, a thermistor chain and an Acoustic Doppler Current Profiler (ADCP), provide real-time data via the project's website enabling the detection and monitoring of high biomass blooms, along with high-frequency, time-series research data. This study reports on the development of the mooring system, which formed a large component of the BCLME project, and utilises time series data from the mooring to characterise the variability of currents and water column structure in response to local synoptic weather patterns, at time scales important in determining HAB dynamics. In the context of this study HABs are considered to be high biomass blooms as these have historically been problematic in the region leading to faunal mortalities (e.g. Cockcroft *et al.* 2000), and it is possible to detect and monitor such blooms using data from the mooring. The toxicity of some species, or presence of toxic species, can

1 Introduction

Whilst the majority of the phytoplankton in the southern Benguela make a useful contribution to the productivity of the region, supporting a large fishery, harmful algal blooms (HABs) are a regular feature of the west coast of South Africa, particularly during the latter part of the upwelling season (Pitcher *et al.* 1998, Pitcher & Calder 2000), and are usually attributed to species of dinoflagellate. Blooms of harmful algae may affect commercial and recreational activities in the area, with harmful effects attributed to the toxicity of some species leading to faunal mortalities and illness due to contaminated shellfish, or to the collapse of high biomass blooms leading to anoxia (Pitcher *et al.* 1998).

Effective coastal management requires HAB monitoring programmes to be in place, accompanied by scientific programmes aimed at increasing the understanding of processes underlying the dynamics and impacts of HABs (Pitcher & Calder 2000). As part of the Benguela Current Large Marine Ecosystem (BCLME) programme, a project was established to develop an operational capacity for the real-time observation and forecasting of harmful algal blooms in the BCLME region through the deployment of bio-optical moorings. This project led to the development of a demonstration mooring, deployed off Lambert's Bay, in the greater St Helena Bay region (Figure 1-1), from February to June 2004, and a second phase mooring, deployed in January 2005, which is still in use. These moorings, equipped with radiometers providing data analogous to remote sensing reflectance, a fluorometer, a thermistor chain and an Acoustic Doppler Current Profiler (ADCP), provide real-time data via the project's website enabling the detection and monitoring of high biomass blooms, along with high-frequency, time-series research data. This study reports on the development of the mooring system, which formed a large component of the BCLME project, and utilises time series data from the mooring to characterise the variability of currents and water column structure in response to local synoptic weather patterns, at time scales important in determining HAB dynamics. In the context of this study HABs are considered to be high biomass blooms as these have historically been problematic in the region leading to faunal mortalities (e.g. Cockcroft *et al.* 2000), and it is possible to detect and monitor such blooms using data from the mooring. The toxicity of some species, or presence of toxic species, can

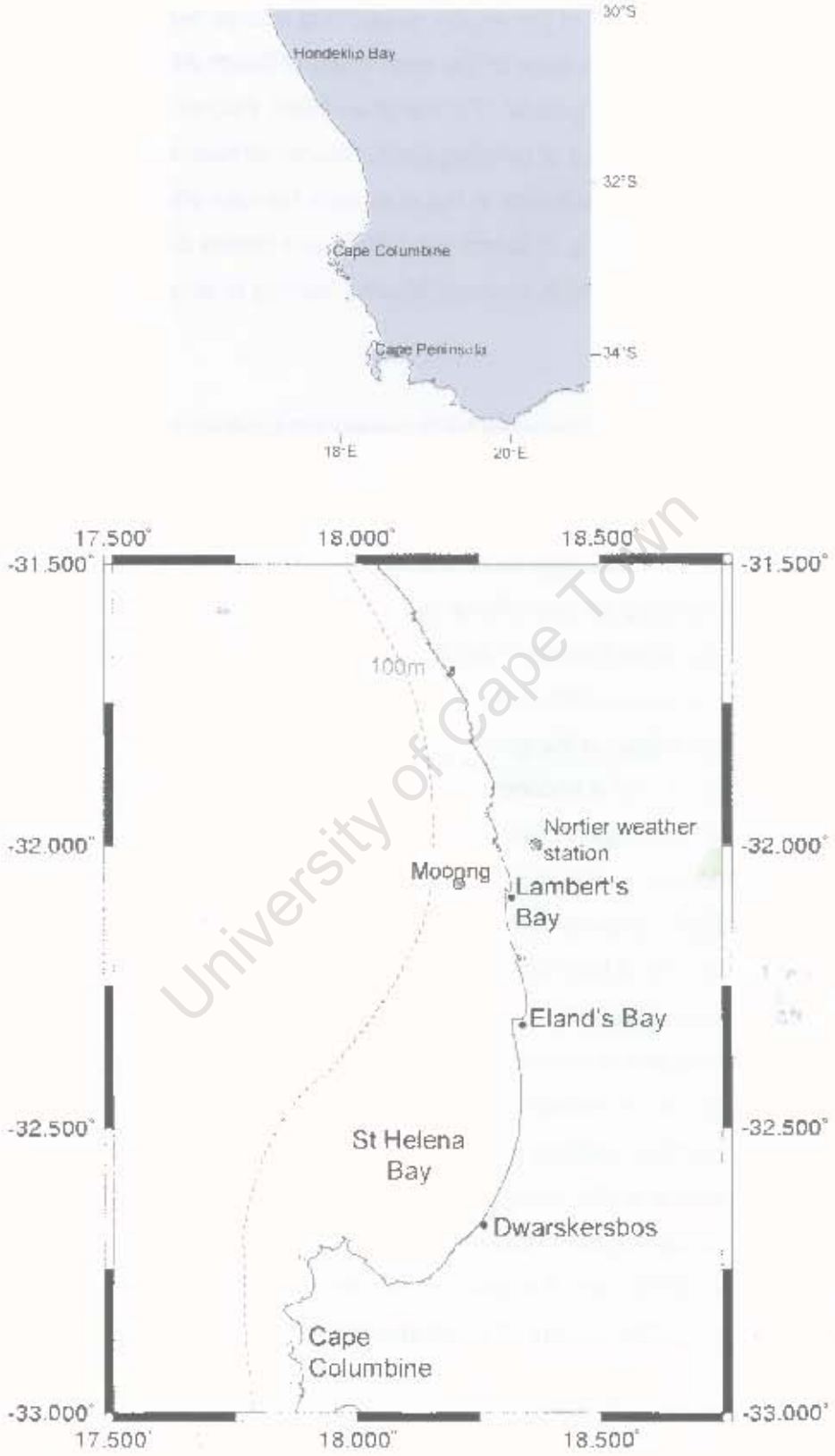

Figure 1-1 Maps depicting the location of the mooring off Lambert's Bay, and the Nortier weather station, in the greater St Helena Bay region on the west coast of South Africa

currently only be monitored in the region via analysis of water samples and is thus beyond the scope of this study.

1.1 Background

The Benguela is one of four major eastern boundary current upwelling regions of the world oceans (Hill *et al.* 1998) extending from the Agulhas Bank at about 37°S, 27°E off the southern tip of Africa to the Angola Front at around 14°S (Shannon & Nelson 1996, Shillington 1998). In contrast to other eastern boundary upwelling regions, the Benguela is bounded by warm water at both the northern and southern ends (Shannon & Nelson 1996). Topographical variation in the coastline of the southern Benguela gives rise to discrete upwelling cells at Hondeklip Bay, Cape Columbine and the Cape Peninsula (Nelson & Hutchings 1983). This study focuses on the greater St Helena Bay region (Figure 1-1), found to the north of the Cape Columbine upwelling cell at 33°S and characterised by a broad shelf. St Helena Bay has historically been the focus of several research initiatives owing to its high productivity and importance as a nursery ground for pelagic fisheries (Hutchings 1992). This region is also particularly susceptible to HABs and their negative impacts.

1.1.1 Winds

Prevailing winds over the Benguela are determined by the South Atlantic high pressure system, the pressure field over the African subcontinent and eastward moving cyclones (Nelson & Hutchings 1983); seasonal shifts in the position of the South Atlantic high lead to seasonally variable winds along the west coast of southern Africa. During the summer winds are predominantly southerly and upwelling-favourable, while the northward shift of the pressure system during winter leads to a higher frequency of non upwelling-favourable winds with a westerly component (Shannon 1985). Wind induced upwelling in the southern Benguela is therefore highly seasonal, with the upwelling season extending from September to March. Historical temperature studies off Lambert's Bay in the St Helena Bay region have shown seasonal upwelling to be at a maximum between December and March in the austral spring and summer, as indicated by lowered surface temperatures; upwelling is at a minimum in August and September in this region (Nelson & Hutchings 1983). At the event scale the eastward passage of low pressure cells and associated frontal systems during the summer months leads to periodic weakening of the South Atlantic high and slackening of south-easterly, upwelling-favourable winds

along the coast (Nelson & Hutchings 1983) causing modulation of the upwelling cycle with a period of 3 – 6 days. The passage of these cyclones during winter causes westerly winds to dominate, at times bringing gale-force north-westerly winds (Risien *et al.* 2004). Analysis of variability in satellite winds over the southern Benguela shows synoptic-scale pulsing to occur in coastal winds throughout the year at periods of 4-12 days. Wind stress events are highest in intensity during summer months when south-easterly winds dominate and generally lower in intensity during austral autumn and winter (between April and mid-July), associated with the northerly migration of the westerly wind belt (*ibid*).

Southerly winds are deflected around Cape Columbine and blow with an onshore component to the north of Columbine (Nelson & Hutchings 1983); hence prevailing summer winds in the St Helena Bay area are south-westerly. Average wind speeds in the region are 3-4 m s^{-1} with a mean southerly component in summer and mean northerly component in winter (Kamstra 1995). Land sea breezes are a common feature of the winds along the west coast of South Africa (Jackson 1947).

1.1.2 St Helena Bay circulation and characteristics

The coastline is aligned in an approximately north-south direction along the northern shores of St Helena Bay, and sub-inertial current flow in this region runs mostly parallel to the bathymetry (Holden 1987). Drift card trajectories have shown nearshore surface current flow in the St Helena Bay region to vary seasonally, with southward current flow dominating in winter and northward current flow dominating in summer (Duncan & Nell 1969). An inshore counter-current develops occasionally during summer, becoming more persistent in autumn (*ibid*). Currents are predominantly barotropic and are dominated at the event scale by wind-related alongshore variation associated with the synoptic weather (Holden 1987). Spectra from current meters deployed in the region exhibit a strong peak at the inertial period of 22.5 hours (*ibid*). Retentive circulation develops within St Helena Bay during summer when generally northward flow exists offshore with cyclonic circulation and associated eddies observed in the coastal region south of Elands Bay (Holden 1985). A barotropic model of the region demonstrates the development of the upwelling plume off Cape Columbine in response to equatorward winds. A cyclonic eddy forms in the lee of the Cape enhancing retentive circulation in the

bay and creating a degree of isolation between nearshore and offshore waters (Penven *et al.* 2000).

A seasonal signal is evident in monthly trends in sea surface temperature derived from satellite imagery for St Helena Bay, with average summer temperatures of around 17 °C and winter temperatures of around 15 °C (Demarcq *et al.* 2003). Standard deviations of sea surface temperatures are much greater in summer months (*ibid*), reflecting the impact of the upwelling cycle on sea surface temperatures. During active upwelling, southerly winds are associated with northward flowing currents on the shelf and a drop in sea surface temperature (Jury & Brundrit 1992). A plume of cold water extending northwards from Cape Columbine, and a narrow strip of cold upwelled water along the coast of St Helena Bay north of Dwarskersbos, can be seen in satellite imagery following upwelling-favourable winds (Taunton-Clark 1985). The upwelling centre at Cape Columbine is associated with a narrow, steeply shelving shelf and a strong northward jet with speeds typically in excess of 50 cm s^{-1} (Nelson & Hutchings 1983). Where the shelf broadens in St Helena Bay, downstream of the upwelling cell, the lower energy environment favours the development of stratification and stability of the water column in summer months (Pitcher *et al.* 1998, Probyn *et al.* 2000). During winter months the combination of winter storms and reduced insolation gives rise to a deep, well-mixed surface layer (Shannon & Pillar 1986).

Remotely sensed chlorophyll data identify St Helena Bay as a region of high biomass (Pitcher & Weeks 2006). Satellite derived mean monthly surface chlorophyll *a* concentrations are highest between December and March, in the upwelling season, and lowest in July (Demarcq *et al.* 2003). The high productivity is a result of the periodic re-supply of nutrients to the euphotic zone through upwelling activity, the relative stability of the physical environment and retentive circulation in the region (Pitcher *et al.* 1992). Within the southern Benguela the negative relationship between temperature and nitrate concentration is well established (e.g. Andrews & Hutchings 1980, Waldron & Probyn 1992), with high levels of nitrate found in newly upwelled waters.

1.1.3 Phytoplankton dynamics and harmful algal blooms

The succession of differing life-forms of phytoplankton is driven by their adaptation to varying conditions of turbulence and nutrient availability, with diatoms dominating in

turbulent, nutrient-rich waters and dinoflagellates dominating in stratified, nutrient-poor environments (Margalef 1978). Dinoflagellates are able to migrate vertically to retrieve nutrients in stratified, low nutrient environments due to their swimming ability (Smayda 1997), facilitating their succession from diatoms in these conditions. Coccolithophorids dominate in warmer, oligotrophic waters (Smayda 1980). Thus levels of mixing and stratification are important as physical processes that affect species and life-form selection and distribution, grouping together phytoplankton with an affinity for, or the ability to withstand, similar environmental conditions (Pitcher & Nelson 2006). Changes in water column conditions in response to the upwelling cycle interrupt and reset patterns of succession (Pitcher *et al.* 1992), with diatoms typically dominating recently upwelled water and dinoflagellates following stabilisation of the water column and the decline of surface nutrients (Shannon & Pillar 1986). In the southern Benguela the development of seasonal stratification leads to an increase in dinoflagellates relative to diatoms as the upwelling season progresses (Pitcher & Weeks 2006). High biomass phytoplankton blooms may cause discoloration of the water, known as red tide. The incidence of red tide in the southern Benguela is not a new phenomenom and was identified as a factor affecting fish stocks by Gilchrist (1914 as cited in Pitcher & Calder 2000). In upwelling systems, red tides form as a typical stage of the phytoplankton succession, rather than being an exceptional disruption of diatom blooms (Smayda 2000).

The role of physical processes in harmful algal bloom dynamics is well established. Whilst levels of mixing determine life-form selection and distribution, mesoscale circulation determines the advection and retention of blooms (Pitcher & Nelson 2006) Often the appearance of a bloom in an area occurs too rapidly to be explained by *in situ* growth and is attributed to advection of the initial population from outside the area (e.g. Sordo *et al.* 2001). There are many instances of advection of HAB species alongshore or onshore through wind driven flows and coastal currents, leading to the accumulation of populations and bloom events (e.g. Sellner *et al.* 2003). In the context of the St Helena Bay region, local winds and topography affect the circulation pattern and are key factors in the introduction, maintenance and transport of blooms in the region (Pitcher & Nelson 2006).

A conceptual model of red tide formation in St Helena Bay (Pitcher & Nelson 2006) shows northward flow to dominate under upwelling conditions with an alongshore coastal jet forming, which separates from the coast north of Cape Columbine. Across-shelf phytoplankton distributions are related to mixed layer depth, with dinoflagellates dominating in nearshore regions where waters are typically more stratified, and diatoms dominating in offshore waters where the mixed layer is deepened by increased wind stress. Development of the coastal jet separates the offshore population of diatoms from the nearshore population dominated by dinoflagellates. During upwelling-favourable winds, alongshore upwelling and northward flow in the coastal jet lead to the accumulation of dinoflagellates at convergence zones inshore of the coastal jet. An inshore counter current develops during periods of wind relaxation or reversal, as the result of interaction of the coastal jet with local topography, contributing to cyclonic circulation within St Helena Bay and leading to southward transport of the dinoflagellate population.

1.2 Rationale

The locally evolved mooring and system is the only bio-optical mooring in southern Africa, and thus documentation of its development, and the knowledge gained in the process, are important in building capacity in the region. Data from the mooring are used to examine the time scales of variability in the current and temperature fields from the Eulerian perspective of the mooring, their response to local winds and the effect of these processes on phytoplankton dynamics in the context of high biomass blooms. Servicing of the mooring leads to monthly interruption of the data set and therefore the time scales of variability examined are restricted to those with periods of less than two weeks. These time scales are commensurate with cycles of upwelling and relaxation, the variability of which are key factors in the formation of phytoplankton blooms (Pitcher *et al.* 1995) and thus it is appropriate to examine the data at these scales.

The mooring was designed around the use of the radiometers and bio-optics for the detection and monitoring of HABs, and therefore the radiometers form an extensive part of the description of the mooring configuration and development. However, the case studies in this thesis are restricted to the use of current and temperature data from the mooring to examine physical processes important to high biomass blooms and do not make use of the radiometer data. Examples of use of the radiometer data, along with

other data from the mooring, for the detection and monitoring of HABs can be found in Bernard *et al.* 2006 and Fawcett *et al.* 2006.

1.3 Objectives

The aims of this project were two-fold: to develop, maintain and deploy the mooring and associated systems, and to use time series data from the mooring as case studies to characterise the physical processes governing HABs. Further objectives are as follows:

- To document the development and configuration of the system associated with a real-time mooring.
- To investigate the dominant time scales and variability of local wind forcing in the upwelling season, and the response of currents and water column structure to these winds.
- To investigate the effect of seasonal variation in local wind forcing on currents and water column structure.
- To investigate the biological response to physical forcing at the dominant time scales observed in the upwelling season, in the context of high biomass blooms.

1.4 Thesis Organisation

Chapter 2 describes in detail the development and configuration of the moorings, including the instrumentation, data collection and telecommunications system. Deployment and maintenance of the moorings is also discussed. This chapter has arisen both through the need to document the development of the mooring for reference, and as a significant part of the two year project was spent on the development and implementation of the data logging and communication systems for the mooring and maintenance of the mooring. Some recommendations, which have arisen from the mooring deployment, and example diagnostic data are presented at the end of the chapter.

Chapters 3, 4 and 5 describe data sets collected from the mooring in a number of detailed case studies. Time series data from February 2005, which falls in the latter part of the upwelling season, are presented in chapter 3. The dominant time scales of variability in the local wind, and the time scales of variability in, and response of, currents and water column structure to these winds are examined. The results from two further

data sets, one from May 2005 and one from November/ December 2005, are summarised in chapter 4 alongside the data from February 2005. These data highlight the variations observed in local wind forcing, current flow and water column structure at differing times of year. Data collected during a four week field study in March 2005, along with concurrent data from the mooring, are described in chapter 5, examining the role that physical processes play in the algal dynamics of the region. Chapter 6 provides a summary of the findings and some recommendations for future research.

2 System Development

The Namaqua mooring has been developed for the bio-optical detection and monitoring of HABs in the southern Benguela region. Optical instrumentation, despite its limitations, is well suited for the monitoring and characterisation of HABs, allowing for some description of algal abundance and assemblage via their optical properties (Cullen *et al.* 1997, Sellner *et al.* 2003). Due to the interaction of algal cells with the light field, the measurement of remote sensing reflectance (Morel & Prieur 1977, Zaneveld 1995), and the application of reflectance algorithms (Roesler & Perry 1995, Bernard 2005) to such data, allows for some description of the phytoplankton present in the surface waters. Information derived from these data may include indications of chlorophyll *a* concentration, cell size and relative accessory pigment concentration (Bernard 2005); species and toxicity determination are currently not possible using these methods. The development of the bio-optical mooring, and its availability as an instrument platform, led to the integration of other sensors into the mooring system. The additional data provided by these sensors is useful both in the detection and monitoring of high biomass blooms, and in the longer term understanding of bloom dynamics and formation in the southern Benguela region. Moorings provide a suitable platform for making observations on appropriate scales to examine bio-optical and physical interactions (Dickey 1991). Incorporation of a fluorometer, thermistor chain and ADCP into the system allows for the monitoring of algal biomass, the temperature structure of the water column (which is of importance in the formation and maintenance of dinoflagellate-dominated blooms), and provides current data enabling the potential transport pathway of a bloom to be established.

Key considerations in the development of the mooring (Bernard 2004) were:

- The development of a robust and cost-effective system providing real-time remote sensing reflectance data.
- The buoy should utilise sensors capable of being field calibrated and should be easily deployed and serviced from small vessels.
- Buoy and sensor configuration should be designed to minimise shading of the optical sensors.

- A data logging system should provide on-board storage of data, remote communication of data and be configurable for autonomous interrogation of the system.
- On-board power systems should be self-sufficient, powering the sensors and data logging systems and providing back-up power.
- The use of proven sensor and control systems in a modular design.

2.1 Instrument Package

2.1.1 Radiometers

In order to measure remote sensing reflectance (R_{rs}) two radiometers are required: one sensor measuring downwelling irradiance ($E_d(0^+)$) and one measuring upwelling radiance ($L_u(0^+)$). These parameters are measured on the buoy using two RAMSES hyperspectral radiometers (TriOS, Germany): an above surface irradiance sensor (RAMSES-ACC) and a subsurface radiance sensor (RAMSES-ARC). These sensors were utilised on the Volvo Ocean Race yachts in 2001-2 as part of the Volvo Ocean Adventure (Byfield *et al.* 2002) and have proved themselves to be robust and able to withstand prolonged exposure to a harsh environment. Successful field trials carried out using the radiometers on a temporary mooring in the Benguela region, and the low cost of the sensors compared to similar instruments, led to the selection of the TriOS RAMSES radiometers as being the most suitable for use on the buoy. Both radiometers sample from 320 – 950 nm with 3.3 nm per pixel. Integration time is automatically selected by the radiometer according to the ambient light conditions and ranges from 4 ms to 8 s. A silicon photodiode array is used as the detector within the sensors. The irradiance sensor is fitted with a cosine collector while the radiance sensor has a field of view of 7° in air (10° in water). The spectral accuracy of both radiometers is 0.3 nm with a detection accuracy of between 6 and 10%. An inclinometer incorporated into the radiance sensor enables the collection of tilt and roll data for each radiometer measurement, allowing for quality control of the measurements (Mueller *et al.* 2003a).

2.1.2 Fluorometer

A SCUFA II fluorometer (Turner Designs, USA) is used to measure stimulated chlorophyll fluorescence intensity, which provides an indication of chlorophyll *a* concentration and algal biomass. The instrument emits an excitation beam from a blue LED at 440 nm and detects the fluorescence signal at 680 nm using a silicon photodiode

positioned at 90° to the light beam. Automatic gain control is used within the instrument, and optical filters restrict the emitted and detected light to the wavelengths of interest. There is an inverse relationship between fluorescence and temperature that is independent of the chlorophyll concentration of the medium (Lorenzen 1966). The SCUFA uses temperature compensation to correct the fluorescence readings and outputs both raw and corrected fluorescence readings.

2.1.2.1 Limitations of Fluorescence Data

There are a number of limitations associated with stimulated fluorescence data that should be taken into account when using it as a proxy for chlorophyll *a* concentration or biomass. The irradiance conditions, species composition, and nutritional and physiological state of the phytoplankton population are all known to affect fluorescence values (Cullen *et al.* 1997). A strong diurnal cycle exists in the fluorescence signal of natural phytoplankton populations, in which the normalised fluorescence per unit chlorophyll is attenuated at midday when insolation is highest, due to photochemical and non-photochemical quenching (Dickey & Falkowski 2002). In stratified conditions, some phytoplankton, including motile dinoflagellates, are capable of undertaking vertical migration at night to acquire nutrients, which may lead to a lower abundance of phytoplankton, and thus fluorescence, in surface waters at night (*ibid*).

2.1.3 Thermistor Chain

The temperature profile of the water column is monitored using a 50 m Templine thermistor chain (Apprise Technologies, USA). The chain comprises of 17 digital semiconductor temperature sensors, accurate to 0.1 °C, positioned 2 m apart for the top 20 m of the thermistor chain and 5 m apart for the remaining 30 m. This thermistor chain uses direct addressing for the thermistors, enabling many thermistors to be interrogated using a single command, which has the advantage of greatly reducing the number of wires needed for multiple thermistors. The major advantage of this is that only one serial port is required to receive data from a number of thermistors, reducing the demands on the data logger.

2.1.4 Acoustic Doppler Current Profiler

A surface mounted Workhorse Sentinel 300 ADCP (RD Instruments, USA) is used for profiling currents through the water column. The ADCP operates at 300 kHz using four

convex beams with a beam angle of 20°. For use with the buoy the instrument is set up with a depth cell size of 2 m allowing for 24 cells through the water column at the mooring location. The blank after transmit distance is set to 1.76 m, with the first cell located at 4.18 m. Total ensemble length is 1:52.50 minutes with 40 pings of 2.81 seconds averaged together during an ensemble. A number of quality control and error checking routines are performed internally within the ADCP, which flag the data as bad if it does not meet the predefined criteria. These include a correlation threshold, a false target threshold, a minimum percentage of good water-profiling pings obtained within an ensemble, and an error velocity threshold (the error velocity is the difference between the two measurements of vertical velocity and provides an indication of the standard deviation of the data). The measurements have a specified accuracy of 0.5% of the water velocity ± 0.5 cm s^{-1} and a resolution of 0.1 cm s^{-1}.

An ADCP can be surface or bottom mounted with corresponding advantages and disadvantages of each configuration. A bottom mounted ADCP is stable in its deployment location but is unable to resolve currents close to the surface due to sidelobe contamination, and unable to measure currents close to the bottom due to the blanking distance. Data retrieval from the ADCP has to be via recovery of the ADCP using divers or an acoustic release, or by the use of acoustic modems configured to communicate with a surface data logger. A surface mounted ADCP cannot measure near surface currents due to the deployment depth and blanking distance, is subject to wave motions which may increase the standard deviation of velocity and direction estimates, and cannot resolve near bottom currents due to sidelobe contamination from the seabed. Data are easily retrieved from a surface mounted ADCP by direct connection to a data logger or recovery of the instrument by boat. Comparisons of surface and bottom mounted ADCP data (e.g. Lohrmann 1998, Kashino *et al.* 2005) have found differences of around 5 cm s^{-1} throughout the water column between measurements from instruments in the two configurations, which appeared to be independent of wave height and were attributed to buoy induced velocities. Despite the potential introduction of small errors into the velocity data, a surface mounted configuration was selected for the ADCP deployment due to the ease of deployment and data recovery. The effects of the blanking and deployment depth from a surface mounted unit, and sidelobe contamination from a bottom mounted unit lead to similar losses in surface current data, which is of the greatest interest in this application.

2.1.5 GPS

GPS position is recorded using a LeadTek GPS 9532 (Leadtek, UK). This allows the time to be updated accurately every 24 hours with the GPS time and the position of the buoy to be monitored should it become unattached from the mooring.

2.1.6 Modifications

The thermistor chain became wrapped around the mooring line and was lost from the system in April 2004. During the development of the second mooring (January 2005) it was replaced with a shorter 30 m thermistor chain of the same design, with a 2 m thermistor spacing between 0 m and 20 m and 5 m spacing from 20 m to 30 m. This thermistor chain subsequently became damaged and was replaced by a 24 m thermistor chain with 2 m thermistor spacing. Where possible, when a thermistor chain was not available, Starmon mini (Star-Oddi, Iceland) temperature recorders were deployed in self logging mode for data continuity. These temperature recorders have an accuracy of ± 0.05 °C.

The initial GPS unit was damaged by ingress of seawater and was replaced with a GPS 35 LVS (Garmin, USA), which was integrated into the second buoy. Following failure of the second unit it was decided that a GPS was not essential to the operation of the buoy and it was not replaced.

Although the data logging system was designed to include an ADCP, insufficient space on the demonstration bio-optical buoy led to the ADCP being deployed in self-logging mode on the marker buoy. The design of the second mooring and scientific buoy allowed for the integration of the ADCP into the scientific buoy and for the data to be collected by the system. The ADCP runs from an internal battery pack and is not supplied power by the system.

The selection of a spar buoy design for the second mooring means that the buoy undergoes vertical motion in response to the wave field. In order to produce remote sensing reflectance measurements from the radiometer data, the radiance data must be propagated to the surface. This requires knowledge of the depth at which the radiance measurement was made. The design of the demonstration buoy as a surface following platform meant that the depth of the radiance sensor remained relatively constant and

could be measured before deployment. In order to obtain a measurement for depth on a vertically moving platform a PDCR 1830 pressure sensor (Druck, UK) was incorporated into the system, located next to the radiance sensor. The sensor measures depth by means of a diaphragm and compensates for atmospheric pressure by using a vented cable.

2.2 Mooring Design

2.2.1 Demonstration Mooring

The demonstration buoy, designated as Bokkom, was designed as a surface following buoy constructed from a 316 grade stainless steel frame. The frame comprised of a central cage with a floatation unit and an outer ring with the radiance sensor mounting and additional buoyancy for stability (Figure 2-1). A plate at the top of the buoy provided mounting for the GSM and GPS antennae, a navigation light and the irradiance sensor (which requires an unimpeded view of the sky over a 180° hemisphere). Four solar panels were mounted at an angle of 45° on brackets at the top of the main cage. The Ocean-i unit and Templine control boxes were mounted in the main cage above the floatation. The thermistor chain was routed from the Templine control box down the side of the floatation and through the water column; a small weight was attached to the end of the chain. Closed cell polyethylene foam, encapsulated in polyurethane for protection and rigidity, was used for the floatation. The radiance sensor was mounted at the edge of the outer ring where it had an unimpeded downward view, shading from the buoy superstructure was minimised, and the frame offered some protection for the sensor. Continuation of the main cage underwater provided housing for the SCUFA and the battery pack, which was the heaviest item on the buoy and provided some ballasting. A stabilising weight attached by three stainless steel wire strops was suspended 3m below the main cage.

The main surface flotation of the mooring was constructed from encapsulated glass flotation units mounted in a frame with a navigation light mounted on the top, and was anchored using rope and chain to railway line on the seabed. The scientific buoy was connected to the surface mooring unit via a 5 m tether (Figure 2-1).

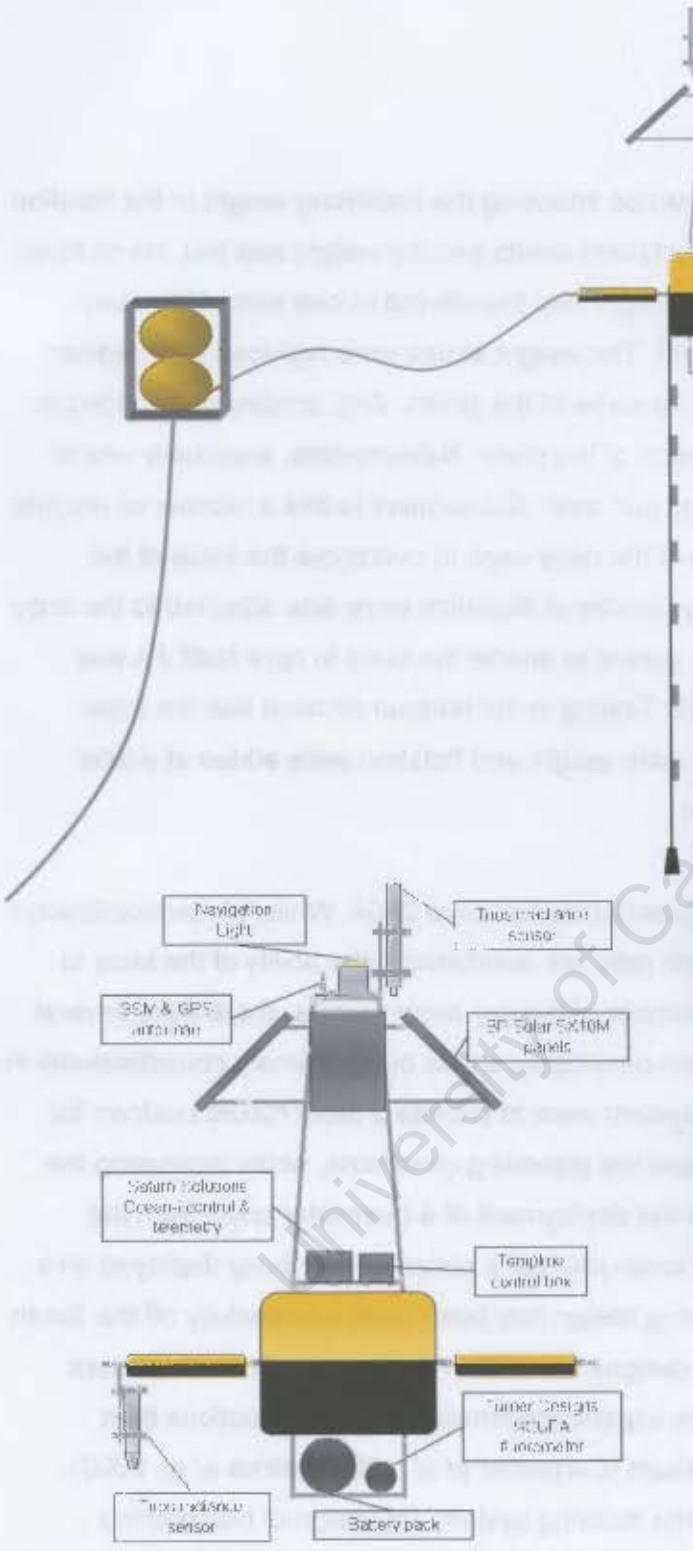

Figure 2-1 Schematics (courtesy of S. Bernard) and photograph of demonstration mooring and buoy (Bokkom)

2.2.1.1 Modifications

Early on in the deployment the wire strops attaching the stabilising weight to the flotation ring parted due to chaffing at the attachment points and the weight was lost. As all three strops did not part at the same time, weight was transferred to one side of the buoy structure causing the buoy to turn over. The weight strops were replaced with heavier duty chain with large O-rings to absorb some of the stress. Zinc anodes were added to the chain to reduce the rate of corrosion of the chain. Nevertheless, eventually one of the chains parted causing the buoy to turn over. Subsequent to this a number of weights were attached directly to the bottom of the buoy cage to overcome the issue of the strops parting and inverting the buoy. Blocks of floatation were also attached to the buoy superstructure underneath the solar panels to enable the buoy to right itself if it was knocked horizontal by waves or swell. Testing in the harbour showed that the initial weight attached was insufficient, so more weight and flotation were added at a later stage to enable the buoy to self-right.

The buoy suffered irreparable structural damage in June 2004. Whilst the demonstration buoy collected a valuable three month data set, establishing the ability of the buoy to detect algal blooms, and fulfilled a number of the key requirements, there were several matters to be taken into account when developing a new buoy. Primary considerations in the development of a new mooring system were to provide a more robust platform for data collection, better able to withstand the prevailing conditions, whilst increasing the ease of deployment and allowing for the deployment of a thermistor chain from the scientific buoy. This resulted in the construction of a pencil or spar buoy deployed on a dual tight line mooring. Such a mooring design has been used successfully off the South African coast and similar spar buoy designs have been deployed in Antarctic waters (e.g. Demer *et al.*, 2003). Spar buoys experience smaller tilt and roll motions than surface following buoys such as Bokkom (Carpenter *et al.* 1995, Detrick *et al.* 2000), resulting in a reduction of stress on the mooring system. Redesign of the mooring allowed the ADCP to be incorporated into the bio-optical buoy and the data from it to be logged by the system.

2.2.2 Second Phase Mooring

Key components of a spar buoy design are to ensure that the buoyancy is just sufficient to keep the buoy hanging from the surface, and that the bulk of the weight is located as

far below the water surface as possible. To keep the windage of the buoy as low as possible the mast of the buoy was designed with a small surface area. The payload at the top of the mast was kept to a minimum, consisting of the GPS and GSM antennae, the irradiance sensor and navigation light. A flexible solar panel was wrapped around the length of the mast. The deployment requirements of the radiance sensor (as before) are that it should be vertically orientated, as close to the surface as possible and free from shading by the buoy structure. To meet these criteria a stainless steel arm was attached to one side of the buoy around the flotation unit; the SCUFA fluorometer, radiance sensor and depth sensor were attached to this arm.

The buoy, designated BOB, was constructed from PVC pipe encapsulated in fibreglass (Figure 2-2). Two smaller diameter pipes were attached to the lower section of the buoy adding to the strength of the structure and providing housing for the cables running through the buoyancy unit down to the Ocean-i unit. A stainless steel cage bolted to a flange at the bottom of the buoy houses the Ocean-i unit, battery and ADCP. These are the heaviest components of the system, providing ballast at the bottom of the buoy as well as a clear line of sight for the ADCP. In an ideal system the ballast should be as far below the waterline as possible. This poses difficulties, as increasing the length of the buoy makes handling of the buoy from a small boat more problematic, and causes loss of surface current data from the ADCP. A compromise was reached in which the length of the structure below the waterline is around 2 metres; ADCP data collection starts at 4 metres. Buoyancy of the structure should be minimised below the waterline to enhance the stability of the structure. Housing the instruments in the open stainless steel cage reduced buoyancy along with allowing the lower section of the PVC pipe to be flooding through a vent hole at the top of the pipe. The surface flotation unit is comprised of closed-cell foam (Sondor SPX33, Sondor Industries, South Africa) encapsulated in fibreglass.

The new mooring was designed as a dual anchor tight line mooring in order to decrease the stress transmitted to the scientific buoy by a single point tether, and to reduce the

chances of the thermistor chain becoming entangled. The mooring was orientated into the predominant swell, which is considered to be south-west for the deployment off Lambert's Bay (Figure 2-2). The system was anchored to the seabed at both ends, with

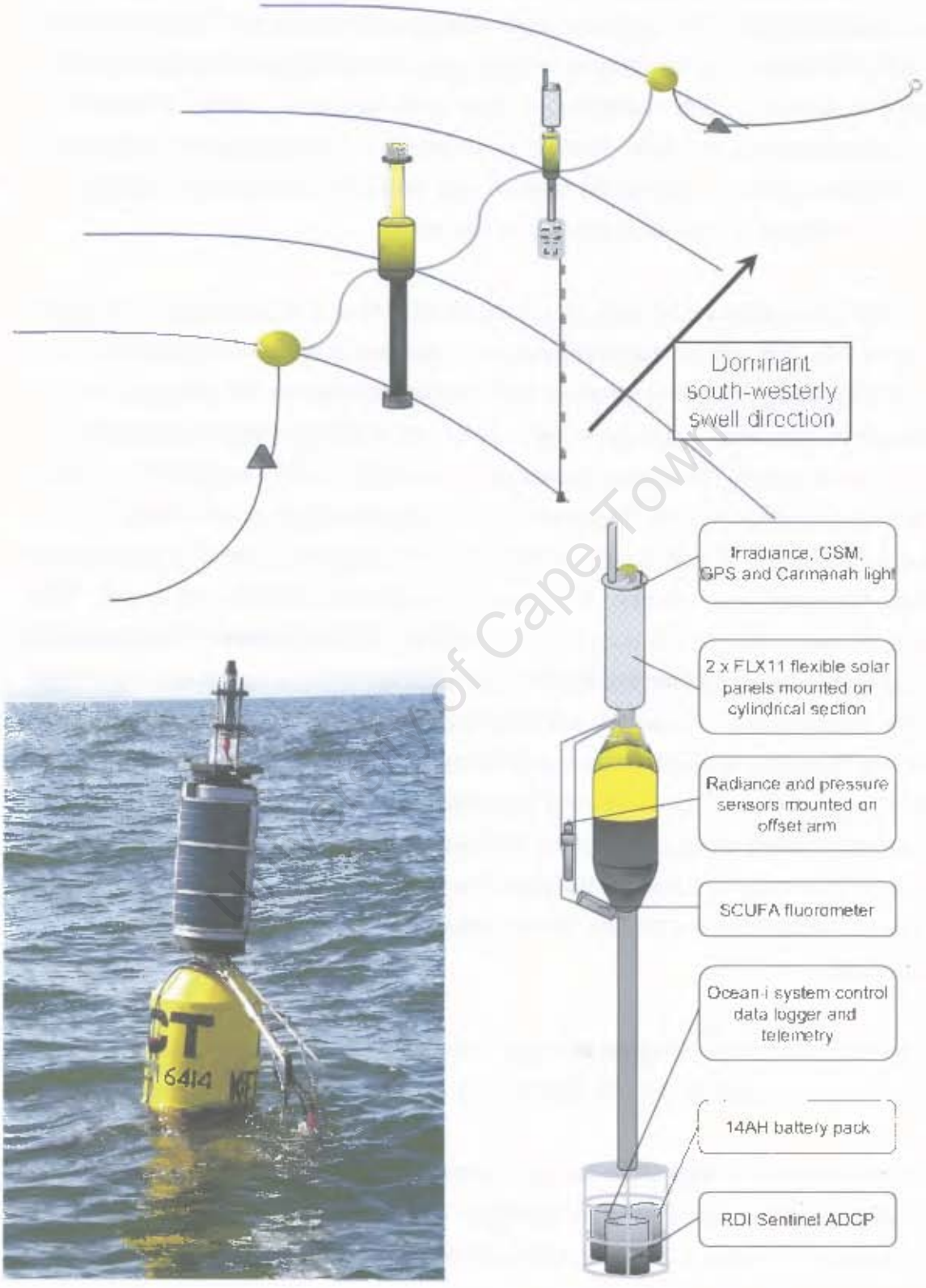

Figure 2-2 Schematics (courtesy of S. Bernard) and photograph of second phase mooring and buoy design (BOB)

plumb weights to act as dampers connected to trawl floats at the surface. A marker buoy, designated BOMB, with a light and radar reflector, and the scientific buoy, BOB, were strung between the two sets of trawl floats on 6 m strops. In this configuration the entire mooring rides the swell and stresses at individual tether points are reduced. The marker buoy remains on the mooring when the scientific buoy is removed for servicing, providing enhanced visibility and safety.

2.2.2.1 Modifications

The scientific spar buoy was designed with a 1.5 m long mast above the water line on which a flexible solar panel was mounted. During field trials it quickly became apparent that this mast was too long, leading to increased tilt/ roll of the buoy, and causing the mast to break at the flange at its base. The mast of the buoy above the flotation unit was shortened by one metre and fibreglassed into a single section to improve the structural strength and sea-keeping abilities of the buoy. Reduction of the mast length decreased the area available for the mounting of solar panels leading to the use of two smaller solar panels (see 2.3.1). These panels were attached back to back on the shortened mast. A stainless steel sleeve was inserted into the tube at the bottom of the buoy between the instrument cage and the flange to disperse the stress and drag from the cage through the structure, relieving stress on the flange. Whilst the buoy was out of the water holes were drilled through the bottom of the buoy structure in order to bolt the stainless steel sleeve into the pipe and increase the integrity of the structure. The total length of the buoy was reduced to 3.9 m; the decrease in length of the structure above the waterline adds to the ease of handling of the buoy and increases its sea-keeping abilities. Stress from the mooring is transmitted intermittently to the scientific buoy when waves pass along the mooring. This was reduced by attaching a weight to the seaward mooring line between the marker buoy and scientific buoy to dampen some of the pull from the mooring line.

Despite the new mooring design, the thermistor chain became entangled around the landward mooring line and was damaged. To prevent this from recurring a shorter 24 m thermistor chain was used, and the spacing between the scientific buoy and landward mooring line was increased from 6 m to 15 m.

After nine months of deployment the marker buoy, trawl floats and lines were heavily fouled, despite the use of anti-fouling paint, causing the trawl floats to start to sink and placing large stresses on the mooring lines and components. This led to the removal of the scientific buoy from the mooring and the eventual loss of the mooring system.

2.3 Control System

A robust control and data logging system to supply power to the instruments, interrogate, collect, and store data from the instruments and transmit the data in real-time is vital to the optimum operation of the buoy as a monitoring system (Mueller *et al.* 2003b).

The control system used on the buoy is an Ocean-i unit (Saturn Solutions, UK). This system has been used extensively with TriOS radiometers, particularly during the Volvo Ocean Adventure (Byfield *et al.* 2002), and was therefore a logical selection for use with the radiometers on the buoy. Adaptation and development of the Ocean-i system to operate on a buoy using a multitude of sensors alongside the radiometers formed a crucial component of the buoy development.

The Ocean-i unit is based around an Advantech PCM-7210 integrated XScale single board computer running Windows CE 4.1 that controls the data sampling routine for the instruments, stores, and transmits the data. The use of XScale technology provides a low power environment in which the control system is implemented. Control software for the Ocean-i unit is written using Visual Basic .NET. Six serial ports are available for use with the instrumentation, all of which use a RS232 data interface for communication. Four of the RS232 serial ports are available on the platform itself while a further two serial ports are provided by the inclusion of a daughter board (MUX board) which also provides power management for the system. Microsoft Windows based user software, Ocean-i Console, allows user set-up of certain parameters and selection of the data acquisition routine for the instruments through a local or remote connection. Data are stored on a removable CompactFlash card.

A Comtech OEM-GPRS-2E (Comtech, UK) dual band, HSCSD (High Speed Circuit Switched Data) capable GSM (Global System for Mobile Communication) modem is integrated into the Ocean-i unit for remote access of the system and data transfer. A SIM card must be inserted into the modem in order to access a GSM network.

A BecoSolar (Becosolar, UK) shunt regulator is incorporated into Ocean-i to interface between the solar panels and battery pack. This limits the voltage to which the battery can be charged, prolonging battery life, and prevents the battery from discharging through the solar panels at night.

The Ocean-i Console software provides a user interface for the configuration, control and management of data from the Ocean-i unit. It can be run on any IBM compatible PC running Windows 95 or above. Connection to the Ocean-i unit can be achieved locally via a serial port and cable connecting to an external port on the Ocean-i unit, or remotely by dialling into Ocean-i via a modem. The Console software allows the user to change the configuration of the data cycle and the Ocean-i set-up, and download data. Data are downloaded from Ocean-i by selecting the times and dates between which data are required using the Console software. These data are then requested from the Ocean-i unit and saved to the PC running the Console software. The data files can then be viewed using the Console software and the radiometer data can be calibrated, reflectance can be calculated, and the data can be exported in a number of file formats. Options exist to select the intervals at which data are collected ranging from every five minutes to once an hour, with a burst length of between one and five minutes and the times between which radiometer data are collected. Radiometer serial numbers must be configured via Console prior to data collection in order for data to be stored correctly. If radiometer data are to be viewed or exported as calibrated data the software must be provided with the location of radiometer calibration files. These files are supplied with the radiometers; background, calibration and wavelength files are required for each radiometer in order to calibrate data. Advanced setup allows the specification of the serial numbers of the radiance and irradiance sensors, which are required for immersion factor and reflectance calculations, and the input of the instrument offset to be applied to tilt and roll data. Communication parameters may also be altered to improve remote connection and data transfer. Diagnostic information and error logs available on connection to the Ocean-i unit provide information on system operation.

2.3.1 Modifications

A number of modifications were made to the Ocean-i unit due to changes implemented during the design of the second mooring system.

In the second configuration Ocean-i was located in the cage at the bottom of the buoy at a depth of around 2 m along with the battery and ADCP, and was therefore re-housed in a depth rated case. The chassis on which the electronics are mounted was designed to include space for housing the thermistor board and batteries in order to eliminate the need for further waterproof housing of the thermistor chain controller.

A reduced area of solar panels and thus power is available in the second buoy configuration, requiring a reduction in the amount of power used by the system where possible. It was discovered that at 12 volts the radiometers drew an ambient current of 40 mA, and that they could be more optimally powered at 7.8 volts reducing the power draw to 7 mA. To facilitate this reduction in power a power supply board for the radiometers was designed and integrated into the Ocean-i unit to step-down the power supplied to the radiometers from 12 to 7.8 volts.

The incorporation of the pressure sensor, which is an analogue instrument, involved the addition of an A/D converter in order to interrogate the instrument. This was built into the Ocean-i unit and has the secondary advantage of enabling power monitoring of the battery.

On a couple of occasions it was not possible to connect to the demonstration buoy remotely from Cape Town. Discussion with MTN revealed that a link break had occurred, in which the landline connection between the Lambert's Bay tower and Cape Town is lost. When this occurs most modems and cell phones require rebooting in order to relocate the network. Although link breaks do not occur frequently, it is important to set the modem up in a way in which it can reboot itself on a daily basis in order to re-establish connection to the network if it is lost. This was achieved by running a wire between the reset pin on the modem connector and a reset pin on the MUX board causing the modem to reset once a day at 00:28 when the system performs a hardware reset and updates the clock.

2.4 Power

Power remains a serious limitation for long-term autonomous systems (both stationary and moving) either requiring expensive cables, limited solar power, or short-lived batteries (Glenn *et al.*, 2000). The Ocean-i unit is designed to run from a 12 volt power

source, which powers the unit and supplies power to the instruments. Supply of power to the system is achieved through the use of a 12 volt, rechargeable, sealed lead-acid battery housed in an underwater casing that is charged by solar panels.

A careful balance must be achieved between power consumption, power supply and battery size in order to create an optimally functioning system. Adequate power must be supplied by the solar panels to charge the batteries and provide back-up power; equally there must be enough drain from the battery during a daily cycle to allow the battery to be cycled thus prolonging battery life. A spreadsheet provided by BP Solar aids in the calculation of the required battery size and number of solar panels required. Important considerations in calculating power requirements of a system are both the active and quiescent power draw of the instruments. Quiescent loads, which are generally of a longer duration, often have the greatest effect on the power requirements of a system.

Table 2-1 illustrates the typical power requirements of instruments used on the buoy, assuming a data acquisition period of two minutes every half an hour (see 2.5). The calculation for the number of solar panels required divides the total load (Ah) by the worst month daily average insolation in the area (ESH) to provide a required array current. Supplying the current of the solar module intended for use allows the calculation of the number of parallel solar modules required to power the system. For the instrument configuration detailed in Table 2-1 the system load is 2.6 Ah which, according to the calculations in Table 2-2, requires an array current of 0.78 A to run the system. The solar panels selected for use on the buoy were BP SX10M modules that supply a current of 0.58 A under ideal conditions; therefore two of these panels are required to run the system. A 12 Ah battery is used which should provide 3 days of back-up power in the absence of the solar panels.

In an ideal situation, solar panels should be situated perpendicular to the incoming sunlight, in order to intercept the maximum amount of sunlight. This is not possible on a buoy due to the difficulties of mounting the solar panels in an ideal position and the motion of the buoy. There are two aspects of solar panel positioning to be considered: the solar azimuth angle which corresponds to the daily east-west track of the sun and the solar declination angle which corresponds to the sun's apparent seasonal height in the sky. Changes in solar azimuth angle can be overcome by orientating the solar panel

DC Device	Load (watts)	Hours of use/day	Daily watt-hours
1. Computer	2.64	1.6	4.22
2. Scufa	0.6	1.6	0.96
3. Computer (standby)	0.024	22.4	0.54
4. MUX board	0.036	24	0.86
5. Modem	0.072	24	1.73
6. GPS	0.75	1.6	1.2
7. Radiance standby	0.48	22.4	10.75
8. Radiance acquiring	0.84	1.6	1.34
9. Irradiance standby	0.372	22.4	8.33
10. Irradiance acquiring	0.756	1.6	1.21
11. Thermistor chain standby	0.0036	23.85	0.09
12. Thermistor chain acquiring	0.23	0.15	0.03
DC load in watt-hours/day			31.26

Table 2-1: Daily power requirements of instruments on demonstration mooring (reproduced from BP Solar spreadsheet).

Array Sizing Procedure		
1. DC load in watt-hours/day	31.26	Wh
2. AC load expressed as DC	0.00	Wh
3. Total load	31.26	Wh
4. System nominal DC voltage	12	volts
5. Total load in ampere-hours (Line 4/Line 5)	2.61	Ah
6. System losses/safety factor multiplier	1.2	
7. Adjusted total daily load (line 5 X line 6)	3.13	Ah
8. Worst month daily average insolation (from map)	4	ESH
9. Required array current (Line 7/Line 8)	0.78	amperes
10. Current at maximum power (I_{mp}) of selected module	0.58	amperes
11. Number of parallel modules required	1.35	
12. Line 11 rounded up to next whole number	2	
13. Number of series modules required	1.0	
Total modules in array (Line 12 X Line 13)	2	

Table 2-2: Solar array sizing calculations given power requirements from Table 2-1 (reproduced from BP Solar spreadsheet).

DC Device	Load (watts)	Hours of use/day	Daily watt-hours
1. Computer	2.64	1.6	4.22
2. Thermistor chain standby	0.0036	23.85	0.09
3. Computer (standby)	0.024	22.4	0.54
4. MUX	0.036	24	0.86
5. Thermistor chain acquiring	0.23	0.15	0.04
6. Modem	0.072	24	1.73
7. GPS + Scufa	1.35	1.6	2.16
8. Radiance standby	0.1014	22.4	2.27
9. Radiance acquiring	0.624	1.6	0.1
10. Irradiance standby	0.0624	22.4	1.4
11. Irradiance acquiring	0.5304	1.6	0.85
12. Rad power supply	0.102	24	2.45
13. Press board standby	0.048	24	1.15
14. Press board acquiring	0.06	1.6	0.1
15. Pressure sensor	0.06	24	1.44
DC load in watt-hours/day			19.4

Table 2-3: Daily power requirements of instruments on second mooring (reproduced from BP Solar spreadsheet).

towards north in order to gain the most daily sunlight from a fixed position. In the case of a buoy, which itself moves, this can be achieved by having a number of solar panels positioned around the buoy so that one is usually facing the sun, or by using a wrap-around solar panel. Solar declination angle can be dealt with from a fixed position by mounting the panel at an angle of its latitude + 10° to intercept the maximum amount of sunlight in winter. The inability to mount solar panels in an ideal orientation on a buoy requires that a higher powered or larger number of solar panels should be used in order to generate a similar amount of power to one ideally situated panel of the same output. Four of the 10 W modules were mounted on the demonstration mooring at an angle of 45°.

2.4.1 Modifications

The change in design of the mooring system had two consequences for the power balance of the system: the use of a spar buoy design led to the selection of flexible solar panels to charge the system, changing the amount of power that could be supplied to

the system and necessitating a reduction in the power requirements of the system where possible (see 2.3.1), and the addition of a pressure sensor altered the power demands of the system. Table 2-3 outlines the power requirements of the altered system; a reduction in the power demand of over 10 Wh per day was achieved.

The second mooring was field trialled with a FLX-32 (Uni-Solar, USA) flexible solar panel wrapped around the mast. Although the orientation of the panel was sub-optimal, with an operating current of 1.94 A the calculations indicated that 0.25 of these panels would be required, and therefore one deployed sub-optimally was considered sufficient. Following the field trial, and the modification of the buoy to a shorter mast, it was no longer possible to use the 32W panel due to space constraints and two FLX-11 panels were selected. These panels have an operating current of 0.62 A; calculations indicate that 0.8 optimally located modules would be required to power the system.

The two flexible 11 W panels successfully kept the battery charged and the system running during the summer months; however the solar panels supplied insufficient power during shortened daylight hours in winter. In a system with such a delicate power balance a slight reduction in daylight hours quickly reduces the operating period of the buoy. This was temporarily overcome by changing the batteries more frequently; future winter deployments must consider the addition of further solar panels, larger battery packs or an alternative power source such as wind power.

2.5 Sampling Routine

Implementation of an adequate sampling regime is important in order to observe the processes that the buoy is designed to monitor (Dickey 2003). In the development of a moored system, sampling frequency must be balanced with the available power, storage capacity and data transmission capability. Sampling at too high a frequency drains power from the system and quickly uses up storage space while sampling at too low a frequency means that it is not possible to resolve higher frequency signals.

Instruments deployed previously in Lambert's Bay in self-logging mode have used a sampling period of 10 minutes. The determination of physical processes such as internal waves, which are the highest frequency events of interest in this application, requires a sampling period of around 6 minutes. The storage and power demands of such a regime

are too great for the buoy and therefore a sampling period of 30 minutes was selected as a suitable compromise. This can be altered remotely at any time should the required power and storage become available.

Use of the radiometers for the measurement of reflectance means that it is preferable to sample in bursts (collect samples as quickly as possible over a specified period). This enables the filtering of data on tilt/ roll to remove anomalous data, and the production of a mean or median reflectance value for the burst period (Cullen *et al.* 1997). A burst period of two minutes was decided upon as the acceptable minimum sampling period.

The Ocean-i unit was originally developed for the collection and storage of data from the RAMSES radiometers. The hyperspectral nature of the radiometers leads to the generation of a significant amount of data: 528 bytes per radiometer per acquisition. For ease of storage and manipulation all data are stored as records of the same length. Each radiometer acquisition generates a header record of 528 bytes containing the time and date of acquisition and any ancillary data, followed by 528 bytes of data for each radiometer. Where multiple radiometers are present a start command is sent to each radiometer one after another (effectively simultaneously). The use of an automatic integration time by the radiometers prevents their acquisition from being run by a timer. The data management unit must issue a start command to the relevant port, await the returned data and issue another start command on receiving the expected amount of data until the end of the collection period is reached. Two radiometers are used on the buoy, generating three 528 byte records per acquisition: a header record followed by one for each radiometer.

Few other instruments generate as much data per acquisition as the radiometers. Therefore it is possible to store the data from other instruments in the 528 byte header record generated by the radiometer acquisitions. This preserves storage space and lowers transmission times by saving the data in an area already allocated to data. As the radiometers with their varying integration time are the most problematic instruments to control, collection of data from the other instruments has been designed to fit around the radiometer data collection. Designing control software to initiate data collection, process and store data from a number of instruments with differing timing requirements requires careful consideration. Controls for the collection and storage of data from the other

instruments were added to the software on an instrument-by-instrument basis to build up a complete system. The flow charts in appendix I outline the architecture of the burst sampling software that controls the acquisition and saving of data from all the instruments. Two main processes run side-by-side to collect and store the data: the start acquisition process and the update files process. The first process controls the sending of commands to the instruments to initiate data collection; the setting of flags according to the current acquisition status of the instrument determines when data collection is initiated for each instrument. The second process controls the saving of collected data to a file. These processes are interlinked by the receipt of radiometer data, which restarts the acquisition process, and initiates the saving process. Each instrument has differing timing and data protocol requirements that must be taken into consideration when creating an acquisition regime.

2.5.1 SCUFA

Most instruments are supplied power continuously through Ocean-i; data acquisition is initiated by sending an RS232 command and the instruments draw very little standby current when not acquiring. The SCUFA outputs data continuously at a date of 1Hz when powered up. It is not possible to start and stop acquisition by administering a command string. This leads to a large power draw on the system and the lamp being continuously lit, which shortens the life of the lamp. To overcome this, a serial port for the SCUFA was provided on the MUX board that has the ability to control the supply of power. The SCUFA is powered up at the start of a two minute burst and data are output continuously. When radiometer data are received and a header record is written, the data string from the SCUFA port is picked up and the temperature corrected fluorescence and turbidity values at the start of the string are extracted and saved to the header record.

2.5.2 GPS

The GPS requires a 5V power supply and is powered by a USB port power supply on the computer board. This means that the GPS unit only receives power when the computer board is active, before, and during an acquisition cycle. Although the data output of the GPS can be turned on and off by sending commands, it is not possible to poll the unit for a single acquisition. The GPS is used both for setting the system time where necessary, and saving the position of the buoy with the dataset. If the Ocean-i

unit has a hardware reset, a command string is sent to the GPS to stop the output of messages. Once the system is ready to acquire data a second command string is sent to the GPS to start the output of data; messages from the GPS are output at a frequency of 1 Hz. The system attempts to get a valid time from the GPS; GPS messages include a character in the string designating whether the data in the message is valid (i.e. the GPS has obtained a satellite fix since start-up). Once a valid time has been received and used to set the system time, or the cycle times out after five attempts, the output of GPS messages is stopped. An option exists to update the system time with GPS time for accuracy at 00:28. This happens, as above, by forcing the system to perform a hardware reset. At the start of an acquisition cycle the GPS message output is re-started. After a valid position has been received, the output of GPS messages is stopped and the position extracted from the string transmitted by the GPS is saved to the next header record that is written.

2.5.3 ADCP

The ADCP is powered by internal batteries and automatically enters sleep mode to save power after 5 minutes of inactivity. At the start of an acquisition cycle, Ocean-i transmits a 'Wake-up' command to the ADCP, followed by a 'Start Pinging' command. The ADCP internally averages the data collected during an ensemble and transmits a block of data to Ocean-i at the end of an ensemble that consists of the averaged velocity data for the ensemble and header information for the ADCP. The ensemble length was selected to fit into the two minute acquisition cycle of the radiometers, allowing for the storage of data within the existing protocol. When Ocean-i receives the data from the ADCP, it writes it to the next header record in the data file.

2.5.4 Thermistors

The thermistor chain takes approximately 10 seconds to retrieve data from the 17 thermistors. At the start of an acquisition cycle the Templine controller is sent a start command. When the controller has collected temperature data they are transmitted to Ocean-i. On receiving the thermistor data Ocean-i saves them to the next header record that is written, and another start command is issued to the thermistors.

2.5.5 Other Schedule Considerations

The nature of radiometer data dictates that it only needs to be collected during daylight hours, and only when the sun is at a relatively high angle (Mueller *et al.* 2003b). The Ocean-i unit can manage this in two ways: a schedule period can be configured in which radiometer data are only stored by the system between the specified times, or the system can compare the signal to noise ratio of the received irradiance data and discard data where the signal to noise ratio is less than ten on the assumption that it is too dark to collect radiometer data. When it is dark or outside a specified schedule period a header record is saved to the data file containing the data from the other instruments and the radiometer is discarded. Two thirds less storage space is used when radiometer data are not saved. A schedule period of 08:00 to 17:00 is used for the collection of radiometer data during the mooring deployments.

2.5.6 Modifications

The original system was reliant on the GPS to set the clock time if the system underwent a hardware reset, as the single board computer that Ocean-i is based around does not have a real-time clock that is capable of retaining the time. This caused problems when a GPS was not available to the system, in that the time was often lost and reset to the default setting of 01-06-99 12:00, leading to data being collected with incorrect timestamps. The MUX board has a real-time clock on board which enabled the software to be changed to reset the time from the MUX clock following a hardware reset, before attempting to update the time from the GPS. The date is retrieved and set from the name of the latest data file saved on the Compact Flash card.

The incorporation of a pressure sensor (see 2.1.6) into the system during the design of the second mooring required an existing instrument channel to be shared as the six serial ports available in the Ocean-i unit were already in use. Readings from the thermistor chain were originally collected throughout the two minute sampling burst. This was altered to take one reading from the thermistor chain before the start of the sampling burst and then change the baud rate (the thermistor chain operates at 38400 baud whereas the SCUFA operates at 9600 baud) and utilise the same channel to supply power to the SCUFA and collect fluorescence readings for the duration of the two minute burst.

Data from the pressure sensor is required for each acquisition of radiometer data. A command to acquire data from the pressure sensor is sent immediately after an acquire command is sent to the radiometers. The A/D converter that collects and converts data from the pressure sensor collects 16 pressure measurements, which are averaged to remove any noise from the signal, and transmits a single pressure measurement to Ocean-i. This measurement is saved to the header record that corresponds with the radiometer data gathered simultaneously. The A/D converter for the pressure sensor also monitors the power of the buoy's battery. These data are collected at the same time and in the same manner as the pressure data and saved to the next header written.

2.6 Data Storage

Data are stored within the Ocean-i unit on a 256MB removable CompactFlash card. A data file is created for each day, and data collected during each acquisition cycle are appended to this file. All data are stored as binary data; the file is named with the date in the format yy-mm-dd.fdt where yy represents the last two digits of the year, mm represents the month and dd represents the day.

The amount of data generated per acquisition cycle varies due to the varying integration time of the radiometers and therefore a differing number of acquisitions collected in each cycle. In well-lit, low biomass conditions radiometer data are collected rapidly and around 79 Kilobytes (KB) of data are generated from a two minute acquisition cycle. Data are collected more slowly outside the scheduled hours for the radiometers, and one third of the amount of data are recorded due to the lack of radiometer data; around 5KB of data are generated by a two minute acquisition. Assuming that data are collected for two minutes every half an hour, and that radiometer data are collected for nine hours a day, approximately 1.65 Megabytes of data are generated per day. This allows for 155 days of storage on the CompactFlash card: this can be considered a conservative estimate of the length of time for which data can be stored given that it is calculated assuming well-lit conditions. The format in which the data are stored within the header and radiometer records is detailed in appendix II.

Data can be downloaded from the CompactFlash card either locally or remotely using the Ocean-i Console software, or by removing the card and using a card reader. Downloading data using Ocean-i Console converts the data from a binary to an ASCII

file during the download process; this enables the viewing and conversion of data with Ocean-i Console and user manipulation of the data. Retrieval of the data using a card reader requires further conversion of saved files into an ASCII format before they are of use.

2.7 Buoy Servicing and Calibration

Instrumentation deployed on coastal moorings are highly susceptible to biofouling and thus must be serviced frequently and/ or employ strategies to prevent fouling in order to maintain data quality (Twardowski *et al.*, 2005). This is particularly important in areas of high biomass such as St Helena Bay (Pitcher & Weeks 2006). Biofouling on optical collectors or light sources, as in the case of the radiometers and SCUFA, leads to degradation in the quality of measurements. Steps can be taken to reduce the problem of biofouling through the use of an antifouling compound that slows down the growth of organisms. Non-optical sensors such as the ADCP can be coated with an antifouling paint. Optical sensors require a clear field of view or unimpeded light source so another solution has to be found. The SCUFA is supplied with a copper screen that clips over the head of the instrument. Copper is a micronutrient which becomes toxic at higher concentrations, interfering with enzymes on cell membranes and preventing cell division (Chavez et. al. 2000). As copper corrodes in seawater oxidised molecules are released into the water inhibiting biological growth. Both the SCUFA and radiance sensor on the buoy are wrapped in thin copper sheeting to reduce biofouling (Figure 2-3).

One of the important considerations in the development of the buoy was that it should be serviceable from a small boat. Ship time is expensive and has to be scheduled well in advance. Servicing from a small boat provides greater flexibility with regards to scheduling, is more cost-effective, and is important in maintaining the system in order to make effective measurements and minimise downtime. Servicing of the buoy in Lambert's Bay is carried out at approximately monthly intervals in conjunction with Marine and Costal Management routine sampling trips. Buoy servicing includes cleaning of the buoy and instruments to remove biofouling, downloading and backing up of all data, testing the drift of the radiometers with a field calibration unit (FieldCAL, TriOS, Germany), implementation of any necessary software upgrades to the Ocean-i unit and repair, maintenance and adaptation of the buoy itself to improve performance and prolong its lifespan.

Figure 2-3 Photographs of BOB removed from mooring for monthly servicing, illustrating levels of bio-fouling on buoy and instruments. The SCUFA and radiance sensor can be seen wrapped in copper sheet which helps to reduce local fouling (left)

2.8 Data Transmission

The incorporation of a GSM modem into the Ocean-i unit enables the remote access of the system and download of data. Cellular phone telemetry enables two way communication (e.g. Dickey *et al.* 1993) and eliminates both licensing and the need to establish shore receiving facilities (Glenn *et al.* 2000). Access to the system is via a modem with calls initiated from the user side allowing greater control over the system. The use of a HSCSD enabled GSM modem offers the possibility of higher data transfer speeds. HSCSD data transfer is reliant on the modem having a number of downlink and uplink slots for the transfer of data. Unfortunately most HSCSD modems are designed for receiving high volumes of data and transmitting small volumes of data. The consequence of this is that only one uplink slot is available on the Ocean-i modem restricting data transfer rates to ~ 14 kbps, though the modem is capable of receiving data at a higher rate. Network delays mean that a realistic data transfer rate of ~ 10 kbps can be achieved. Whilst not particularly fast, this is a higher data transfer rate than could be expected from a non-HSCSD enabled modem.

MTN were selected as the service provider to use for the modem on the buoy as they provide the best network coverage for the area. A landline or GSM modem can be used for communication at the user end; in this case a GSM modem is used as mobile-to-mobile calls prove to be the most cost effective.

2.9 Data Collection and Processing

It was initially envisaged that the buoy would be accessed remotely several times a day from Cape Town and all the data would be downloaded. The rate of data transfer and cost of calls (R 1.70/ minute peak rate, R 0.95/ minute off-peak) caused the amount of data to be downloaded per day to be revised.

Transmission of a two minute acquisition cycle of 79 KB at a rate of 10 kbps should take around one minute twenty seconds. In reality there is an overhead in transmission time to allow for dialling, connection, establishment of communications and disconnection in addition to the data transfer. To download an entire day's data, collected for two minutes every half an hour, at these transfer rates would require around half an hour connection time per day costing over R 1000 per month. For these reasons it was decided to download one half hourly sample twice a day. This is enough to monitor the general conditions in the area and provide an indication of the development of high biomass blooms; should an event of interest occur further data can be downloaded by manually dialling into the system. The entire data set is downloaded locally when the buoy is serviced for processing and analysis of the time series data.

An autodial routine was developed as part of the Ocean-i Console software to autonomously dial into the buoy and download the last half hours data. Using the Scheduled Tasks application in windows, the Ocean-i Console software is called by a command line at specified times during the day. The software uses the current time to calculate the times between which to download data the previous half hours data, assuming that data are collected on the hour and on the half hour. It then dials into the buoy, downloads and saves the data between the required times, disconnects from the buoy, exports the data in a specified file format and closes the software.

Matlab R13 (The MathWorks) is used for the processing, output and display of the data. A routine was written to export the data from Ocean-i Console in a format that can easily

be utilised as an input file for Matlab. This takes the data from a two minute acquisition cycle and writes it as space delimited ASCII data to four files, one for each of the radiometers, one containing header information including time, data, tilt and roll and one containing ancillary data from the SCUFA and thermistors. The file format was modified with the development of the second mooring to produce separate files for thermistor, SCUFA and ADCP data and to add pressure and power values into the header file. The output data files are saved to a directory where they can be utilised by Matlab. These files are automatically created by Ocean-i Console for any data downloaded autonomously.

Windows Scheduler is used to run Matlab five minutes after Ocean-i Console has downloaded data. A script file is called which processes the two-minute acquisition cycle data, applies a locally developed reflectance algorithm (Bernard 2005) to the data, and uploads the output to the web page. Data are downloaded from the buoy, processed and uploaded to the website (www.hab.org.za) autonomously twice a day at 09:00 and 15:00. A rolling seven day time series of data is generated from the daily samples to provide an insight into the change in conditions. Other data available on the website include background information on harmful algal blooms and ocean colour and chlorophyll *a*, sea surface temperature satellite images for the last three days where available.

2.10 System Deployment

2.10.1 Mooring Location

The mooring is deployed on the southern Benguela shelf three and a half kilometres offshore from Lambert's Bay in 52m of water (Figure 1-1). The availability of a slipway at Lambert's Bay eases the deployment and servicing of the buoy, which is crucial to the maintenance of a successful system. Research concerning HABs has been carried out in the region for a number of years (e.g. Pitcher *et al.* 1998) and is ongoing. Studies carried out in the area provide additional data that complement the data collected by the buoy, which together contribute to the understanding of HABs in the area.

2.10.2 Deployment Dates

Full deployment logs indicating servicing periods and instrument failures can be found in appendix III. Overall deployment dates were as below:

Bokkom deployed 28th February 2004 – 17th June 2004
BOB deployed 26th January 2005 – 21st July 2005 and 10th November 2005 – present (new mooring).

2.11 Recommendations

Throughout the development and deployment of the buoys and mooring systems, a number of issues have arisen. The future development of similar mooring systems, or the continued running of the present one, would benefit from taking these into consideration.

As mentioned in section 2.4, the power supply and demands of the system are delicately balanced and currently unable to support the continued running of the system during shortened daylight hours. Further consideration needs to be given to additional and alternative sources of power such as a greater area of solar panels or a wind generator, or the provision of larger battery packs to support the system during winter.

In its current configuration the ADCP is mounted at the bottom of the buoy and starts collecting data at 4m with the centre of the first bin being around 5m (see 2.1.4). The surface current is of interest and relevance in the advection of HABs, and it may therefore be desirable to measure currents in the surface 5m. This could either be achieved by reconfiguration of the buoy and mooring system, or through the addition of a single point current meter mounted to measure the near-surface currents.

The current rates of data transfer using GSM, even with HSCSD, are slow and do not allow for the download of more than snapshots of data in real-time. Communications are continuously evolving and newer technologies allowing for higher data transfer rates should be considered if they are stable and compatible with the current system.

Failure of instruments and components is a feature of any system, particularly one deployed long-term in a harsh environment. Continuity of data can only be assured with the availability of spare instruments that can be interchanged with non-functioning instruments as necessary. In an ideal situation a complete replacement buoy system with instruments would be available. Systems could be swapped in and out whilst the

second system was serviced and maintained, minimising gaps in the data due to routine servicing as well as instrument failure.

The availability of personnel to respond to instrument failure and servicing demands is as important as the availability of spares. Currently a small team of two to three people, all of whom are required for each trip, with access to one boat and skipper are responsible for maintaining the buoy. A larger pool of people, with access to alternate boats and skippers, should be able to schedule regular servicing of the system and respond more quickly to instrument failure, helping to maintain an optimally functioning system.

Experience gained from deployment of the current mooring system suggests that the entire mooring should be removed and serviced or replaced on a six monthly basis to prevent loss of the mooring due to wear and fouling. This should be scheduled during a period when data gathering is not considered critical (e.g. winter). As HABs are less likely to occur during winter, and the passage of winter storms leads to the greatest strain on the mooring system, it may be prudent to remove the buoy and mooring system for a few months during winter and replace it before the transition to spring conditions.

The size and weight of the scientific buoy presents the greatest difficulty when deploying and servicing the buoy from a small boat. Although this was considered during the design of the buoy, the current buoy still weighs around 100 kg and is cumbersome to handle. Any weight that could be saved in the refinement or re-design of the scientific buoy would considerably ease the handling of the buoy.

2.12 Example Data: Buoy Diagnostics and Performance

Sample diagnostic data from BOB in January/ February 2005 are shown in figures 2-5 to 2-7, illustrating the heave of the buoy in response to the wave field, the tilt and roll of the buoy, and the battery power.

Tilt and roll angles for the buoy are calculated as the root mean square of the separate tilt and roll measurements. Values for the tilt of the buoy vary between 0 and 45 degrees within a two minute sampling burst indicating a large range of movement, although the majority of the variation is confined between 0 and 20 degrees. Median values for a two

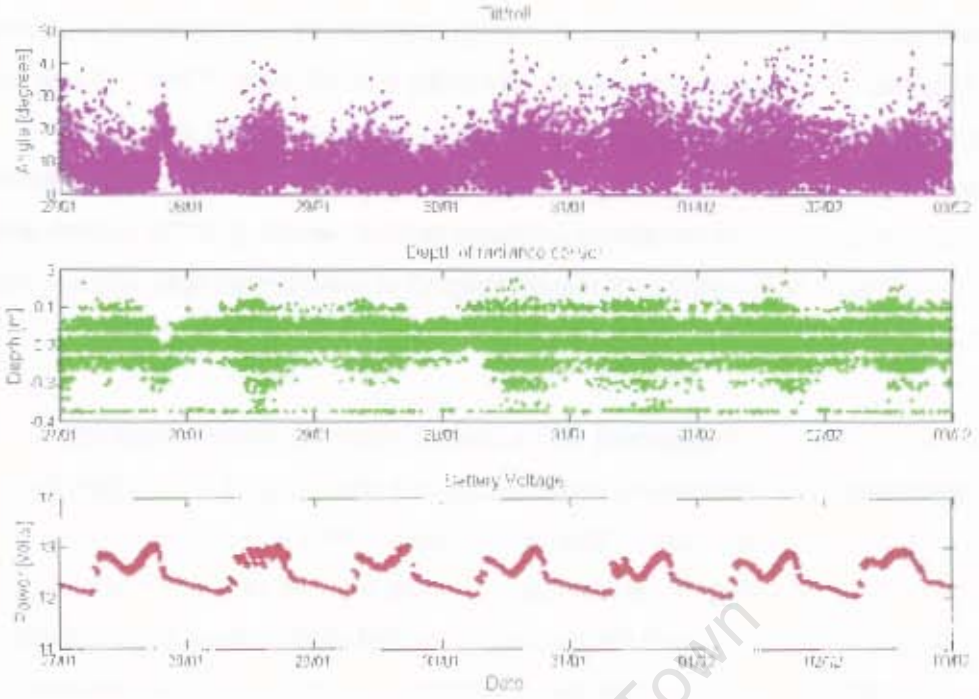

Figure 2-4 Half hourly diagnostic data from the mooring illustrating variations in tilt and roll (top), the depth of the radiance sensor (middle) and battery voltage (bottom) for a week in January/ February 2005

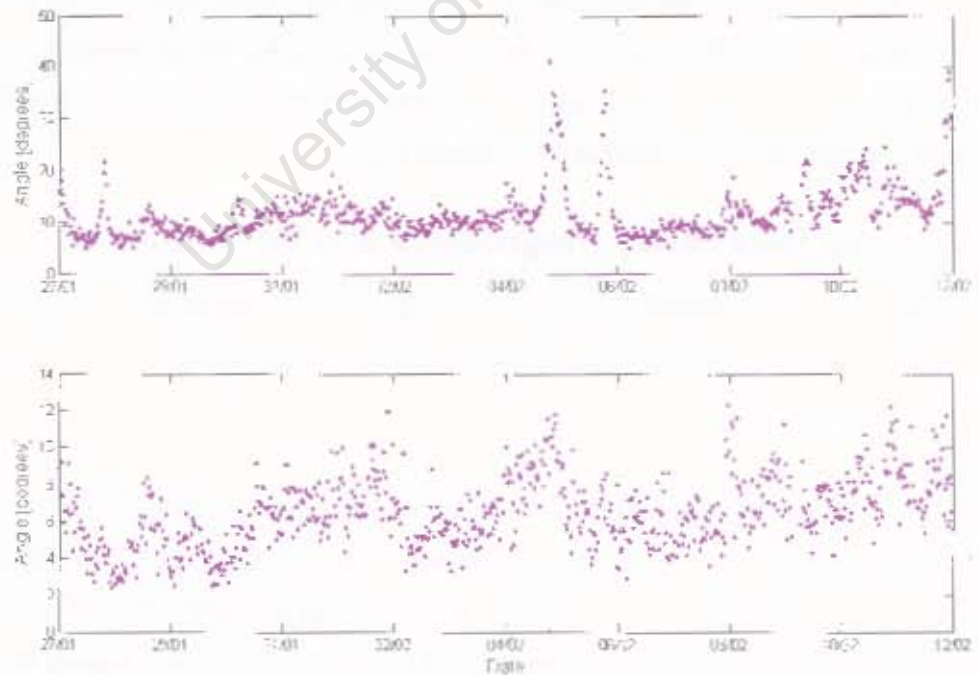

Figure 2-5 Half hourly median (top) and standard deviation (bottom) tilt and roll measurements from the mooring for a week in January/ February 2005

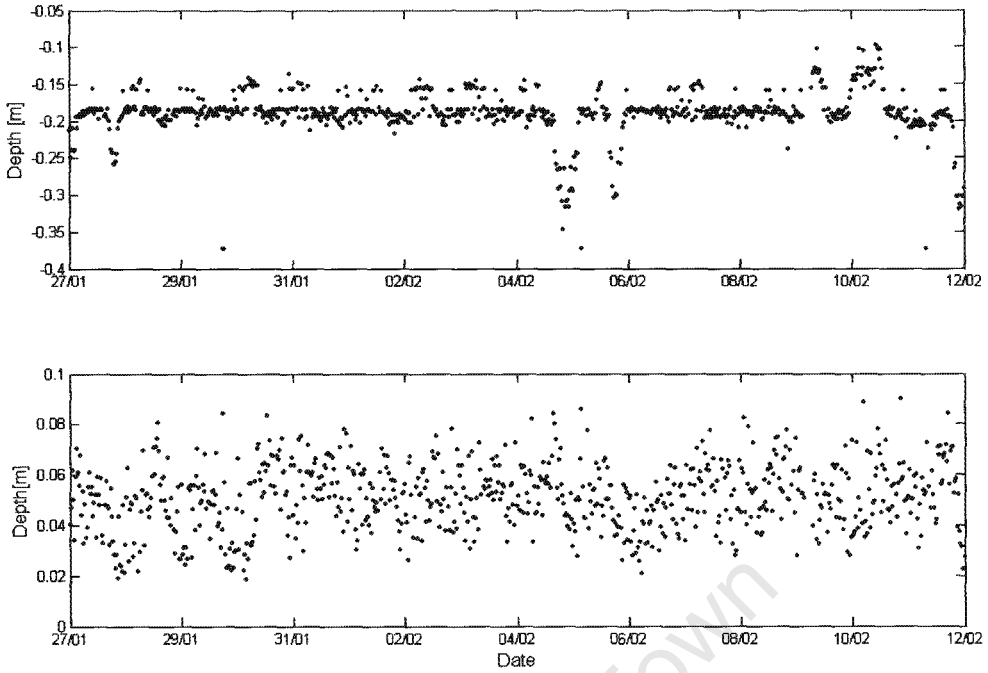

Figure 2-6 Half hourly median (top) and standard deviation (bottom) radiance sensor depths from the mooring for a week in January/ February 2005

minute burst are generally between 10 and 15 degrees while the standard deviation for the same period is between 5 and 10 degrees. Not all measurements are compromised by a high value of tilt and roll, and there are enough low values within a sampling burst to filter the data on these. Where the tilt and roll values remain high throughout a sampling burst (e.g. late on the 27th February) it is attributed to a strong surface current; as the instrument cage at the bottom of the buoy structure has the largest area it causes the greatest drag and the buoy tends to lean into the current. This has been confirmed by visual observation while at the mooring site.

The depth of the radiance sensor varies between around 0.1 and 0.3 m during a sampling burst as waves pass along the mooring. Median values for a two minute burst are 0.15 to 0.2m with a standard deviation of 0.08 to 0.02m. Higher and lower median depth values are associated with periods of high tilt and roll where the buoy is leaning into the current; depending on the direction of the current the radiometer arm is either leaning further into or out of the water and therefore the median depths for these sampling bursts are more extreme than usual.

The two 11W solar panels provide adequate power to the system with the battery voltage dipping to 12 volts in the early morning and being recharged to around 13 volts during the day; overall the battery power remains fairly constant illustrating a well balanced system. The dip in power towards midday may be due to the radiometers starting to collect data at 8am pulling a relatively large amount of current, or the automated dial in and download of records at 9:30 am causing a large current draw by the modem.

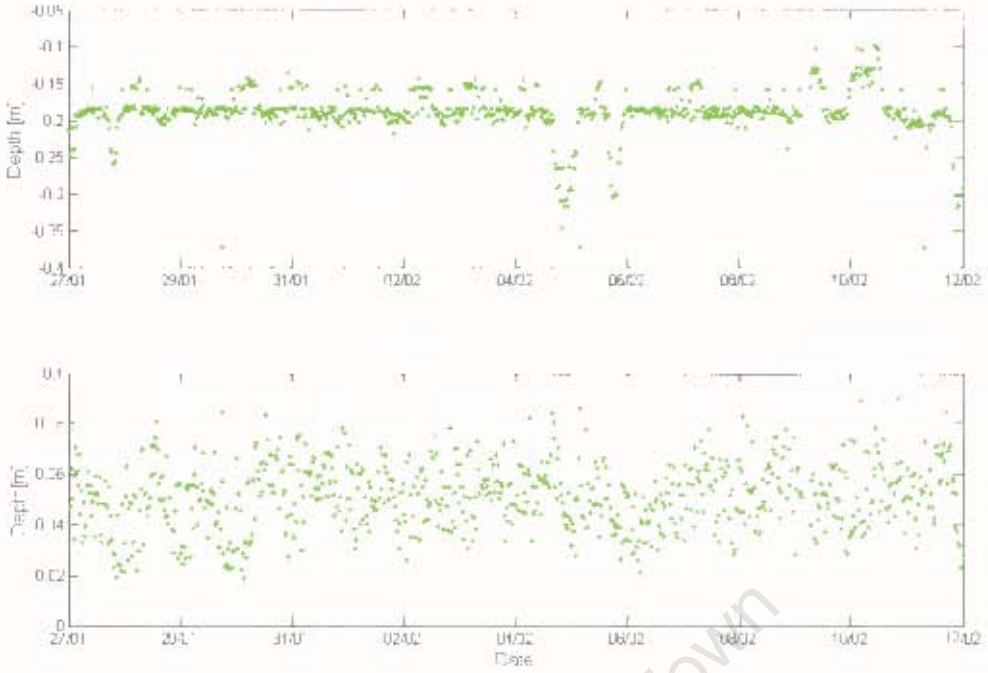

Figure 2-6 Half hourly median (top) and standard deviation (bottom) radiance sensor depths from the mooring for a week in January/ February 2005

minute burst are generally between 10 and 15 degrees while the standard deviation for the same period is between 5 and 10 degrees. Not all measurements are compromised by a high value of tilt and roll, and there are enough low values within a sampling burst to filter the data on these. Where the tilt and roll values remain high throughout a sampling burst (e g. late on the 27th February) it is attributed to a strong surface current; as the instrument cage at the bottom of the buoy structure has the largest area it causes the greatest drag and the buoy tends to lean into the current. This has been confirmed by visual observation while at the mooring site.

The depth of the radiance sensor varies between around 0.1 and 0.3 m during a sampling burst as waves pass along the mooring. Median values for a two minute burst are 0.15 to 0.2m with a standard deviation of 0.08 to 0.02m. Higher and lower median depth values are associated with periods of high tilt and roll where the buoy is leaning into the current; depending on the direction of the current the radiometer arm is either leaning further into or out of the water and therefore the median depths for these sampling bursts are more extreme than usual.

The two 11W solar panels provide adequate power to the system with the battery voltage dipping to 12 volts in the early morning and being recharged to around 13 volts during the day; overall the battery power remains fairly constant illustrating a well balanced system. The dip in power towards midday may be due to the radiometers starting to collect data at 8am pulling a relatively large amount of current, or the automated dial in and download of records at 9:30 am causing a large current draw by the modem.

3 Variability and time scales of physical processes: February 2005

In the southern Benguela the wind has a direct effect on shelf currents, local upwelling and mixing, and therefore plays a critical role in the dynamics of phytoplankton blooms (Pitcher *et al.* 1995). The likelihood of occurrence, and the extent of potentially harmful algal blooms on the west coast of South Africa, is greatest during the latter part of the upwelling season (Pitcher & Calder 2000). For these reasons a set of physical data from late January and February 2005, collected by the mooring deployed off Lambert's Bay, are used as a case study to characterise the physical processes of the nearshore environment from the Eulerian perspective of the mooring.

3.1 Data Analysis

Data from the mooring were collected as outlined in chapter 2, and were analysed and presented using Matlab R14 (The MathsWorks). Concurrent wind data were obtained from the South African Weather Service for the Lambert's Bay Nortier station, which uses R.M. Young (USA) wind sensors. The weather station is located inland, 8.4 km north-east of the buoy position (Figure 1-1). All wind data were plotted as the direction towards which the wind is blowing to ease visualisation of the wind data with the current data. Winds are referred to in the meteorological convention as the direction from which the wind is blowing. Currents have been rotated by 21.5° to the east to be aligned to true north. The coastline runs approximately north/ south at the mooring location; rotated currents are considered to be aligned roughly alongshore and across-shelf. Positive currents are directed to the north and east in all figures. Sidelobe contamination is considered to affect the bottom 6% (3 m in 50 m of water) plus one depth cell (2 m) of the ADCP data and therefore data from the ADCP were only considered valid to 45 m depth. Due to the location of the ADCP in the cage at the bottom of the bio-optical buoy 2.5 m below the waterline, and the blank after transmit depth of 1.76 m, the centre of the first depth cell is located at 5 m. Sea surface temperature images are daily composites of Advanced Very High Resolution Radiometer (AVHRR) data from sensors carried on board the NOAA-17 and NOAA-18 polar orbiting satellites. NOAA-17 has a morning overpass time on the west coast of South Africa and NOAA-18 has an afternoon overpass time. The spatial resolution of the AVHRR is 1.1km at nadir and the accuracy

of computed sea surface temperatures is in the order of 0.5 °C (Brown *et al.* 1985, Minnett 1991).

Filtered data were generated using a pl64 filter that has a half amplitude period of 33 hours and a half power period of 38 hours. The filter removes energy at periods shorter than 38 hours, thus removing tidal, diurnal and inertial signals, while preserving energy at lower frequencies including the mean (Limeburner 1985 as cited in Largier *et al* 1993). The filter script was supplied by Robert Beardsley to the Woods Hole Sea-Mat Matlab Tools for Oceanographic analysis website (http://woodshole.er.usgs.gov/operations/sea-mat/) and downloaded from there. High frequency data were obtained by subtracting the filtered low frequency data from the original data set. Statistical analyses for correlation coefficients were carried out with a bootstrap analysis using 1000 resampled data sets as most of the data are not normally distributed, with a Fischer transform performed on the replicated data to ensure a normal distribution; original data were tested for normal distribution using a Lilliefors test. The 2.5th and 97.5th percentile of the replicated data were used to determine significance at the 95% confidence level. Wavelet analysis was performed on the data to examine variations in power within the time series data (Torrence & Compo 1998). Time series are expanded in time-frequency space, allowing the determination of the dominant periodicities of variability and their variation in time (Torrence & Compo 1998, Grinsted *et al.* 2004). Matlab scripts for running wavelet analyses on time series were provided by Jean-Luc Mélice (University of Cape Town). The wavelets are obtained from a single function Ψ by translations and dilations (Equation 3-1), where $a > 0$ is the dilation parameter and b is the time translation

$$\Psi_{a,b}(t) = \frac{1}{a}\Psi\left(\frac{t-b}{a}\right)$$

Equation 3-1

parameter. In this investigation the Morlet wavelet was used, which is a complex cosine wave modulated by a Gaussian function (Equation 3-2) with i = [-1$^{1/2}$] and where

$$\Psi(t) = \pi^{1/4} e^{-t^2/2} e^{i\omega_0 t}$$

Equation 3-2

$\omega_0 = \pi[2/\ln 2]^{1/2}$ is chosen to be large enough to ensure that $\Psi(t)$ satisfies the admissibility condition which practically is equivalent to

$$\int_{-\infty}^{\infty} \Psi(t)dt = 0$$

Equation 3-3

By inverting the scale of the Morlet wavelet, the continuous wavelet transform becomes a time frequency analysis where the dilation parameter *a* corresponds to the period and the translation parameter *b* corresponds to the time. In Equation 3-1 the normalisation 1/a is used instead of the usual 1/(*a*)1/2. With this the components of the continuous wavelet transform may be directly compared to each other and the Morlet wavelet can be interpreted as a bandpass linear filter of weight 1/*a* centered around $\omega = \omega_0/a$. This allows the extraction of the different local components of the signal such as it's local value, amplitude and phase for each point of the (*b*,*a*) time-frequency space (Mélice *et al.* 2001). Scripts from the FATHOM Matlab toolbox for Multivariate Ecological & Oceanographic Data Analysis were used for vector manipulation and plotting; this toolbox is provided free online by David Jones (University of Miami).

3.2 Results

Data are presented for the period from the 27th January to 22nd February 2005.

3.2.1 Wind

Winds for the period (Figure 3-1) were principally south-westerly with periods of reversal to north-westerly lasting up to five days in duration. Southerly winds were generally larger in magnitude with a mean strength of 4.1 m s^{-1} and reaching a maximum of 9.3 m s^{-1}, while northerly winds had a mean strength of 2.9 m s^{-1} and a maximum of 5.3 m s^{-1}. Winds were southerly 54% of the time and westerly 75% of the time. Across-shelf winds were predominantly diurnal with a stronger eastward (onshore) component.

A diurnal signal that is consistent throughout the data set, but stronger during the second half of the data, is found in wavelet analysis of the alongshore wind (Figure 3-2). The

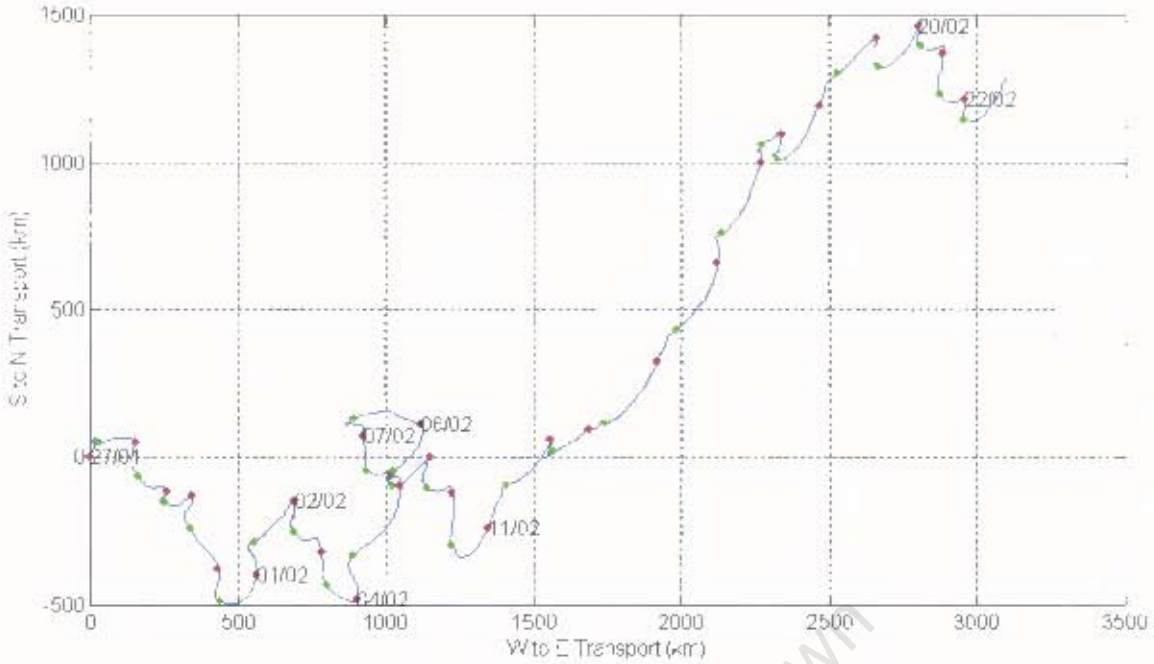

Figure 3-1 Progressive vector diagram of wind data from the Lambert's Bay Nortier weather station between the 27th January and 22nd February 2005. Red dots and dates are positioned at midnight, green dots are positioned at midday. Data starts at the origin (0,0).

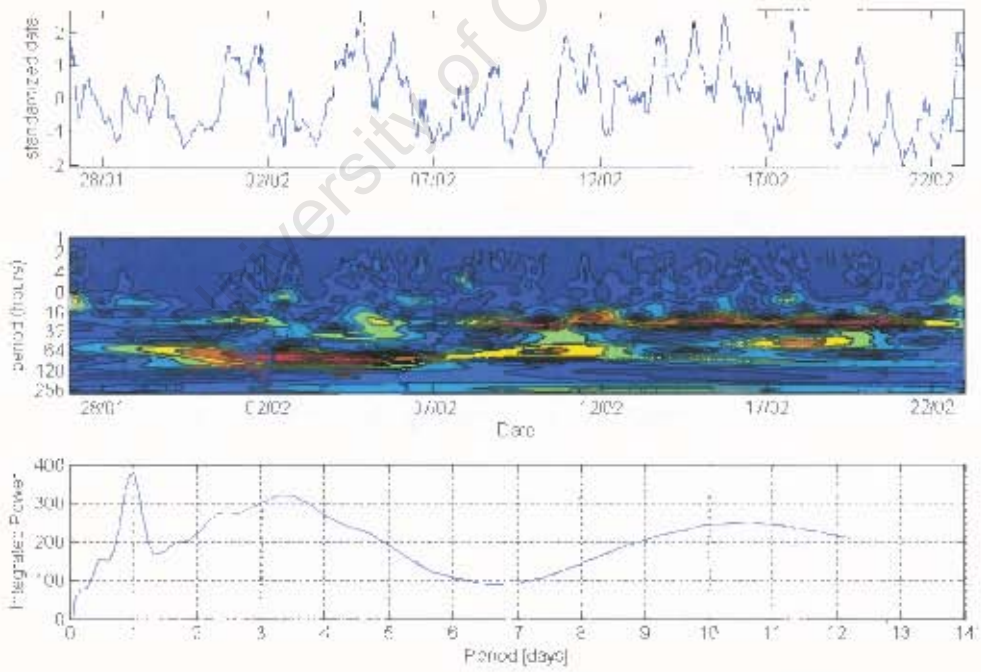

Figure 3-2 Wavelet analysis of alongshore wind data from Nortier weather station. Top: time series of the alongshore with the linear trend removed. Middle: amplitude of the signal over the time period of the data set. Bottom: integrated power of the signal over the data set period.

early part of the data set contains a 3.5 day signal, which appears to vary between 2.5 and 3.5 days throughout the data. A longer period signal at 10.5 days is present in the middle of the data. Across-shelf wind data exhibit a strong and consistent diurnal signal.

3.2.2 Currents

The first half of the data set was dominated by south-westward flowing near-surface currents (Figure 3-3) during periods of predominantly northerly winds, with two brief reversals to northward flow in conjunction with wind reversals. Consistent southerly winds between the 11th and 20th February corresponded with a reversal to north-eastward near-surface currents. Anti-clockwise oscillations were evident in the flow between the 27th and 29th January and the 16th and 22nd February. South-westward flow was also evident in the near-bottom currents (Figure 3-3), with periods of reversal to north-eastward flow between the 1st and 6th February and the 11th and 16th February, consistent with southerly, upwelling-favourable winds and the onshore movement of deep water.

Maximum current velocities were found in the surface waters and were particularly strong in a northward direction reaching speeds of up to 71 cm s^{-1} (Table 3-1). Mean currents at all depths were towards the south and west at low speeds of around 2 cm s^{-1}. Near-surface currents (5 m ADCP bin) were southward flowing for 69% of the data set and westward flowing for 64% of the data set, while currents at 45m flowed southward 69% of the time and westwards 57% of the time.

Wavelet analysis of near-surface alongshore current data (Figure 3-4) indicates high power at frequencies of 22.5 hours, 3.5 days and 9.25 days. The signal at 22.5 hours is present throughout most of the data set, although strongest during the second half of the data set. The 3.5 day signal is also largely consistent throughout the data, though strongest in the middle period of the data set, and likewise for the 9.25 day signal. Wavelet analysis for the across-shelf near-surface currents (Figure 3-5) exhibits similar behaviour with signals found at 21 hours, 3.5 and 9.5 days during the same periods in the data. An intermittent higher frequency signal is visible in the across-shelf data, particularly during the earlier part of the data, which may account for variability observed in the high frequency data during the first half of the data set.

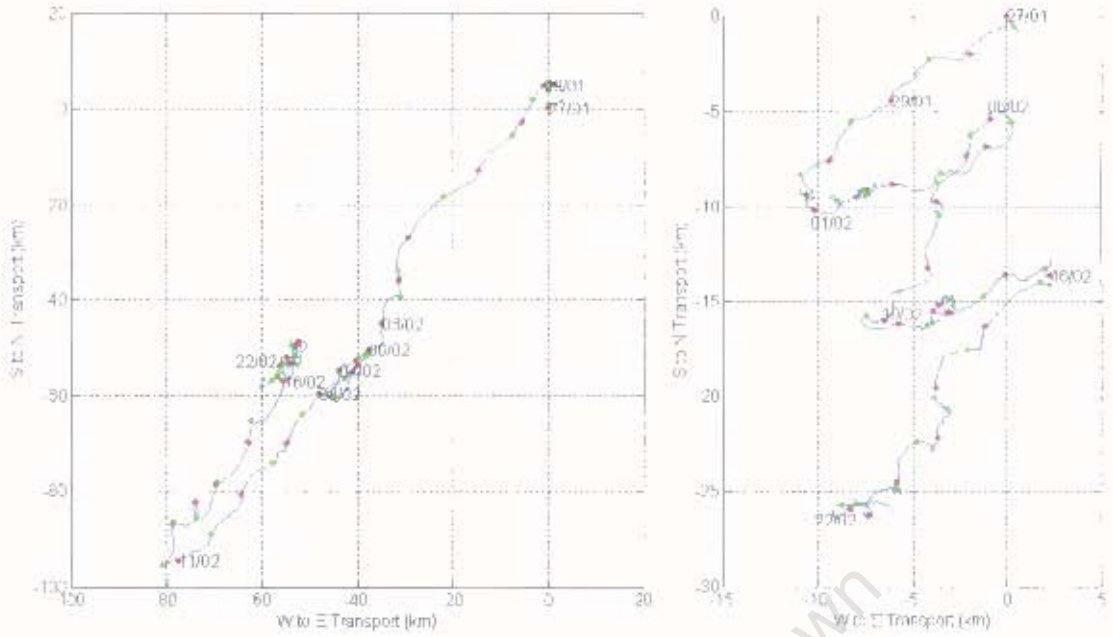

Figure 3-3 Progressive vector diagram of ADCP current data for the 5 m bin (left) and the 45 m bin (right) from the mooring (BOB) between the 27th January and 22nd February 2005.

	5m ADCP bin alongshore current	5m ADCP bin across-shelf current	45m ADCP bin alongshore current	45m ADCP bin across-shelf current
Mean	-2.2 cm s^{-1}	-2.6 cm s^{-1}	-1.7 cm s^{-1}	-0.6 cm s^{-1}
Standard deviation	13 cm s^{-1}	9.9 cm s^{-1}	3.5 cm s^{-1}	4.3 cm s^{-1}
Maximum +ve	71.3 cm s^{-1}	32.6 cm s^{-1}	11.6 cm s^{-1}	13.3 cm s^{-1}
Maximum -ve	-31.8 cm s^{-1}	-31.9 cm s^{-1}	-11.9 cm s^{-1}	-13.4 cm s^{-1}

Table 3-1 Characteristics of alongshore and across-shelf current data gathered from the ADCP deployed on the mooring (BOB) between the 27th January and 22nd February 2005. Positive values are directed to the north and east.

3.2.2.1 Low Frequency Currents

At low frequencies (greater than 1.6 days), the alongshore components of the wind and near-surface current data exhibit reversals in direction of between two and five days duration (Figure 3-6). Reversals in current direction were well correlated with reversals in wind direction, with current reversals appearing to lag wind reversals. The extent of the current reversal appeared to be dictated by the magnitude of the shift in wind direction. Larger changes in wind direction such as that on the 4th February were followed by

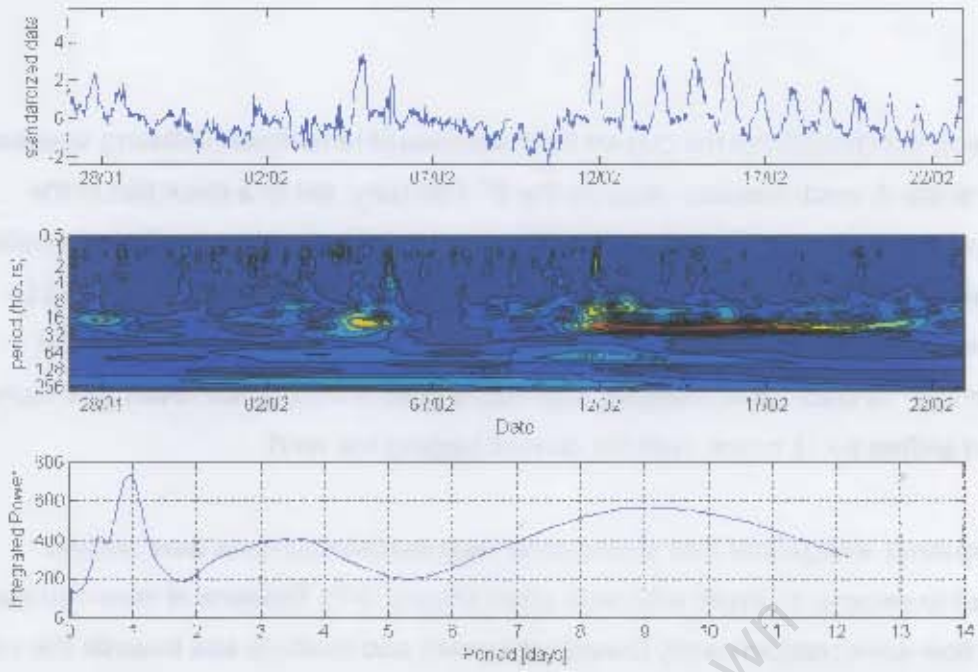

Figure 3-4 Wavelet analysis of alongshore current data from the ADCP bin at 5m. Top: time series of the alongshore current with the linear trend removed. Middle: amplitude of the signal over the time period of the data set. Bottom: integrated power of the signal over the data set period.

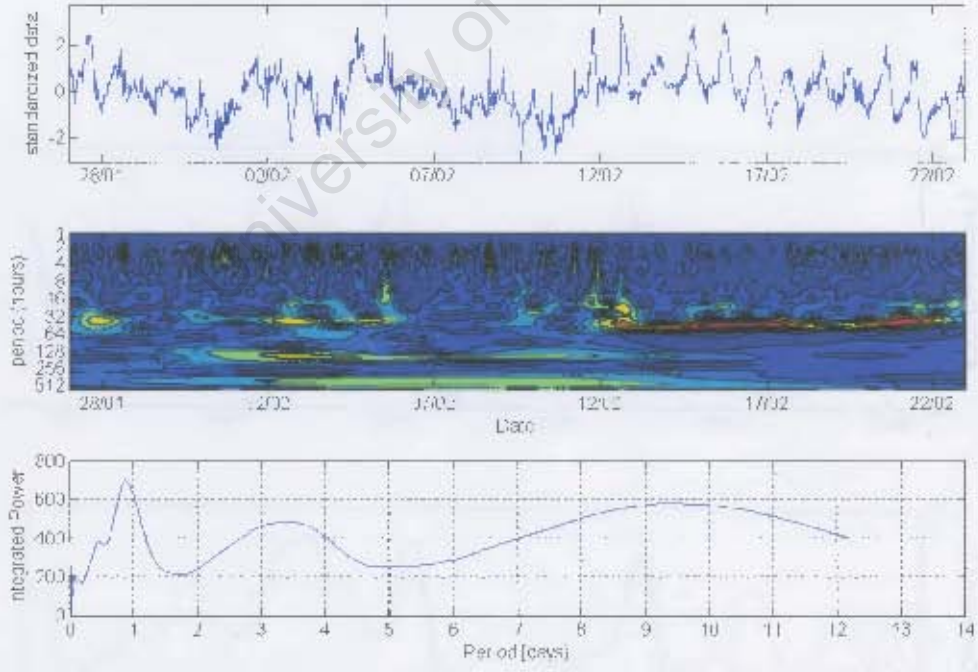

Figure 3-5 Wavelet analysis of across-shelf current data from the ADCP bin at 5m. Top: time series of the across-shelf current with the linear trend removed. Middle: amplitude of the signal over the time period of the data set. Bottom: integrated power of the signal over the data set period.

changes in the direction of the current from southward to northward flowing whereas smaller shifts in wind direction, such as the 8th February, led to a reduction in the magnitude of the flow in the original direction but not a reversal in direction. Correlations were calculated for the filtered wind and 5 m current data with wind data shifted by between 0 and 24 hours to examine the effect of different lag periods. Maximum correlation (r^2 of 0.55 – 648 samples, significant at 95% confidence level) was found with the wind shifted by 12 hours, with the current lagging the wind.

Low frequency alongshore and across-shelf near-surface currents were usually observed to reverse in phase with each other (Figure 3-7). Patterns of near-surface current flow were predominantly towards the north and onshore and towards the south and offshore, with alongshore currents reaching the highest magnitudes. The predominantly barotropic nature of low frequency currents is illustrated in Figure 3-8. (In this context barotropic currents are defined as those in which there is no vertical shear.)

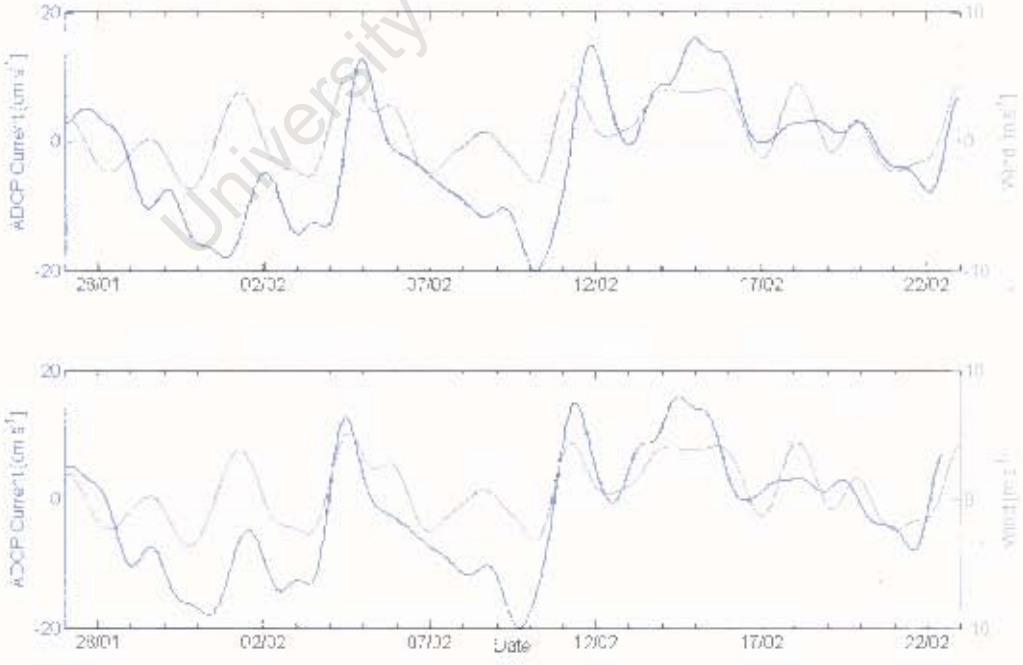

Figure 3-6 Low pass filtered alongshore ADCP current from 5 m bin and alongshore wind from Lambert's Bay Nortier weather station between 27th January and 22nd February 2005. In the bottom diagram the alongshore wind has been shifted by 12 hours illustrating the correlation between alongshore current and wind reversals at this phase lag.

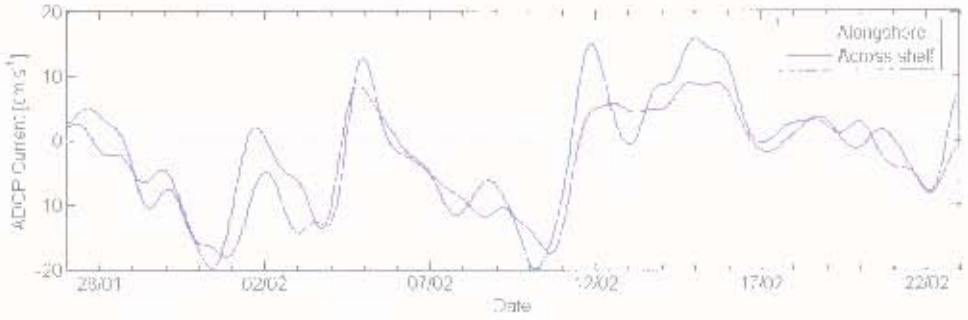

Figure 3-7 Low pass filtered alongshore and across-shelf ADCP current from 5 m bin between 27th January and 22nd February 2005

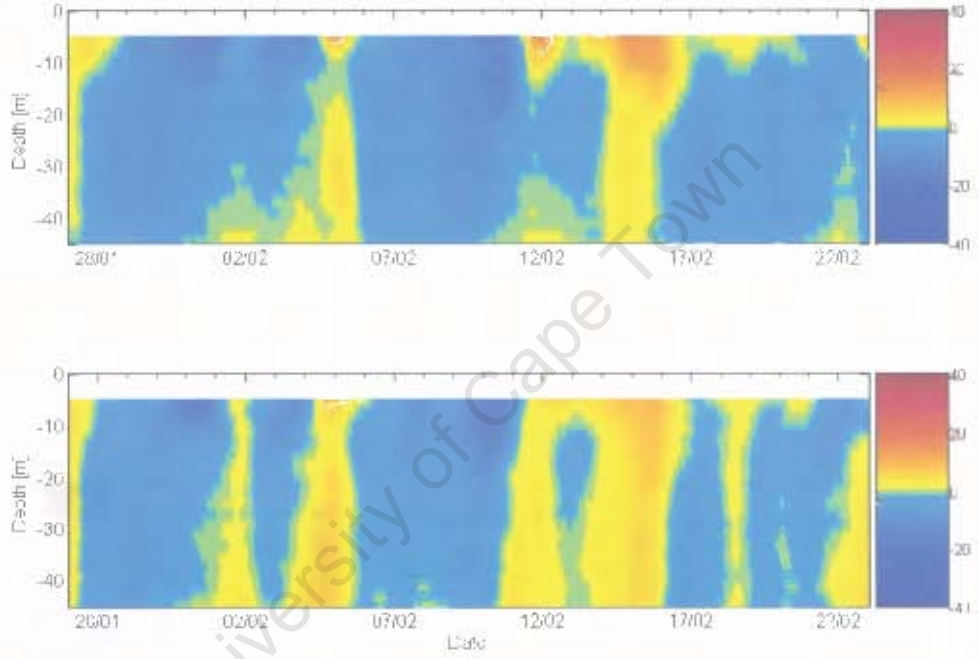

Figure 3-8 Low pass filtered current velocities [cm s^{-1}] for ADCP bins between 5 m and 45 m for alongshore component (top) and across-shelf component (bottom) between the 27th January and 22nd February 2005.

3.2.2.2 High Frequency Currents

High frequency currents (those at periods of less than 1.6 days) were predominantly baroclinic (exhibiting vertical shear) in both the alongshore and across-shelf directions (Figure 3-9). This was particularly evident during the second half of the data set (10th February onwards), where currents in the top 15 m of the water column flowed in the opposite direction to currents deeper in the water column. This resulted in strong vertical shear in the water column at depths of around 10 to 20 m. Consistent with the signals in

the wavelet analysis, near-surface currents in the first half of the data were generally small (less than 10 cm s^{-1}) and fluctuated in direction on an intermittent time scale, while the second half of the data was characterised by stronger currents of up to 30 cm s^{-1}, which changed direction on a regular time scale of around once day.

A progressive vector plot of the near-surface high frequency currents in the second half of the data set (Figure 3-10) shows currents performing anti-clockwise oscillations of around 3 km in diameter. The oscillations were elliptical in nature due to the relatively stronger alongshore component of the current. Displacement due to these oscillations was generally offshore and then southward between midnight and midday, onshore in the early afternoon and northwards in the late afternoon and evening.

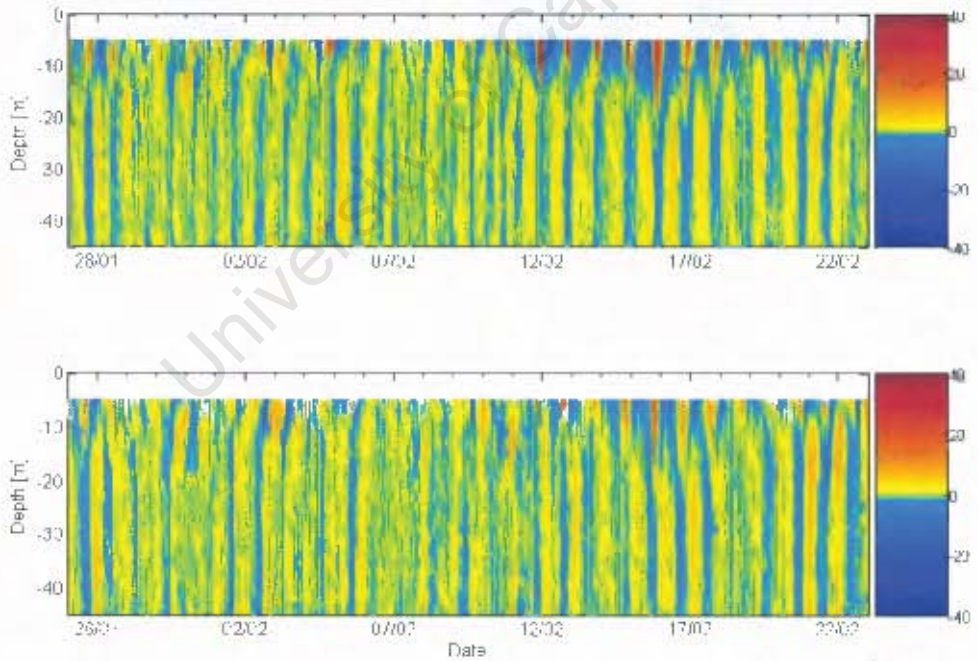

Figure 3-9 High frequency current velocities [cm s^{-1}] for ADCP bins between 5 m and 45 m for alongshore component (top diagram) and across-shelf component (bottom diagram) between the 27th January and 22nd February 2005.

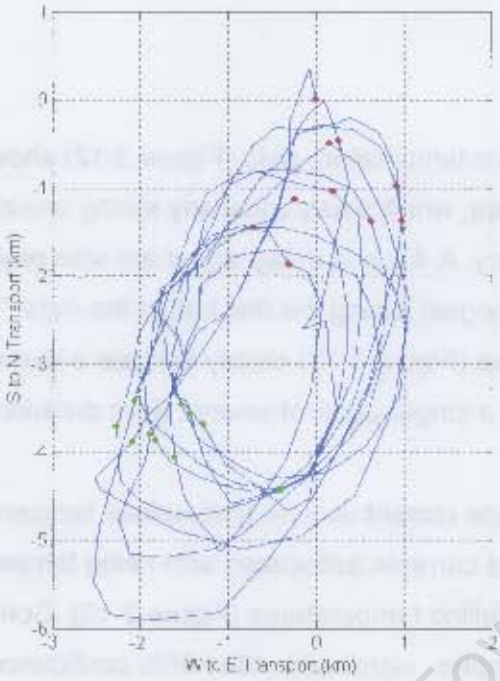

Figure 3-10 Progressive vector diagram of high frequency ADCP current from 5 m bin between 12th and 22nd February 2005. Red dots are positioned at midnight, green dots at midday.

3.2.3 Temperature and water column structure

Time series temperature profile and current data for the period are displayed in Figure 3-11. The water column structure was characterised by periods of warming of surface waters, which extended to 10 to 15 m depth, interspersed with episodes of cooling of the water column due to upwelling and mixing. Periods of persistent warm surface waters are observed to be coincident with southward currents. Onshore flow in the 45 m currents (Figure 3-3) between the 4th and 6th, and 11th and 16th February was associated with cooling of the entire water column, consistent with upwelling. Surface currents were directed northwards and onshore during these periods. Diurnal warming and cooling was exhibited by surface waters. Surface temperatures for the period range from 10.8 °C to 19.9 °C (Table 3-2), while temperatures at 30 m exhibited a much smaller range, from 9.6 °C to 10.8 °C. The mean difference between surface and 30 m temperatures was 5.3 °C, with a maximum difference of 9.5 °C on the 7th February and a minimum difference of 1.1 °C on the 16th February. It is evident from this that there are periods when the water column was relatively well mixed, and periods of strong stratification.

Wavelet analysis of surface temperature data (Figure 3-12) shows a diurnal signal present throughout the data, which was particularly strong around the 27th January, 5th February and 12th February. A 4.5 and 9 day signal are also present through the data set, though they were strongest during the first half of the data. The standardised data for the surface temperature (Figure 3-12) clearly indicate a diurnal cycle of warming and cooling superimposed on a longer cycle of several days duration.

Low frequency near-surface current vectors and surface temperature data were well correlated, with southward currents associated with rising temperatures and northward currents associated with falling temperatures (Figure 3-13). Correlation between the data has an r^2 of 0.57 (648 samples, significant at the 95% confidence level). Persistent southward flow between the 28th January and 4th February led to a rise in surface temperature of 6 °C. A shift to northward flow on the 9th February was associated with a 3 °C drop in temperature, while prolonged northward flow from the 10th to 17th February resulted in a 7 °C drop in the temperature of the surface water.

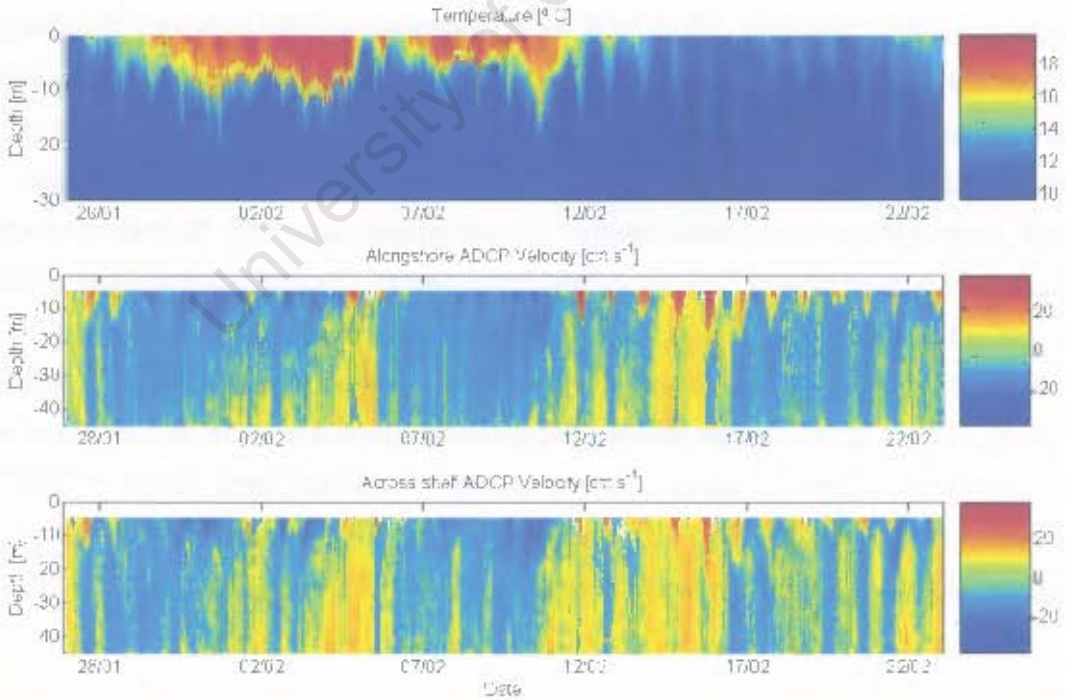

Figure 3-11 Time series of temperature profile data between 0 and 30 m depth and current profile data for alongshore and across-shelf ADCP bins between 5 and 45 m depth from the mooring (BOB) between the 27th January and 22nd February 2005

	0 m temperature	30 m temperature	Daily range in surface temperature	Difference between 0 m and 30 m temperature
Mean	15.5 °C	10.1 °C	2.5 °C	5.3 °C
Standard deviation	2.7 °C	0.3 °C	1.1 °C	2.4 °C
Maximum	19.9 °C	10.8 °C	5.2 °C (5th Feb)	9.5 °C (7th Feb)
Minimum	10.8 °C	9.6 °C	0.9 °C (3rd Feb)	1.1 °C (16th Feb)

Table 3-2 Characteristics of temperature data gathered from the thermistor chain deployed on the mooring (BOB) between the 27th January and 22nd February 2005. All temperatures are in degrees Celsius.

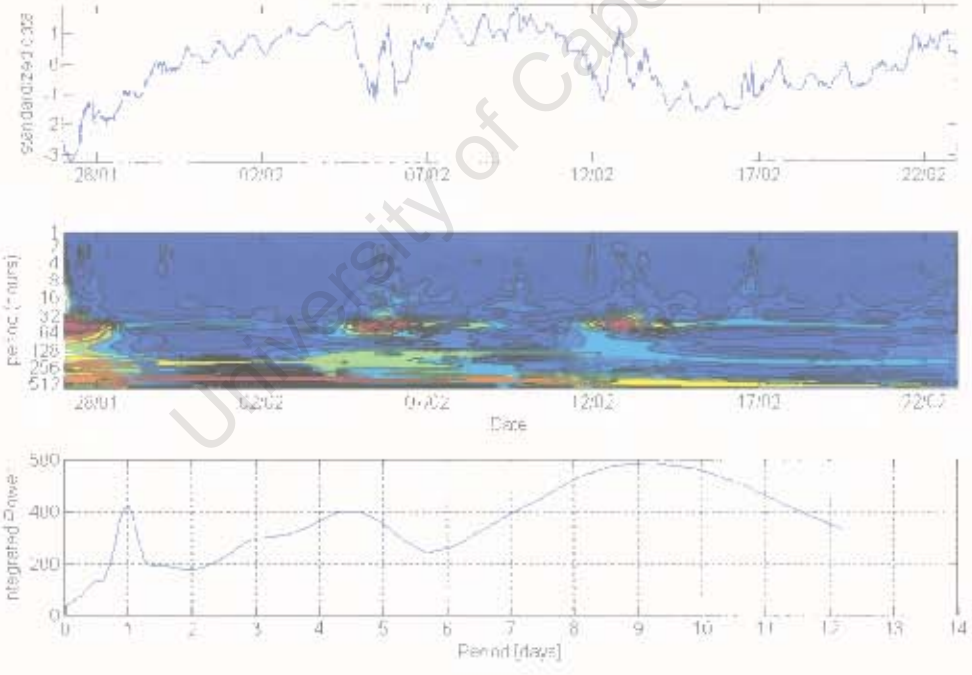

Figure 3-12 Wavelet analysis of surface temperature data from mooring. Top: time series of surface temperature with the linear trend removed. Middle: amplitude of the signal over the time period of the data set. Bottom: integrated power of the signal over the data set period.

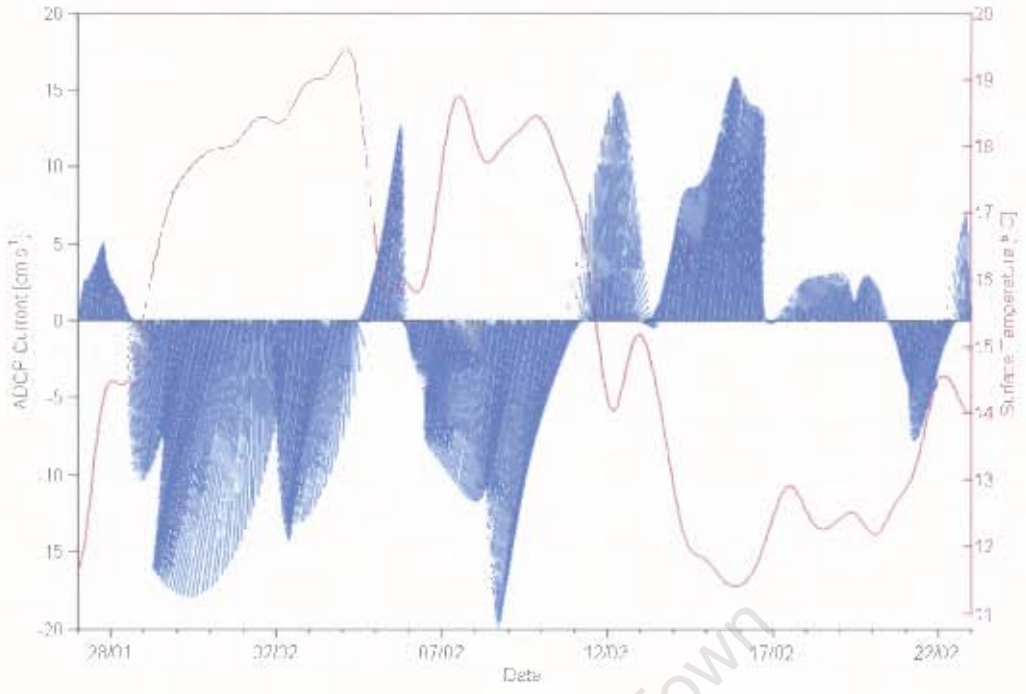

Figure 3-13 Low pass filtered ADCP current vectors from 5 m bin and surface temperature from thermistor chain on mooring between 27th January and 22nd February 2005

The 3rd and 5th February are used as examples to illustrate temperature changes in the surface mixed layer as a result of advection and solar heating. On the 3rd February (Figure 3-14) surface temperatures warmed throughout the day to early evening and then cooled significantly towards the next morning. There was an overall heat gain between 09:30 and 19:00 on the 3rd, as is expected from an overall positive heat flux over the diurnal period (Guastella 1992). The mean total heat flux between 09:00 and 19:00 was 540 Wm^{-2}, calculated from measurements from St Helena Bay for October 1986 (*ibid*). These heat flux data may not be entirely accurate for the 3rd and 5th February 2005 but are considered sufficient to derive an estimate of heating due to insolation. From the temperature profile data for the 3rd February, an integrated temperature rise of 0.39 °C was calculated over the surface 10 m between 09:00 and 19:30.

For a column of sea water, temperature changes in the mixed layer can be calculated by

$$\frac{dT}{dt} = \frac{Q}{\rho_w C_p dz}$$

Equation 3-4

where dT is the change in temperature, dt is the time in seconds, Q is the heat flux, ρ_w is the density of seawater (1025 kg m^{-1}), C_p is the heat capacity of seawater at constant pressure (4180 J Kg^{-1} $^{o-1}$) and dz is the depth of the mixed layer in metres. Assuming a mean heat flux of 540 W m^{-2}, an integrated temperature rise of 0.48 °C would be expected in the surface 10 m over 10.5 hours. Therefore the calculated heat gain between 09:00 and 19:30 on the 3rd February is within that expected by solar heating; the lower actual gain in temperature may be due to reduced insolation on that day as opposed to the day from which the heat flux data are taken. On the 5th February, there was a large heat gain in the surface 8 m between 09:30 to 19:30 and by 01:30 on the 6th February the temperature profile had returned to a very similar profile to that of 09:30 (Figure 3-14). An integrated temperature rise of 3 °C over the surface 8 m was calculated from the temperature profile data. From Equation 3-4, this would require a heat flux of 2382 W m^{-2}, which is five times greater than the available heat flux from insolation.

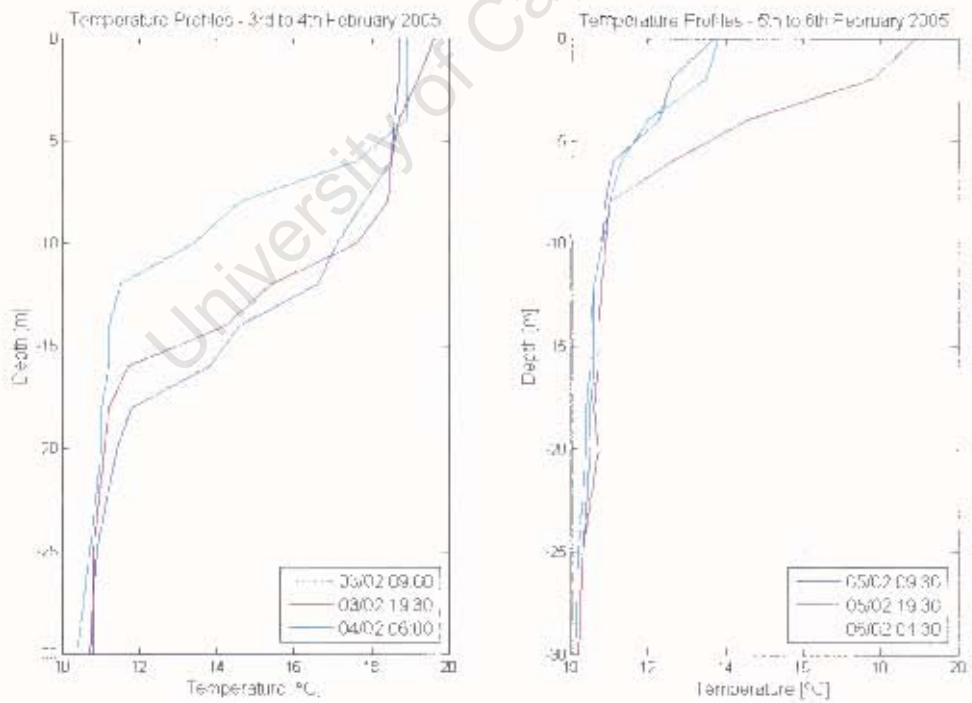

Figure 3-14 Temperature profiles from thermistor chain deployed on mooring for the 3rd and 4th February 2005 (left) and the 5th and 6th February 2005 (right).

3.3 Discussion

The data presented allow the determination of the variability and forcing mechanisms in currents and water column structure. Physical processes affecting phytoplankton bloom dynamics operate over a variety of temporal and spatial scales (GEOHAB 2001). Mesoscale circulation affects the transport and accumulation of phytoplankton populations and nutrients through upwelling cycles, and the development of fronts and convergence zones (*ibid*). Variations in levels of insolation, vertical current shear and wind induced mixing, as well as circulation patterns, affect the dynamics of the surface mixed layer and thus life-form selection and the vertical distribution of phytoplankton (*ibid*). Interaction of these processes at several scales determines bloom timing, location, species and growth.

Processes that impact upon the magnitude and direction of current flow occur at two scales in the data: a two to five day time scale in which reversals in flow are seen, and a shorter time scale of less than a day in which anti clockwise rotations dominate. Where these processes co-occur it has the effect of creating alongshore propagating, anti-clockwise motions.

3.3.1 Low frequency currents

Reversals in the current flow, in both the alongshore and across-shelf direction, were highly correlated with reversals in the local wind field at scales of two to five days, with the magnitude of the wind reversal dictating the magnitude of the current response. Alongshore currents in the data reversed on a cycle of around three and a half days. Wind variations at this scale, at this time of year, are forced by the easterly passage of coastal low pressure cells (Holden 1987). The leading edge of the coastal low leads to equatorward winds, while poleward winds are associated with the passage of the trailing edge (Jury& Brundrit 1992). The dominant wind direction during summer is equatorward under the influence of the south Atlantic high (Holden 1987). Previous observations in the region have attributed reversals in current direction on the shelf, at scales of around 4 days to 3 weeks in summer, to the passage of remotely generated coastal trapped waves, which propagate around the continent in an anti-clockwise direction (Holden 1987, Jury *et al.* 1990a, Jury & Brundit 1992, Schuman & Brink 1990). Alongshore currents oscillate on the same cycles as the synoptic weather, with geostrophically

driven, barotropic reversals in alongshore currents controlled by coastal-low forced shelf waves (Jury *et al.* 1990b). Alongshore current reversals at periods of three and a half days are typical for the Benguela (Nelson 1992), but slightly shorter than the periods attributed to the passage of coastal trapped waves.

The maximum correlation, with the current lagging the wind by 12 hours, between local alongshore wind and near-surface currents is similar to the 8 to 12 hour time lag observed in the upper 20 m of the water column in data from the northern Californian shelf collected during the Coastal Ocean Dynamics Experiment (CODE) (Winant *et al.* 1987). Poleward and barotropic flows of 12 cm s^{-1} in the absence of wind were found from the intercept of the regression line at the optimum lag period on the northern Californian shelf (*ibid*). This value was –3.8 cm s^{-1} locally for the ADCP bin at 5 m, implying poleward alongshore flow in the absence of wind. Modelling of wind forced flow off northern California in the CODE region demonstrated that coastal capes affect the variability of alongshore upwelling currents, and can lead to the development of an alongshore pressure gradient that forces a poleward current during relaxation of equatorward, upwelling-favourable winds (Gan & Allen 2002a, Gan & Allen 2002b). Measured data from the CODE region show that a decrease in equatorward wind leads to a reversal to poleward alongshore currents without the need for a complete reversal in wind direction (Gan & Allen 2002a). Model results find the poleward current to be forced by negative pressure gradients, which develop on the equatorward side of capes, in response to acceleration of alongshore currents as they flow around a point (*ibid*).

It seems likely from the similarity in response of alongshore currents to the local wind field between those observed locally and those observed during CODE, and the location of the mooring in St Helena Bay downstream of a Cape, that negative pressure gradients may be responsible for the poleward flow observed in the mooring data during relaxation of equatorward winds. If the reversals were forced by remotely generated coastal trapped waves, it is unlikely that they would appear as closely correlated to local winds, due to the wave having propagated several hundred kilometres along the coast from its generation site and the associated wind field. The correlation between local wind and current reversals may be explained in terms of remote forcing by coastal trapped waves if the period associated with the modulation in pressure at the generation site is a multiple of the time taken by the coastal trapped wave to travel to the monitoring site

(Nelson 1992). Estimates for the speed of travel for coastal trapped waves in the region ranges between 50 and 200 km per day (*ibid*).

3.3.2 High Frequency Currents

High frequency alongshore and across-shelf currents during the study period were largely baroclinic in nature, exhibiting periods of oscillation, which wavelet analyses showed to occur with a period of 22.5 hours.

The tidal regime in the area is semidiurnal with a spring range of around 2 m (Shillington 1998) but tidal currents are generally small in comparison to wind driven flow (Simpson *et al.* 2002). Data from current meter moorings deployed in around 170 m of water off the Cape Columbine and St Helena Bay coast during winter 1982 displayed evidence of semi-diurnal tides (Holden 1986). Other studies in the region have found tidal currents to be negligible, attributed to small tidal elevations and the near simultaneous timing of high tide along the west coast (*ibid*). Tidal currents are not detected in the mooring data where signals would be expected in the across-shelf current data at 12.4 and 24.8 hours, consistent with a semi diurnal tidal system.

Rotations in the alongshore and across-shelf current data with a period of 22.5 hours are attributed to inertial oscillations and have often been observed in current meter and drifter data in the region (e.g. Bailey & Chapman 1991, Holden 1985, Holden 1987). The Coriolis force acts to the left in the southern hemisphere, leading to anti-clockwise rotations. The local inertial frequency at the mooring is 22.5 hours calculated as $T=2\pi/f$ where f is the Coriolis frequency which is 0.773×10^{-4} s^{-1} at the mooring latitude of 32.083 °S. Inertial oscillations are locally generated, in response to a fluctuating wind stress (Pollard & Millard 1970). A strong diurnal wind was evident during the second half of the data set when inertial oscillations were particularly strong in the current data, reaching velocities of around 30 cm s^{-1}. Winds rotated with a more northerly and onshore component from midday to midnight and a more southerly and offshore component from midnight throughout the morning, consistent with a land-sea breeze. Similar to these results, data from Namibia show strong anti-clockwise diurnal oscillations extending through the water column, with currents of similar magnitude in the alongshore and across-shelf directions, that are often larger in magnitude than the mean flow causing the current to reverse (Simpson *et al.* 2002). At latitudes close to 30° a near resonant

response occurs as the inertial frequency is close to that of diurnal tides and forcing winds (Craig 1989), which increases the energy transfer between atmosphere and ocean (Simpson *et al.* 2002). A potentially important aspect of inertial oscillations is the 180° shift in phase in the current profiles during the study period at depths of around 10 to 15 m. This is considered to be due to the presence of a coastal boundary, which causes a pressure gradient to develop in response to surface winds. Wind forcing is transferred through the water column by the pressure gradient, with a phase shift of 180° (Simpson *et al.* 2002).

Inertial oscillations in response to the diurnal wind are considered to be particularly important in regions with weak tidal currents (Hyder *et al.* 2002), although the elliptical motion associated with inertial rotations has no effect on net transport. Transport is driven by low frequency currents, with inertial oscillations often superimposed on a mean northward or southward flow. Blooms off Lambert's Bay have often been observed to move onshore in the afternoon, which may be associated with the onshore part of the inertial oscillation that occurs after midday. The 180° phase shift between upper and lower layers leads to large current shears across the thermocline, enhancing mixing within the thermocline layer (Knight et al. 2002). It appears from the data that the majority of the vertical shear in the water column was due to inertial oscillations; currents with the high frequency component removed appear predominantly barotropic. During the second half of the data set when inertial oscillations were dominant, the depth of the top of the thermocline was often associated with strong northward pulses of current in the surface layers attributed to inertial oscillations (Figure 3-15).

3.3.3 Water column structure

Two main processes affecting the temperature are: diurnal variation in near-surface temperatures, which may be attributed to solar heating, and longer 3 to 6 day temperature variations associated with current reversals and the upwelling cycle.

Upwelling in the Benguela due to Ekman transport is well documented, with a modulated upwelling cycle of 3 to 6 days typical of the Cape Columbine cell (Nelson & Hutchings 1983). During active upwelling, equatorward winds are associated with northward shelf currents and a drop in sea surface temperature. Relaxation phases are characterised by reduced equatorward or poleward winds, southward flowing shelf currents and

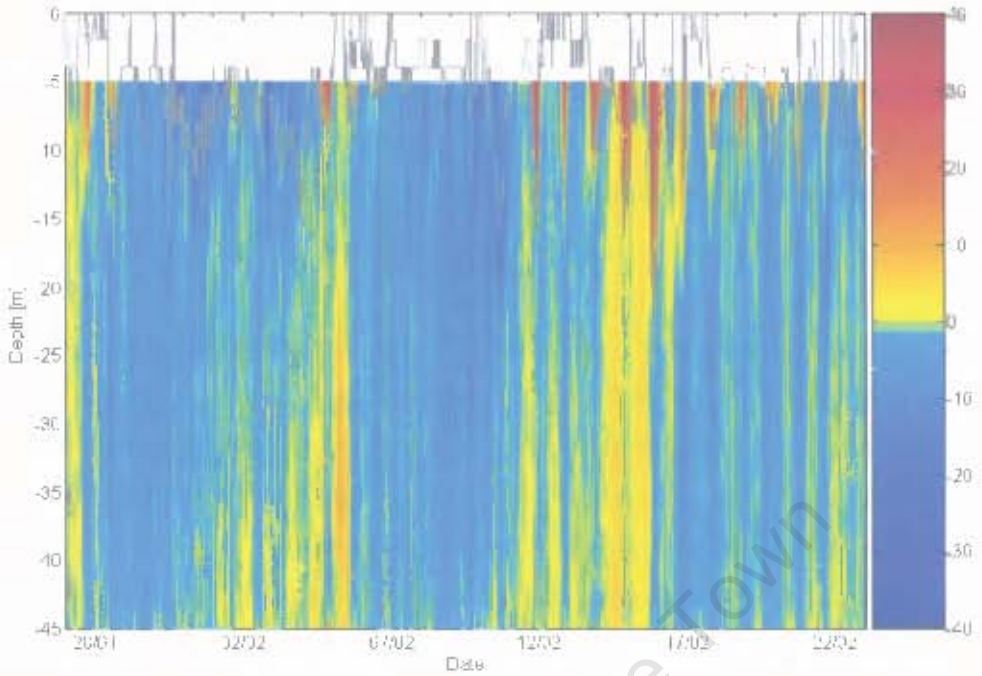

Figure 3-15 Time series of alongshore ADCP current [cm s^{-1}] from 5 m bin. The depth of the top of the thermocline is plotted in grey.

increasing sea surface temperatures (Jury & Brundrit 1992). These processes were clearly visible in the data set with low frequency current reversals responding to wind reversals: water temperatures decrease with northward currents while surface temperatures increase with southward currents.

Surface temperature data during the study period exhibited a clear diurnal signal, indicating that solar heating contributes to raising water temperatures. The association of increasing temperatures with southward flowing currents, and the often large increases in surface temperature over a day (up to 5 °C), imply that advection also contributes to heat gain at the mooring location. This is supported by the temperature profile data, where slabs of warm water extending down several meters appear that cannot be explained solely by surface heating and mixing. Heat budget calculations for the southern Benguela during midsummer estimate that there is a heat input of 255 W m^{-2} per day, predominantly due to incident radiation, which can produce a temperature rise of 0.52 °C day^{-1} integrated over a 10 m surface mixed layer. Temperature increases greater than this are attributed in part to advection (Guastella 1992). In one of the example heat budget calculations (see 3.2.3), 20% of the observed temperature increase can be attributed to insolation, while it is assumed that around 80% of the heat

gain was due to advection of warm water to the mooring location. During the CODE experiment on the northern Californian shelf 50 to 60% of the warming during relaxation of upwelling-favourable winds was attributed to solar heating, with most of the rest accounted for by alongshore advection when currents reverse and flow polewards during wind relaxation (Send *et al.* 1987). Wavelet analysis of the depth of the top of the thermocline exhibited a high powered integrated signal at the inertial period implying that inertial oscillations affect water column structure. This may be due to increased mixing caused by shear induced by inertial oscillations at depths of around 10 to 15 m, or the rotational transport of the water mass by inertial oscillations. Studies of mixed layer dynamics find that surface mixed layers deepen most rapidly in response to wind stress within half an inertial period (Brink 1983).

During periods of increasing temperature, the warm surface mixed layer deepened with time if southward flow persisted. Satellite images for the 4th to the 7th February 2005 (Figure 3-16) assist in explaining changes seen in the temperature profile data, although the limitations of the satellite data in that they measure skin temperature should be borne in mind. On the 4th February temperature profile data show warm surface waters of 18 °C extending to depths of around 10 m, and the satellite image shows the bay to be filled with warm surface water, with a tongue of 18/19 °C water extending from north to south along the coast. Upwelling at Cape Columbine, as seen in the image for the 5th February, led to cooling of the surface water in the bay and the temperature profile shows a dramatic cooling of the entire water column with the thermocline rising to near-surface and surface temperatures dropping to 14 °C. An intrusion of warm water, with surface temperatures of around 18 °C, extending down to 7 m appeared in the temperature profile later on the 5th February, which was replaced by cooler waters again on the 6th. This is assumed to be the tongue of warm water visible in the satellite image for the 6th February, advected into the area from the north, with its appearance and disappearance in the temperature profile being due to movement of the tongue of water in relation to the mooring. The intrusion of the warm water, advected into the mooring area by the southward current, is consistent with the heat budget calculations for the 5th of February, which suggest that around 80% of the change in the temperature profile may be attributed to advection. Surface waters warmed and the thermocline deepened throughout the 6th and 7th February when the satellite image shows decreased upwelling at Cape Columbine and warm surface waters extending throughout St Helena Bay. The

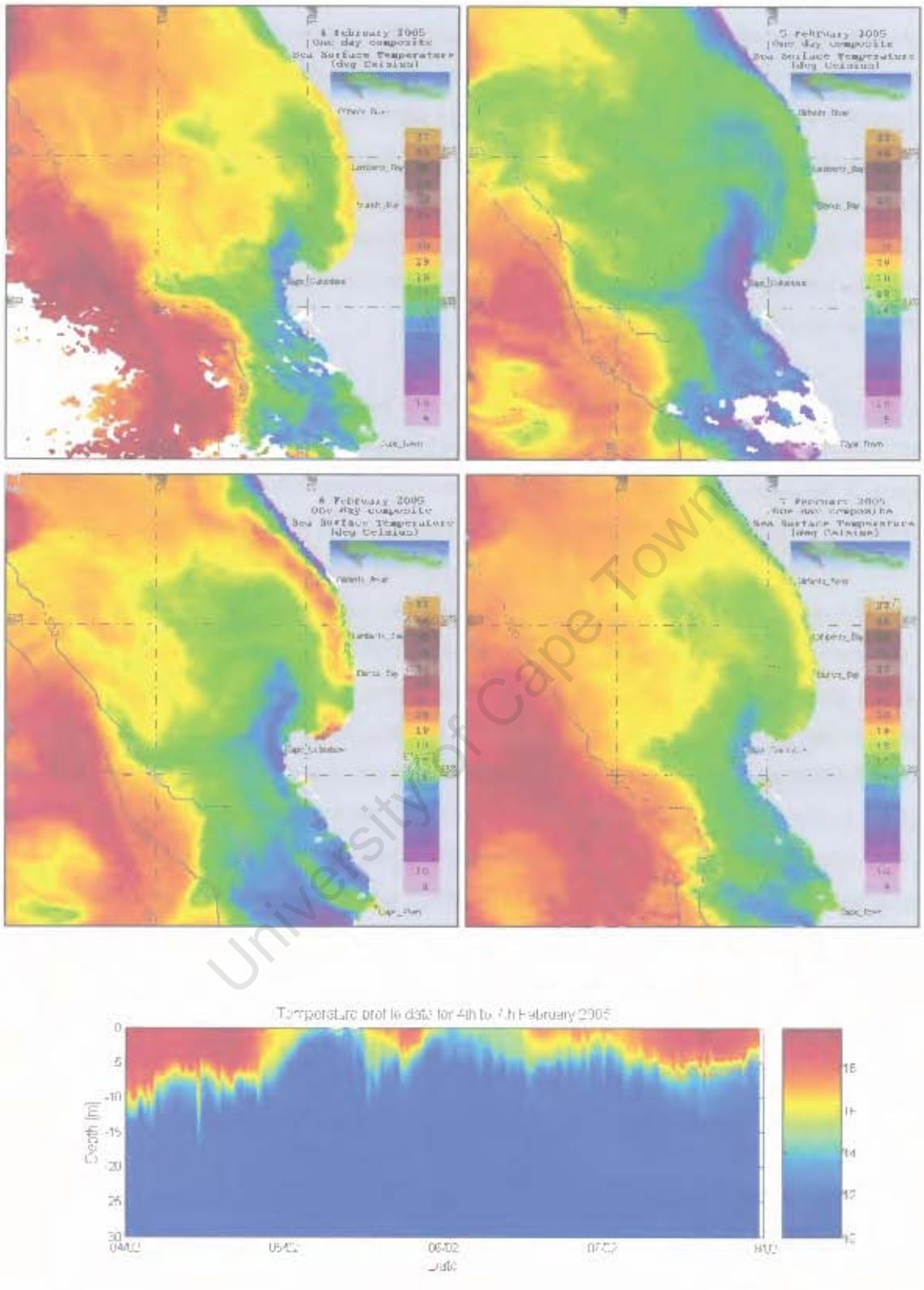

Figure 3-16 One day composite satellite sea surface temperature images from NOAA AVHRR satellite and temperature profile data (°C) from thermistor chain deployed on mooring for 4th to 7th February 2005

warm surface water observed initially on the 4th February was associated with southward flowing surface. A switch to northward flowing currents half way through the 4th February, and persisting through the 5th February, led to the introduction of the cooler, upwelled water on the 5th. Inertial oscillation driven currents later on the 5th February may explain the appearance and disappearance of the warm water in the temperature profile. Water column temperatures increased on the 6th and 7th February associated with southward flow.

3.3.4 Summary

Currents during the study period vary at two time scales, both of which are forced by local winds. Diurnal fluctuation in wind strength and direction due to a land-sea breeze effect drive inertial oscillations, inducing shear in the water column near the thermocline depth. Wind reversals at periods of two to five days, associated with synoptic weather patterns, force reversals in alongshore currents at these scales; a 12 hour lag is observed between wind and current reversals. The location of the mooring in the nearshore environment, downstream of Cape Columbine suggests that negative pressure gradients contribute to forcing southward flow during wind relaxation and reversal. Water column structure is affected by insolation driven changes in temperature and mixed layer depth, and advection. Persistent warm near-surface temperatures and stratification were associated with southward flow.

4 Comparison between winds, currents and water column structure in three data sets from different periods

Upwelling-favourable winds in the southern Benguela are associated with anticyclonic air flow around the South Atlantic High (Nelson & Hutchings 1983). Migration of the high pressure cell northwards in autumn, and south eastwards in spring, leads to seasonal modulation of upwelling-favourable winds (*ibid*). Upwelling-favourable winds are most persistent during spring and summer in the southern Benguela accounting for up to 70% of the total winds (as opposed to around 10% of the total winds during winter) (Andrews & Hutchings 1980), with the upwelling season extending from September to March (Shannon & Nelson 1996). During summer the passage of cyclones south of the continent causes a periodic weakening of the South Atlantic High and relaxation of upwelling-favourable winds. In winter the effect is to bring strong, potentially gale force, north-westerly winds (Nelson & Hutchings 1983). Phytoplankton biomass varies seasonally in the southern Benguela, with highest levels of biomass during the latter part of the upwelling season and lower levels during winter conditions (Pitcher & Weeks 2006).

Two other periods of data have been processed in a similar way to the data from February 2005 (see 3.1 for methods). February is considered to fall late in the upwelling season. The main features and physical processes observed in these data are summarised here, and are indicative of seasonal changes. One data set comprises 24 days of mooring data from the 5th to 29th May 2005, representative of winter conditions, and the other data set consists of 32 days of mooring data from 10th November to 12th December 2005, considered to be early in the upwelling season. Concurrent wind data from the Nortier weather station are available for both data sets.

4.1 Results

4.1.1 Winds

Differences are observed between the wind data from the three periods (Figure 4-1), as is expected due to seasonal migration of the South Atlantic High. The characteristics of the alongshore wind during these periods are summarised in Table 4-1. Southerly, upwelling-favourable winds were highest in magnitude and most persistent in duration

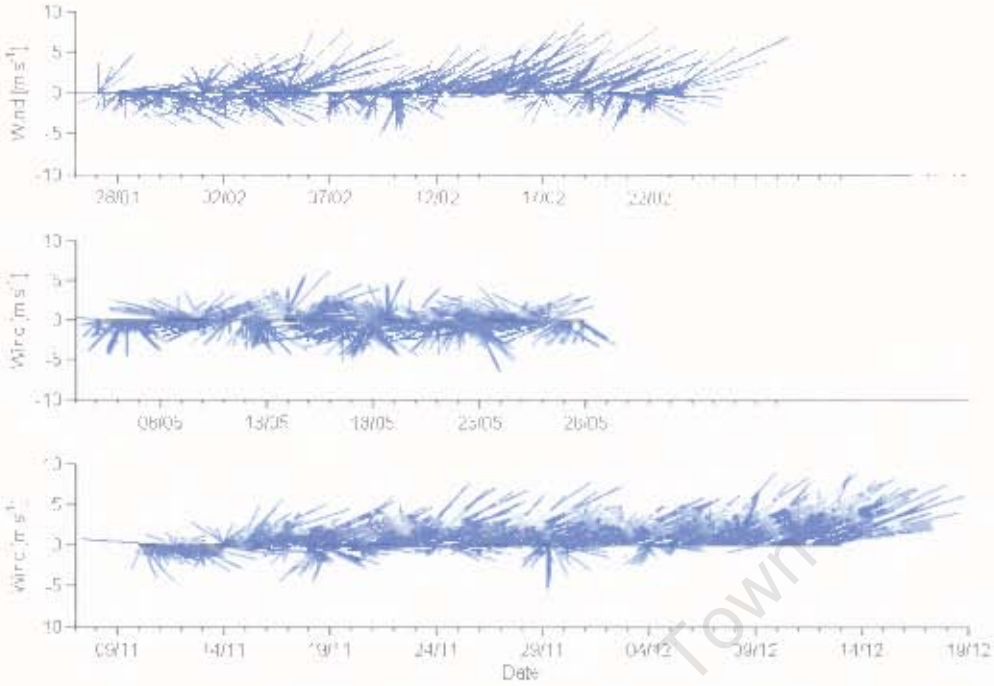

Figure 4-1 Wind vectors from Lambert's Bay Nortier weather station from the late upwelling season (top), winter conditions (middle) and the early upwelling season (bottom) in 2005.

	Late upwelling season	Winter conditions	Early upwelling season
Percentage northerly/ southerly	46% / 54 %	56% / 34 %	25% / 75 %
Mean southerly	4.1 m s^{-1}	3.6 m s^{-1}	4.6 m s^{-1}
Mean northerly	2.9 m s^{-1}	3.3 m s^{-1}	2.3 m s^{-1}
Max southerly	9.3 m s^{-1}	8.5 m s^{-1}	10.7 m s^{-1}
Max northerly	5.3 m s^{-1}	8.5 m s^{-1}	5.5 m s^{-1}

Table 4-1 Characteristics of alongshore wind data from Lambert's Bay Nortier weather station for the three data sets from the late upwelling season, winter conditions and early in the upwelling season in 2005.

early in the upwelling season, with short periods of reversal to northerly winds up to three days long, while winds during winter conditions were predominantly north-westerly. The late upwelling season was characterised by periods of upwelling-favourable winds interspersed with longer periods of relaxation and northerly winds up to five days in duration. Wavelet analyses of alongshore winds (Table 4-2) found the highest powered

signal at the diurnal period in the early and late upwelling season, while this signal was considerably weaker during winter conditions. Signals with a period of a few days in the three data sets were consistent with reversals between southerly and northerly winds.

	Data	Primary Peak	Secondary Peak	Third Peak
Late upwelling season	Alongshore Wind	1 day	3.5 days	10.5 days
	Alongshore ADCP 5m Current	22.5 hours	9.25 days	3.5 days
	Across-shelf ADCP 5m Current	21 hours	9.5 days	3.5 days
	Surface Temperature	9 days	24 hours	4.5 days
Winter conditions	Alongshore Wind	5 days	2.3 days	1 day
	Alongshore ADCP 5m Current	22.5 hours	5.3 days	2.1 days
	Across-shelf ADCP 5m Current	22.5 hours	5.3 days	2.8 days
	2m Temperature	1 day	5 days	4 days
Early upwelling season	Alongshore Wind	1 day	5 days	2.6 days
	Alongshore ADCP 5m Current	1 day	5 days	2.8 days
	Across-shelf ADCP 5m Current	22.5 hours	5 days	
	2m Temperature	1 day	6.5 days	5 days

Table 4-2 Periods at which the three highest powered peaks are found using wavelet analysis for various data for the three data sets

4.1.2 Currents

In response to variations in the prevailing winds, differences were observed in the near-surface currents (Figure 4-2). Characteristics of the near-surface currents are summarised in Table 4-3. Alongshore near-surface currents during winter conditions were predominantly southward, with the maximum velocities occurring in this direction, while early in the upwelling season maximum velocities and the majority of near-surface current flow was directed northwards. Maximum velocities late in the upwelling season were towards the north, although the predominant flow direction was southward.

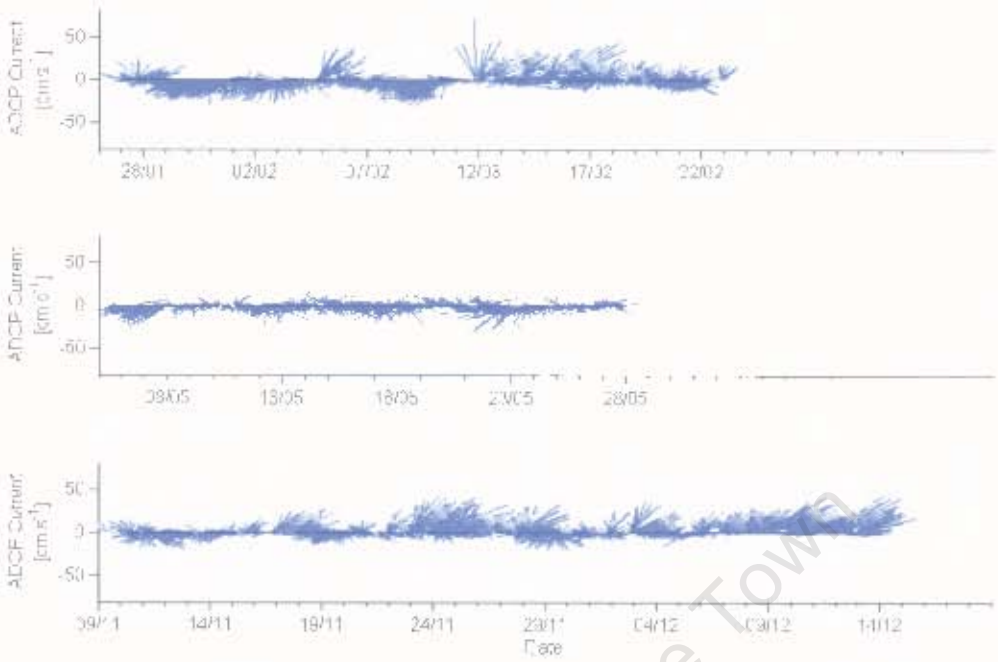

Figure 4-2 Current vectors from ADCP bin at 5 m from the late upwelling season (top), winter conditions (middle) and the early upwelling season (bottom) in 2005.

	Late upwelling season	Winter conditions	Early upwelling season
Percentage northward/ southward	31% / 69%	30% / 70%	59% 41%
Percentage eastward/ westward	36% / 64%	36% / 64%	53% / 47%
Max southward	31.8 cm s^{-1}	33.6 cm s^{-1}	26.3 cm s^{-1}
Max northward	71.3 cm s^{-1}	16.5 cm s^{-1}	46.3 cm s^{-1}

Table 4-3 Characteristics of near-surface currents from ADCP bin at 5 m from the late upwelling season (top), winter conditions (middle) and the early upwelling season (bottom) in 2005.

Wavelet analyses (Table 4-2) found the highest powered signal near the inertial frequency in all data sets (although this signal appears to be at the diurnal rather than inertial period in the alongshore near-surface currents early in the upwelling season), with a signal around five days (three and a half days late in the upwelling season) consistent with reversals in direction.

Correlation between low pass filtered alongshore near-surface currents and winds (Figure 4-3) is observed in all data sets with the highest correlation early in the upwelling season (r^2 of 0.68 with the currents lagging the wind by 13 hours - 782 samples, significant at 95% confidence level) and the lowest correlation during winter conditions (r^2 of 0.21 with the currents lagging the wind by 13 hours - 539 samples, significant at 95% confidence level).

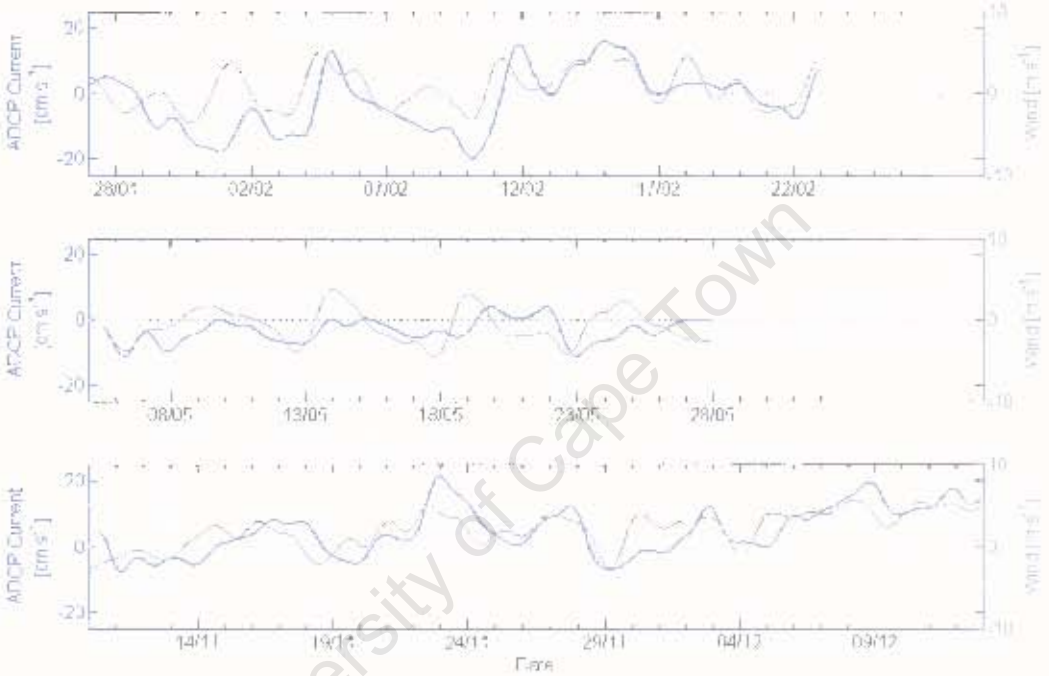

Figure 4-3 Low pass filtered alongshore current from ADCP bin at 5 m and alongshore wind from Lambert's Bay Nortier weather station from the late upwelling season (top), winter conditions (middle) and the early upwelling season (bottom) in 2005.

4.1.3 Temperature and water column structure

A temporary thermistor chain, consisting of self-logging temperature recorders (see 2.1.6) attached to a rope, was deployed on the mooring when the thermistor chain was unavailable. For the data collected under winter conditions the temperature recorders were deployed at 2, 4, 6, 8, 10 and 15 m, while for data from early in the upwelling season they were located at 2 m intervals between the surface and 10 m and 5 m intervals from 10 to 20 m.

Water column structure and temperatures varied dramatically between the three periods (Figure 4-4). Near-surface temperature ranges and water column temperature differences are summarised in Table 4-4. Data from late in the upwelling season were characterised by warm surface waters, extending to depths of around 10 m, persisting for several days, interspersed with periods where the water column is cool and well mixed. Near-surface temperatures exhibited a range of 8.7 °C. In contrast, during winter conditions, the water column was well mixed and temperatures were considerably less variable, with a range in near-surface temperatures of less than 2 °C and a maximum difference of 2.6 °C between near-surface and 15 m temperatures. Water column temperatures early in the upwelling season were cool and well mixed for periods of a week or more; surface waters warmed between upwelling events but to a lesser extent than late in the upwelling season. Wavelet analyses of near-surface temperatures (Table 4-2) show a peak in power at the diurnal period in all data sets, consistent with daily heating due to insolation. Secondary peaks in power at periods of several days represent periods between warming and cooling of near-surface waters, attributed to upwelling cycles and current reversals.

	Late upwelling season	Winter conditions	Early upwelling season
Maximum 2 m temperature	19.4 °C	15.2 °C	17.1 °C
Minimum 2 m temperature	10.7 °C	13.5 °C	10 °C
Max difference between 2 m and 15 m	8.4 °C	2.6 °C	4.2 °C
Min difference between 2 m and 15 m	0.1 °C	0 °C	0 °C

Table 4-4 Characteristics of water column temperatures from mooring thermistor chains for the three data sets from February, May and November/ December 2005.

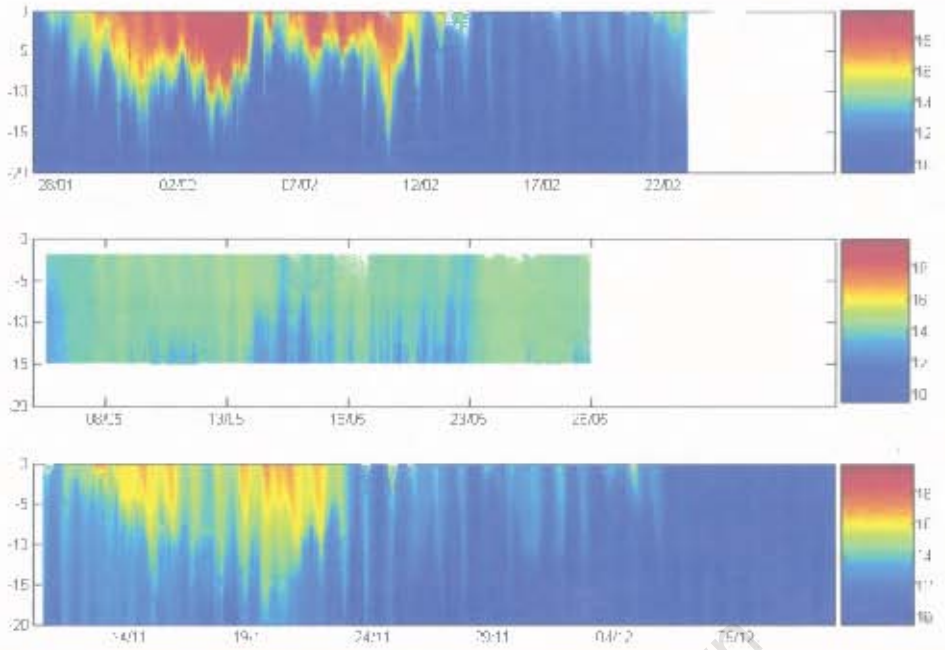

Figure 4-4 Temperature profiles [°C] from thermistor chain deployed on mooring from the late upwelling season (top), winter conditions (middle) and the early upwelling season (bottom) in 2005.

4.2 Discussion

Although the data sets presented are short stand alone time series, differences in the winds, currents and water column structure between the data sets are indicative of a seasonal signal.

4.2.1 Differences in winds and current response to wind forcing

Whilst the data for the three periods are quite different, with winter conditions dominated by northerly winds and southward alongshore currents, and the early part of the upwelling season dominated by southerly winds and northward alongshore currents, in all data sets near-surface currents appeared to respond to changes in direction and magnitude in the local wind field

Winds during winter condition were predominantly northerly, consistent with a northward shift in the pressure system during winter leading to a greater frequency of north-westerly, non-upwelling-favourable winds (Shannon & Nelson 1996). In contrast, summer positioning of the South Atlantic High leads to a high frequency and magnitude of upwelling-favourable winds (Shannon 1985) as observed in early part of the upwelling

season, with only brief periods of relaxation or reversal. Towards the end of summer and autumn the pressure gradients responsible for upwelling-favourable winds weaken (Pitcher *et al.* 1992), consistent with more prolonged periods of wind relaxation and reversal later in the upwelling season. Wavelet analyses show high power at the diurnal period throughout the upwelling season, which is attributed to the existence of a greater temperature differential between land and sea temperatures in spring and summer months, driving land-sea breezes.

Seasonal differences in water movement for St Helena Bay were observed through drift card release in the 1950's and 1960's (Duncan & Nell 1969). The drift was mainly northward in spring and summer with an occasional inshore counter-current, which became stronger during autumn. During winter the drift was predominantly southward, occasionally interspersed with a pattern more typical of summer. These observations are in keeping with those made here from the mooring data. High power at the inertial frequency, and corresponding inertial oscillations, were observed in current data from all data sets. They were most prevalent during periods of strong, diurnally varying winds, consistent with the requirement of a fluctuating wind stress for the generation of inertial oscillations (Pollard & Millard 1970).

Limited literature is available regarding currents and temperatures in winter in the southern Benguela due to a lack of observations. Current meter moorings deployed off the west coast in deeper water (150-200 m) during winter 1982 exhibited current variations at the semi-diurnal tidal frequency, the inertial frequency and low frequency reversals at periods of 5 to 6 days (Holden 1986). Low frequency fluctuations were attributed to the southward passage of remotely forced coastally trapped waves. Those data differ from the data presented here in that the currents were found to be 5 hours ahead of the wind in phase (*ibid*), as opposed to the 13 hour lag observed during winter conditions. Data collected in northern California as part of the CODE found mean currents during winter to be more uniform with depth than summer, poleward and correlated with wind stress, with the current lagging the wind by around half a day (Lentz & Chapman 1989). These observations are more in keeping with those made during winter here, and although the correlation is less good than that for late in the upwelling season, alongshore currents appeared to be correlated with local alongshore winds implying local forcing or local generation of shelf waves as discussed in chapter 3.

Alongshore currents early in the upwelling season were predominantly northward, and well correlated with alongshore winds, with brief reversals to northerly winds leading to current reversals. Processes affecting current magnitude and direction are assumed to be similar to those discussed in chapter 3. The increased frequency and magnitude of northward currents was due to the increased strength and incidence of equatorward, upwelling-favourable winds during spring, corresponding with wind-induced upwelling reaching a maximum at this time of year (Nelson & Hutchings 1983).

Differences in current flow between the data sets are highlighted in Figure 4-5. Mean alongshore currents were southward late in the upwelling season and during winter conditions, while surface currents were northward early in the upwelling season, consistent with increased upwelling.

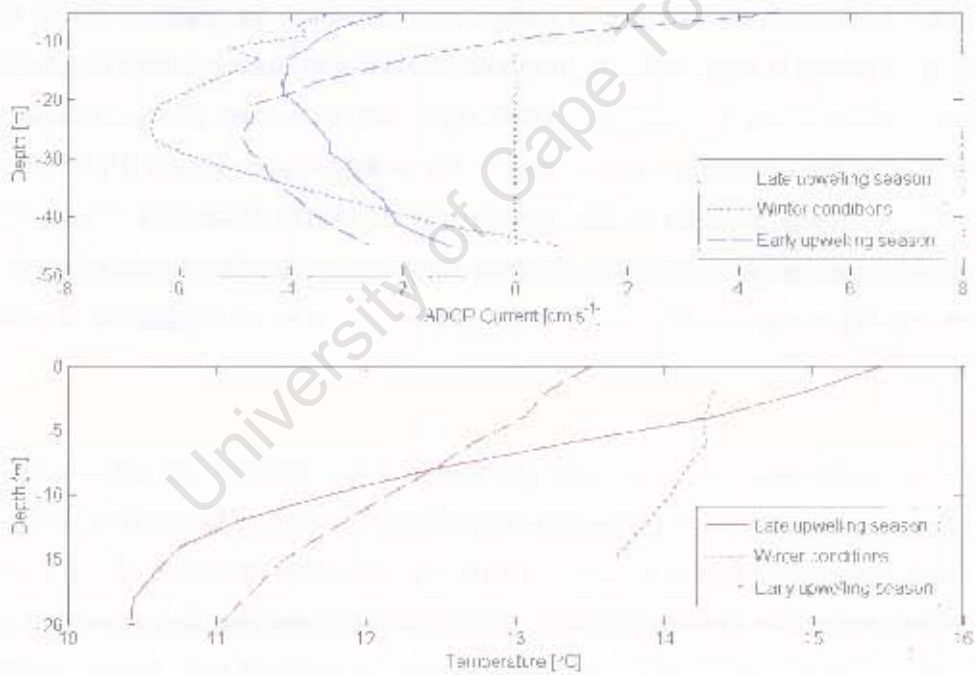

Figure 4-5 Mean current profiles from ADCP bins between 5 and 45 m (top) and mean temperature profiles from thermistor chains deployed on mooring (bottom) for late in the upwelling season, early in the upwelling season and winter conditions in 2005.

4.2.2 Differences in water column structure

Despite the observed difference in maximum and minimum temperatures and water column structure between the three data sets, in all cases there was a correlation between alongshore currents and surface temperatures, with southerly winds and northward currents leading to decreasing surface temperatures, and southward currents associated with increasing surface temperatures.

Temperatures during winter conditions were substantially less variable than during summer months, and the water column was more mixed than during the upwelling season. These differences are attributed to a decrease in upwelling and insolation in winter months, as well as increased mixing due to winter storms. Winter temperature profile data from California show mean water temperatures to be greatest during winter when the wind stress is least, and the mean vertical temperature gradient to be more uniform with depth (Lentz & Chapman 1989). Although mean near surface temperatures are higher late in the upwelling season, due to the availability of around 2.5 times more heat flux from incident radiation in late summer than in winter (Guastella 1992), mean temperature profiles were warmer and vertical temperature gradients lower during winter conditions, similar to the CODE data, and consistent with a lower frequency of upwelling-favourable winds.

Water temperatures were generally cool and levels of stratification low early in the upwelling season due to a high incidence of southerly, upwelling-favourable winds and the intrusion of recently upwelled waters. Warm periods were observed at the start of the data set, concurrent with wind relaxations, southward currents and the advection of warmer water (see chapter 3) but these were shorter in duration than those observed in later in the upwelling season and did not reach the same maximum temperatures.

Seasonal differences in water column structure are highlighted in Figure 4-5. Stratification was greatest late in the upwelling season consistent with high levels of insolation and increased duration of relaxation from upwelling-favourable winds. The water column was well mixed during winter conditions.

4.2.3 Implications for HABs

In a wind driven upwelling system most of the dynamic processes occur in direct response to wind forcing through the creation of a friction layer, currents and sea-level slopes (Nelson 1992). Therefore seasonal variations in wind strength and direction in the southern Benguela lead to differing patterns of current flow and water column structure as observed in the data. Red tides occur most frequently towards the end of summer and autumn, when a decrease in upwelling-favourable winds and increase in calm days contributes to stabilisation of the water column (Horstman 1981). An increased frequency and duration of periods of relaxation from upwelling, and greater water column stratification was observed in the data from later in the upwelling season, than in the data from earlier in the upwelling season, consistent with the reported increase in the frequency of dinoflagellate dominated blooms during the latter part of the upwelling season, given that blooms are associated with wind relaxation and stratified conditions (Pitcher & Boyd 1996). During winter decreased levels of insolation, and an increase in north-westerly winds causing storm-mixing leads to a lower but more even distribution of phytoplankton through the water column (Brown & Hutchings 1985 as cited in Pitcher *et al.* 1992).

5 Phytoplankton response to physical forcing: March 2005

Physical forcing is known to be of importance to phytoplankton, regulating nutrient, temperature and light conditions. In an upwelling system such as the southern Benguela where wind is a major determinant of hydrodynamic variability (Pitcher *et al.* 1995), patterns of phytoplankton are linked to the magnitude and frequency of upwelling events, water column stratification and nutrient availability (Kudela *et al.* 2005). Wind driven variations in currents drive transport of phytoplankton, while water column structure and associated levels of mixing and nutrients determine the composition of the phytoplankton community (Cullen & MacIntyre, 1998). Seasonal patterns of spring diatom blooms followed by dinoflagellate dominance, associated with increasingly stratified conditions, are interrupted and reset by episodic wind forcing, altering the environmental conditions and thus favouring different algal species and assemblages (Kudela *et al.* 2005).

Physical processes in response to the wind, at time scales of less than two weeks, have been detailed in chapter 3. The dominant responses to wind forcing are current reversals, both at time scales of less than a day and three to six days, and associated changes in water column structure due to heating, mixing and advection. A field study was carried out off Lambert's Bay between 15th March and 6th April 2005, during which daily sampling was undertaken at the mooring location. Daily temperature and chlorophyll profiles were obtained using a Sea Bird CTD and Wetstar fluorometer. Surface phytoplankton samples were fixed in buffered formalin and counted using the Utermöhl method (Hasle 1978). Data from the mooring, with the inclusion of fluorescence data, were available between the 19th March and 6th April 2005. These data were used to examine the physical processes and conditions associated with detected changes in phytoplankton abundance and composition. Data analysis, including filtering and wavelet analysis, were carried out as outlined in chapter 3.

5.1 Results

5.1.1 Wind Data

Winds for the five days prior to the field study (8th to 15th March were predominantly southerly and upwelling-favourable (Figure 5-1). Reversals to north-westerly winds,

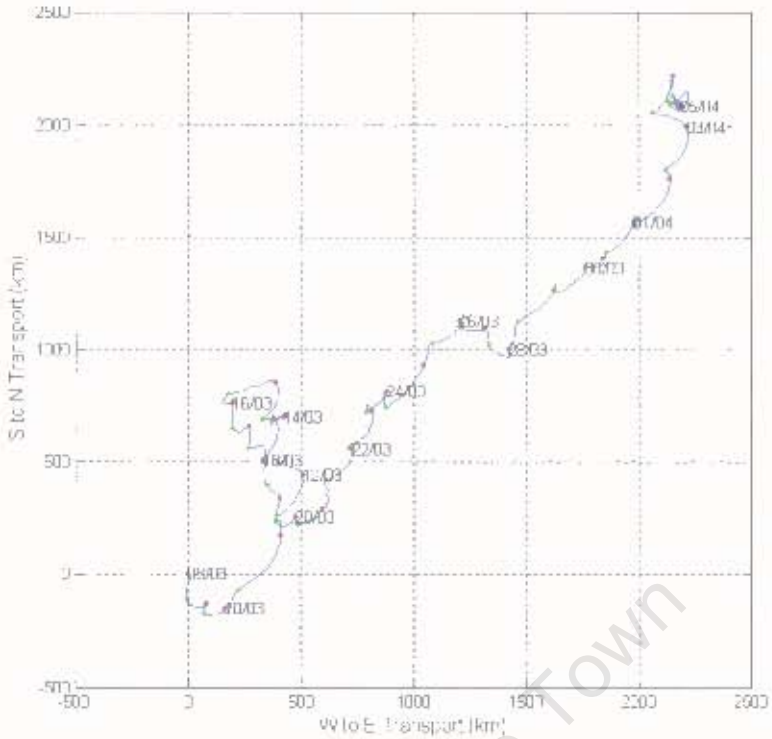

Figure 5-1: Progressive vector plot of wind data from Lambert's Bay Nortier weather station between the 8th March and 5th April 2005. The plot commences seven days prior to the study period. Red dots and dates are positioned at midnight, green dots are positioned at midday. Data starts at the origin (0,0).

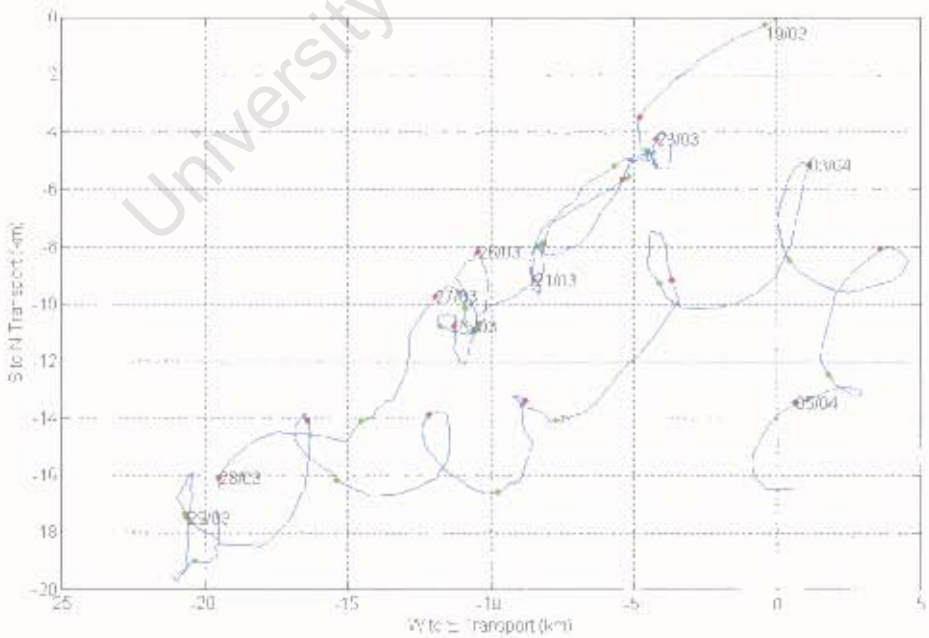

Figure 5-2: Progressive vector plot of ADCP current vectors for the bin at 5m from the mooring (BOB) between the 19th March and 5th April 2005.

lasting between two and five days, are seen on the 16th March, 26th March and 4th April. A strong diurnal component is visible in the south-westerly wind data between the 20th March and 4th April, in which the wind is weak in the morning, stronger and more onshore in the afternoon and backs towards offshore in the evening and early hours of the morning, consistent with a diurnal land-sea breeze effect. Wavelet analyses of wind data for this period (Table 5-1) exhibit a strong signal at the diurnal period in the alongshore and across-shelf data, which may be attributed to the diurnal sea breeze. A longer period signal at four days in the alongshore data, and 3.5 days in the across-shelf data, is indicative of reversals between southerly, upwelling-favourable winds, and north-westerly winds.

Data	Primary Peak	Secondary Peak	Third Peak
Alongshore Wind	1 day	4 days	1.6 days
Across-shelf Wind	1 day	3.5 days	
Alongshore ADCP 5m Current	22.5 hours	3.75 days	
Across-shelf ADCP 5m Current	21 hours	4 days	10.5 days
Surface Temperature	3.75 days	1 day	7 days
6m Temperature	22.5 hours	3.5 days	1.6 days
10m Temperature	22.5 hours	3.5 days	10.5 days
Fluorescence	10.5 days	4 days	17 hours

Table 5-1 Periods at which the three highest powered peaks are found using wavelet analysis for various data

5.1.2 Physical Response to Wind Forcing

5.1.2.1 Current Data

Near-surface currents were south-westward at the beginning of the mooring data set on the 19th March (Figure 5-2). Flow reversed to northward on the 21st March, following reversal to upwelling-favourable winds, with currents becoming southward again on the 23rd and 24th March. The 25th and 26th March were characterised by inertial currents, superimposed on low velocity currents to the north. Currents were southward between the 26th and 28th March in response to north-westerly winds. With the commencement of

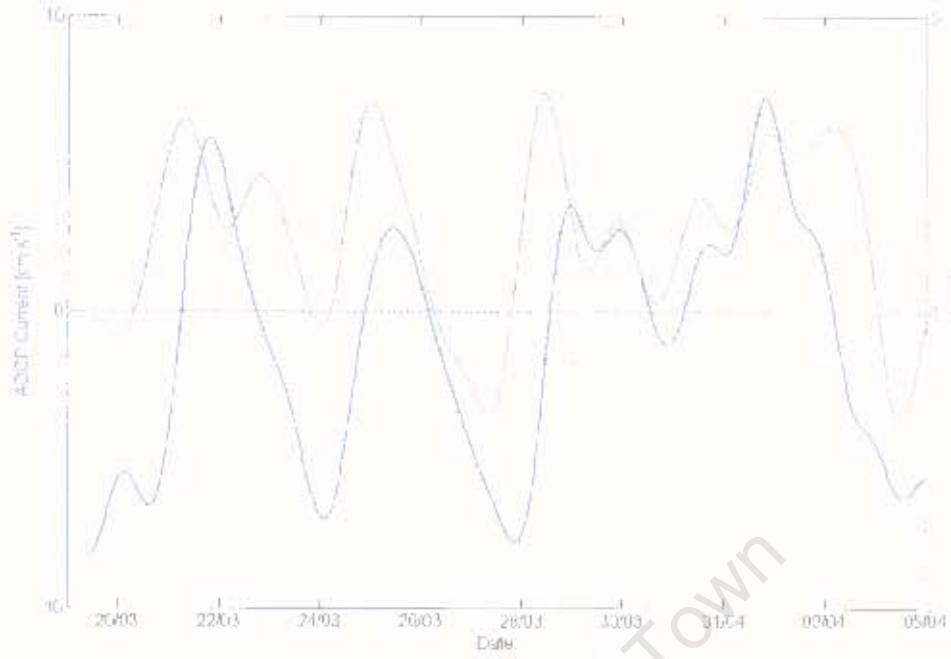

Figure 5-3: Low pass filtered alongshore ADCP current from 5 m bin and alongshore wind from Lambert's Bay Nortier weather station between 19th March and 5th April 2005.

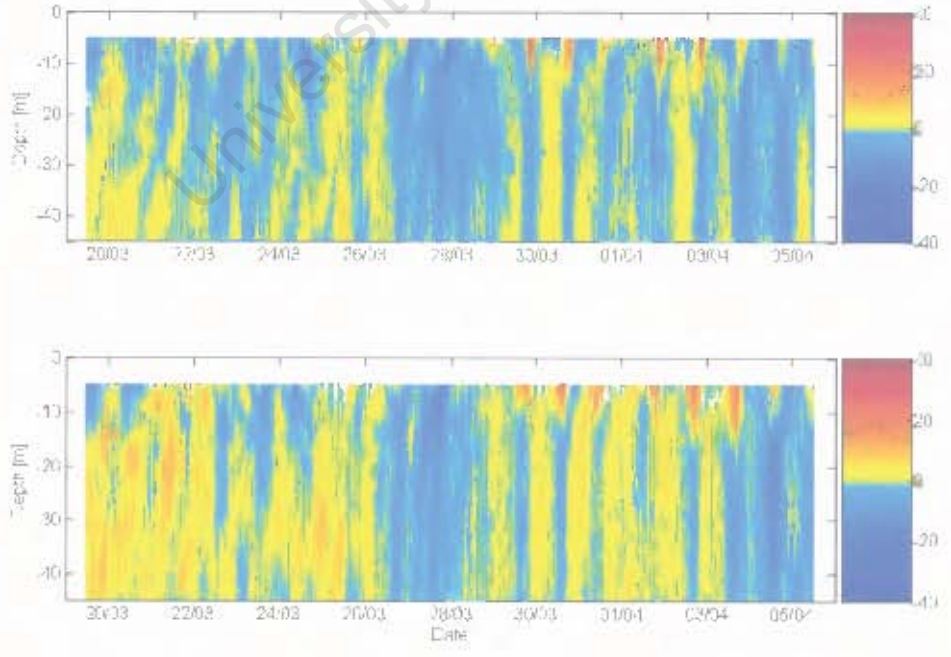

Figure 5-4 Current velocity [cm s^{-1}] for ADCP bins between 5m and 45m for alongshore component (top) and across-shelf component (bottom) between 19th March and 5th April 2005.

south-westerly winds on 28th March the current became northward with a strong onshore component, exhibiting inertial oscillations forced by diurnal winds. Inertial oscillations continued to be observed in the current data, superimposed on southward flow, following the weakening and reversal of winds on the 3rd April.

From this description it is apparent that changes in current direction follow changes in wind direction, as discussed in chapter 3 for the February 2005 data set. Filtered alongshore wind and current data were well correlated (Figure 5-3) with a maximum r^2 of 0.52 (409 samples, significant at 95% confidence level), with the currents lagging the wind by eight hours. The intercept of the regression line at the optimum lag period is –3.6 cm s^{-1}, similar to that found for the data from February 2005, implying poleward alongshore flow in the absence of wind. Wavelet analysis of alongshore current data shows high power at 22.5 hours, coincident with the inertial frequency, and at 3.75 days, corresponding to reversals driven by changes in wind direction (Table 5-1). Across-shelf currents display high power at 21 hours, 4 and 10.5 days. Low frequency alongshore and across-shelf currents were reasonably well correlated, with concurrent reversals and a general north-east, south-west alignment to the flow.

High frequency currents were predominantly inertial, with a strong signal observed in the wavelet analyses between the 24th and 27th March and the 29th March and 4th April, concurrent with strong diurnal winds. A 180° shift in phase at around 10 or 15 m depth, associated with the thermocline, can be seen in the vertical structure of high frequency currents during periods of strong inertial oscillation (Figure 5-4), resulting in vertical shear. Strong northward pulses are seen in the alongshore current profile data between the 29th March and 2nd April, where the northward component of the inertial oscillation is superimposed on existing northward flow. However, as discussed in chapter 3, inertial oscillations appear to have no net effect on the flow or transport and merely add a rotational aspect to the background flow field, with rotations occurring on a daily time scale.

5.1.2.2 Temperature Data

At the start of the study period temperature profile data (Figure 5-5) show a well mixed surface layer of around 14 °C with the thermocline at 10 m. The temperature profile changed rapidly and an extended period of warm, stratified surface waters (with

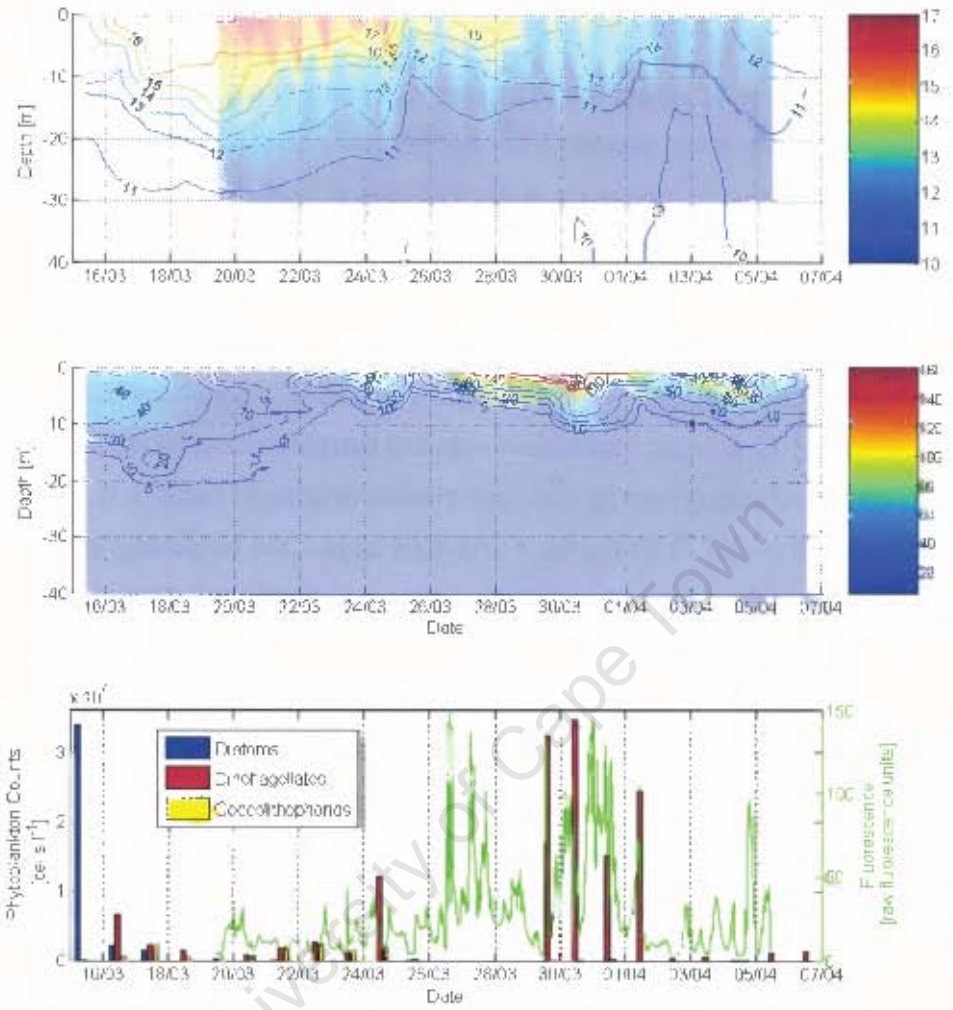

Figure 5-5 Temperature [°C] from mooring thermistor chain (colour plot) and daily CTD casts at mooring location (contour plot) (top), daily chlorophyll [mg m^{-3}] profiles from fluorometer (middle) and daily surface phytoplankton counts with surface fluorescence from mooring (bottom).

temperatures reaching 17 °C) of eight days duration followed. This warm surface water is assumed to be advected into the area from the north by southward currents accompanying the north-westerly winds. Northward and inertial currents on the 25th March, consistent with upwelling-favourable winds, led to rapid cooling of the water column to 13.8 °C at the surface, with the thermocline at 3 m. Temperature profile data show warming in association with southward currents on the 26th March, and a deepening of the surface layer over the following three days. The water column cooled rapidly, in association with southerly winds and northward currents, on the 29th March. Warm pulses of water are observed in the afternoon with onshore currents and cool

pulses of water with northward flow at night. Southerly winds increased in strength on the 2nd of April, accompanied by predominantly northward inertial currents and further cooling of the water column. The water column began to warm again on the 4th April with southward flow following a wind reversal.

Filtered near-surface alongshore current and temperature data confirm the association of warm water with southward currents, and cool water with northward currents, consistent with the expected response to upwelling and relaxation events (Figure 5-6). An overall decrease in surface temperature was observed in the mooring data during the study period. Heat budget calculations (see 3.2.3 for method) for the 22nd to the 24th March (Table 5-2) indicate that the available heat flux from insolation can only explain between 20 and 40% of the observed temperature changes, and that advection must play a role in increasing temperatures. Wavelet analysis of surface temperature data shows high power at the diurnal period, which may be attributed to daily solar heating, and at 3.75 to 4 days, consistent with periods found in wind and current data due to reversals (Table 5-1). Temperature data for 6 and 10 m exhibit high power at the inertial frequency, implying that inertial oscillations were responsible for the intrusion of differing water masses at the mooring location, or changes in mixed layer depth.

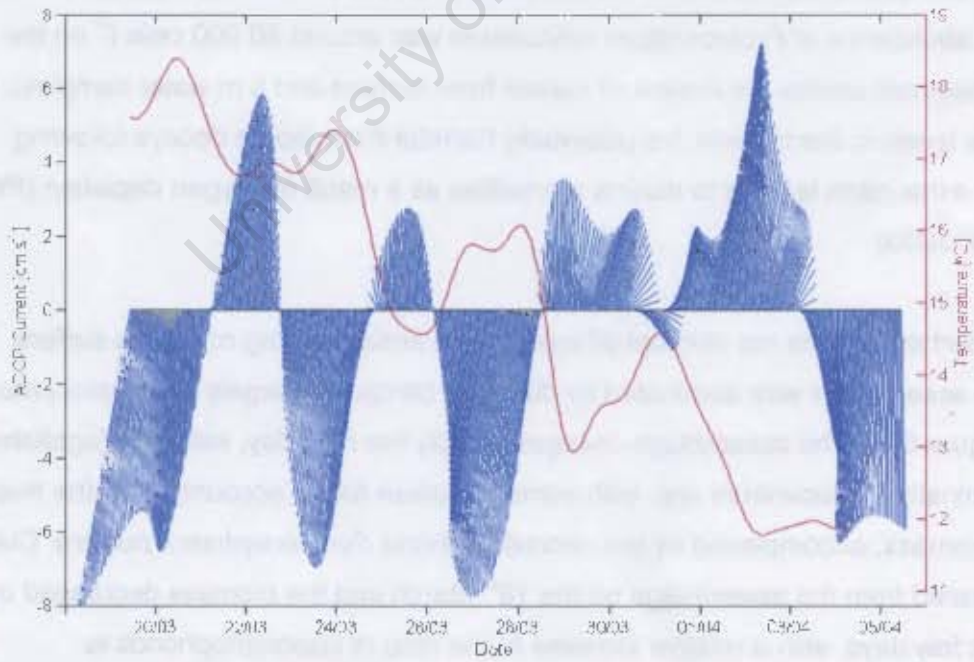

Figure 5-6 Low-pass filtered ADCP current vectors for bin at 5m and surface temperature from mooring thermistor chain between 19th March and 5th April 2005.

Date	Temperature Increase (°C)	Depth (m)	Time (hrs)	Required heat input (W m^{-2})	Estimated available heat flux (W m^{-2})
22nd March	27.4	14	10	3261	662.5
23rd March	6.6	4	7	1963	832.1
24th March	11.43	16	11	1236	238.6

Table 5-2 Components of heat budget calculations for the surface mixed layer for specified dates

5.1.3 Biological Response – Fluorescence and Phytoplankton count data

Two periods of very high biomass, consisting of a dinoflagellate dominated assemblage, were observed during the study period (Figure 5-5). Potentially harmful algae *Dinophysis acuminata* and *Dinophysis fortii* responsible for the production of diarrhetic shellfish poisoning toxins, and *Protoceratium reticulatum,* which produces yessotoxins, formed a component of the high biomass dinoflagellate assemblage. *Dinophysis* species reached a maximum abundance of around 40 000 cells l^{-1} on the 29th and 30th March, while the highest abundance of *Protoceratium reticulatum* was around 90 000 cells l^{-1} on the 1st April (these cell counts are means of counts from surface and 5 m water samples). High biomass levels in themselves are potentially harmful if the bloom decays following nutrient exhaustion leading to marine mortalities as a result of oxygen depletion (Pitcher & Calder 2000).

At the start of the data set chlorophyll levels were around 50 mg m^{-3} in the surface 10 m and the assemblage was dominated by diatoms, composed largely of *Chaetoceros spp.*(Figure 5-5). The assemblage changed rapidly the next day, with dinoflagellates (predominatly *Prorocentrum spp.* with some *Ceratium furca*) accounting for the majority of the biomass, accompanied by the coccolithophorid *Syrachosphaera pulchra.* Diatoms disappeared from the assemblage on the 18th March and the biomass decreased over the next few days, with a relative increase in the ratio of coccolithophorids to dinoflagellates. Chlorophyll values increased in the surface 5 m between the 21st and 24th March; phytoplankton count data indicate a similar mixed dinoflagellate (dominated by *Prorocentrum spp.*) and coccolithophorid (*Syrachosphaera pulchra*) assemblage with a large increase in the ratio of dinoflagellates to coccolithophorids on the 24th March. A decrease in biomass followed the appearance of cooler water on the 25th March.

Unfortunately no daily samples were acquired between the 26th and 28th March, and therefore only mooring data are available. Although fluorescence values were highly variable over this period, they show peaks of 150 (raw fluorescence units) indicating high biomass. Fluorescence dropped with the introduction of cooler water late on the 28th March and then rose rapidly late on the 29th March and continued to be high; chlorophyll profiles indicate surface values of up to 165 mg m^{-3}. The assemblage was dinoflagellate dominated, consisting largely of *Prorocentrum spp.* and *Ceratium spp.* Cooling of the water column was accompanied by a rapid drop in biomass on the 2nd and 3rd April; the remaining biomass consisted of a similar assemblage to the previous few days. An increase in biomass is observed from the afternoon of the 4th, following a reversal in winds and currents, and chlorophyll profiles indicate a sub-surface maximum of around 120 mg m^{-3} on the 3rd, 4th and 5th April. Phytoplankton count data indicate this to be a dinoflagellate dominated assemblage, similar to that detected previously.

The fluorescence signal from the mooring data was highly variable, both within high biomass events, and during periods of lower biomass. Wavelet analysis of fluorescence data leads to the masking of signals during periods of low biomass by the large peaks in signal, and thus power, during periods of high biomass. However, signals are detected at periods of 17 hours and 4 and 10.5 days (Table 5-1), with a fourth peak at 12 hours. The four and ten day signal represent time scales between high biomass events, and at four days shows some correspondence with similar signals found in wind, current and temperature data. A combination of photoinhibition and vertical migration may be responsible for the semi-diurnal signal.

5.2 Discussion

Changes in phytoplankton species composition occur by two main processes: succession and sequence (Smayda 1980). Succession results from the changing physical, chemical and biological characteristics of a given water mass, while sequence is the change in species composition due to a change in water mass type. In the southern Benguela, changes in the water column from a well mixed, nutrient rich environment, to a stratified, nutrient-poor environment, drive changes in phytoplankton composition from diatoms to dinoflagellates (Pitcher & Nelson 2006). Coccolithophorids typically dominate in warm oligotrophic waters and are considered to characterise later stages of succession (Smayda 1980); blooms of *Syrachosphaera pulchra* have for

example been observed in the southern Benguela associated with water temperatures of around 16 °C (Weeks *et al.* 2004). The changes in phytoplankton composition observed during this study period do not represent a typical succession from diatoms to dinoflagellates, rather it is a combination of the two processes with the pattern of succession being altered, and to some extent reset, by changes in water mass brought about by shifts in the wind and current regime. This is typical of upwelling systems, where episodic events lead to the development of spatially and temporally variable sub-habitats (Smayda 2000).

5.2.1 Physical Processes

The close correlation between alongshore winds and currents, and alongshore currents and surface temperatures, were very similar to those observed and discussed in chapter 3 for the February 2005 data set, and are assumed to be due to the same processes. Changes in thermocline depth appear to be largely current driven; by advection of warm surface layers, lifting of the thermocline by upwelled waters, or movement of water masses with inertial oscillations.

5.2.2 Low frequency currents and changes in phytoplankton population

Large changes in biomass and phytoplankton community composition, indicated by fluorescence and phytoplankton count data, occur rapidly and are thus more likely to be due to advection and sequential changes than growth and succession. The diatom dominated assemblage observed initially was associated with a well mixed surface layer of 14°C water, following several days of upwelling-favourable winds. Although the water temperature was warmer than might be expected, the observation is consistent with the occurrence of non-motile diatoms in cool, nutrient-rich water following upwelling (Pitcher *et al.* 1991).

The sudden change in assemblage to a dinoflagellate dominated community the following day was associated with the introduction of a much warmer surface water mass, advected to the mooring location from the north, and was therefore sequential in nature. Continuing southward currents and increasing water temperatures in the following few days led to a complete disappearance of diatoms from the assemblage, and an increase in the number of coccolithophorids relative to dinoflagellates. The increasing coccolithophorid abundance in the water mass was consistent with increasing

temperatures and decreasing or depleted nutrients in the surface waters. The warmest waters, observed on the 19th and 20th March, had a decreased biomass and increased coccolithophorid ratio. Southerly winds, northward currents and a decrease in water temperatures over the following few days resulted in reversal of the pattern of succession; levels of biomass increased and the dinoflagellate dominated assemblage returned. Levels of biomass fluctuated as the bloom and associated water mass were advected by current reversals in response to changes in wind direction, while the assemblage remained unchanged and dominated by dinoflagellates. The changes in species composition were associated with differing temperatures, and thus implied nutrient status, of the water column. These changes reflect a combination of *in situ* changes in phytoplankton succession, and sequential changes through the advection of water populated by later stages of succession to the mooring location.

During the study period the biomass varied from a diatom dominated assemblage, to a mixed dinoflagellate/ coccolithophorid assemblage, to a dinoflagellate dominated assemblage, and from high to low levels of biomass within short time scales. The typical doubling time for phytoplankton on the west coast in the southern Benguela is estimated at 3.2 days from primary production measurements, in comparison to calculated values of 2.2 days at 15 °C and 3 days at 20 °C from Eppley's 1972 equation (Brown *et al.* 1991). Biomass levels at the sampling location often increased by an order of magnitude in a few hours, thus far exceeding possible growth rates. Similarly changes in assemblage occurred too rapidly to be explained by species succession. These rapid variations in biomass and phytoplankton community composition must therefore be attributed to the introduction of populations into the sampling area with changes in water mass. Previous work in the region has shown the relevance of advection in the introduction of high biomass blooms into the region (e.g. Pitcher & Boyd 1996, Pitcher *et al.* 1998), in which dinoflagellates are seen to accumulate at the surface at convergence zones inshore of the coastal jet. These populations move onshore and poleward under relaxation conditions, introducing the bloom to nearshore areas. Observations in 2000 and 2001 demonstrated the appearance of dinoflagellate blooms with increasingly stratified, warmer waters and poleward alongshore currents following wind relaxation (Pitcher & Nelson 2006). An experimental algorithm (Bernard *et al.* 2005) applied to Medium Resolution Imaging Spectrometer (MERIS) images concurrent with the 2005 fieldtrip data substantiates the role of advection in bloom transport (Figure 5-7). The

image for the 30th March shows high biomass in a narrow, meandering strip along the coast, coincident with the high biomass dinoflagellate assemblage detected at the mooring location. The bloom is seen to have moved northward in the image from the 2nd April, consistent with upwelling-favourable winds and northward currents, and decreased biomass recorded at the mooring. On the 5th April, the image shows the bloom to have been transported south, and to extend offshore, while mooring data showed an increase in biomass associated with a switch to north-westerly winds and southward currents.

5.2.3 Effect of high frequency currents

Inertial oscillations were observed in the current data from the mooring in association with diurnally varying winds, particularly during the latter part of the study period. Fluorescence values appeared to peak in the afternoon during this period, possibly due to the onshore component of inertial oscillations moving the biomass towards the mooring location. Warming of the water column in the afternoon exceeded that due to insolation and is likely to be associated with the onshore component of inertial oscillations. Although there is no net transport associated with inertial oscillations, and therefore no relevance of inertial oscillations to bloom advection, they may have an

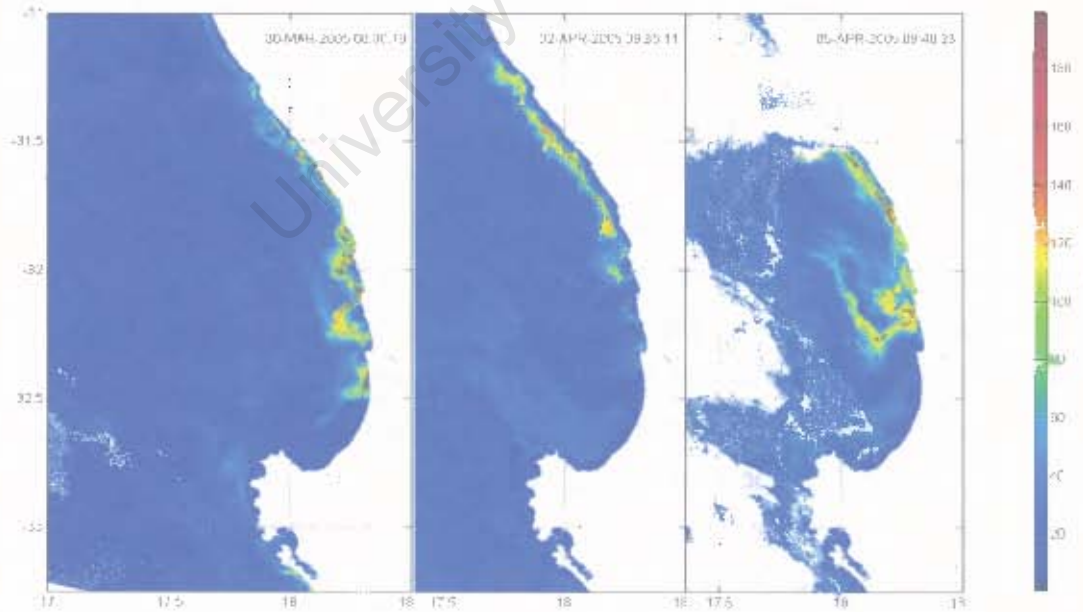

Figure 5-7 MERIS chlorophyll a images of St Helena Bay region illustrating movement of areas of high biomass – chlorophyll levels [mg m^{-3}]are calculated using an experimental algorithm

impact on phytoplankton dynamics through their effect on the mixed layer, as mixed layer dynamics are considered important in phytoplankton life–form selection. Inertial oscillations are likely to be the major energy source driving vertical mixing in regions with weak tidal currents (Rippeth *et al.* 2002). In a modelling study, simulating data from the Mediterranean, the appearance of nutrient pulses in the mixed layer was found to be strongly dependant on inertial currents (Klein & Coste 1984). Mixing occurs across the pycnocline through instability generated by high values of shear found at the depth of greatest stratification (van Haren *et al.* 2003), which may affect the supply of nutrients to phytoplankton blooms and therefore be relevant in the maintenance of blooms. Vertical shear in the water column, such as that associated with inertial oscillations, can lead to the development of thin layers of phytoplankton, which may optimise population growth rate, reduce mortality and affect the transport and retention of a population (Franks 1994, Gentien *et al.* 2005).

5.2.4 Summary

These data illustrate the role of the physical processes described in chapter 3 in the introduction, advection and dispersal of blooms. Current reversals on time scales of a few days, associated with changes in the local alongshore wind direction, and enhanced by local topography, were critical in altering the temperature structure of the water column. Changes in water column structure and levels of stratification determine phytoplankton life-form. Blooms at differing stages of succession, associated with water masses of differing levels of stratification, were advected to the sampling location. Whilst solar heating contributes to rising temperatures, more often than not temperature increases at a single location far exceed those possible due to insolation, and were attributed to advection of water masses southward with currents in response to relaxation and reversal of upwelling-favourable winds. On a shorter time scale, diurnal winds and associated inertial oscillations may contribute to the appearance of warmer water and higher levels of fluorescence at the mooring location during the afternoon. Further effects of inertial oscillations on phytoplankton dynamics, including the impact of vertical shear, mixing across the thermocline and the introduction of nutrients to surface layers are unresolved.

6 Summary

The development of the mooring, and the configuration of the instruments and data collection system have been extensively documented. Insight into the mooring system is provided that may be of use in the deployment of future moorings in the region. This includes considerations associated with the development of the mooring, such as power management, and knowledge gained throughout the project. Within the limitations of the present mooring configuration, a robust system has been developed for the real-time monitoring of algal blooms and associated physical parameters. Existing limitations include the need for frequent, personnel intensive servicing owing to the use of bio-optical instrumentation, and the need for mooring removal and replacement on a six monthly basis due to the use of light weight equipment. The ability of the mooring to detect high biomass blooms in real-time has clearly been demonstrated (e.g. Bernard 2005, Bernard *et al.* 2006, Fawcett *et al.* 2006), and the high-frequency, time-series data stored by the mooring has provided an extensive research data set for the study of physical processes and algal bloom dynamics. Data from the radiometers are also used for ocean colour satellite validation data (Bernard *et al.* 2005).

The initial project was ambitious in simultaneously making, storing and transmitting measurements from a number of instruments, placing high demands on the data logging and power systems. Future moorings may benefit from using fewer instruments, targeted at processes or parameters of interest at the mooring location, resulting in a stable, cost-effective and lighter-weight system.

Whilst the development of HABs in the southern Benguela, and their accumulation inshore, is known to be related to synoptic weather patterns (Pitcher *et al.* 1995, Pitcher & Boyd 1996, Pitcher *et al.* 1998, Pitcher & Weeks 2006), the availability of high-frequency time-series data from the mooring in this study has enabled the time scales of variability in local winds to be characterised, and the response of currents and water column structure to local wind forcing to be determined. These processes play a crucial role in determining HAB dynamics. Comparison between data sets from different times of year provides an indication of the response of currents and water column structure to seasonal variations in meteorological forcing. However, time scales of variability investigated within data sets are restricted to those under two weeks, as removal of the

mooring for monthly maintenance and servicing limits the length of uninterrupted data sets to around 30 days. HAB formation at the event scale is related to the frequency and duration of periods of relaxation from upwelling-favourable winds (Pitcher *et al.* 1995), which are modulated with a period of around 3-6 days (Nelson & Hutchings 1983), and therefore it is appropriate to examine the mooring data at these time scales. Characterisation of the variability and associated processes is carried out from the Eulerian perspective of the mooring, with some supporting use of satellite images to infer the spatial nature of alongshore and across-shelf processes.

During the upwelling season local alongshore winds are predominantly southerly and upwelling-favourable. Variations in magnitude and direction are observed at periods of around 3.5 and 10.5 days, which correspond to relaxation and reversal of upwelling-favourable winds. A strong diurnal signal, consistent with a land-sea breeze effect is always present but varies in magnitude. Near-surface currents exhibit sub-inertial variability at periods of two to five days, commensurate with the passage of coastal lows, wind reversals and cycles of upwelling. Reversals in direction and magnitude lag those displayed by local winds by approximately half a day. Alongshore currents have a tendency to flow polewards in the absence of wind. The constant phase difference between wind and current reversals suggests that current reversals are forced by local changes in wind direction. Reversals to southward flowing currents during periods of wind relaxation are considered to be enhanced by the development of negative alongshore pressure gradients north of capes, which form in response to the interaction of northward currents with local topography under upwelling conditions (Gan & Allen 2002a). At periods of less than a day the signal in the near-surface current data is dominated by variability at the inertial period, in response to a diurnal sea breeze effect. These inertial oscillations lead to anti-clockwise rotations that are superimposed on the low frequency flow field, but have no net effect on circulation or transport. The presence and strength of inertial oscillations depends upon the magnitude and variation in diurnal winds. Vertical shear in the water column, evident in the mooring data, with a 180° phase shift in current direction associated with the thermocline, is induced by inertial oscillations in the presence of a coastal boundary (Simpson *et al.* 2002).

Sub-inertial variations in surface temperature occur on similar time scales to wind and current variations, and are correlated with current reversals. Northward currents are

associated with decreasing surface temperatures and southward currents with increasing surface temperatures, typical of cycles of wind-induced upwelling and relaxation. Increases in surface layer temperatures are often too rapid to be insolation driven, and are attributed to advection of water masses by alongshore currents. Diurnal variations in near surface temperature are attributed to solar heating, while sub-surface temperatures exhibit variation at the inertial period indicating mixing or advection associated with inertial oscillations.

Availability of mooring data throughout the majority of the year has enabled the effects of variations in wind forcing at different times of year on currents and water column structure to be determined. Data sets from early in the upwelling season, late in the upwelling season and winter conditions exhibit similar time scales of variability; however, differences in mean flow and water column structure are indicative of the response of these parameters to seasonal differences in local synoptic weather conditions. Mean winds are south-westerly and upwelling-favourable during summer and north-westerly during winter. At all three times of the year examined, low frequency alongshore current reversals are correlated with reversals in local alongshore winds at periods of two to five days, with current reversals lagging wind reversals by approximately half a day; the correlation is less strong for the winter data. Mean alongshore flow is northwards early in the upwelling season and southwards later in the upwelling season and in winter. Variability at the inertial period is found at all times of year, but is stronger during summer months, corresponding with land-sea breezes causing greater diurnal variation in the wind in summer. Relationships between near surface temperatures and alongshore currents are similar at all times of year, with decreasing temperatures associated with northward flow and increasing temperatures with southward flow. Similar to the current data, differences in temperatures and water column structure between data sets are attributed to the seasonality of local meteorological forcing. Early in the upwelling season, persistent southerly winds lead to upwelling and a cool, well mixed water column which warms and becomes stratified during brief periods of relaxation. Surface temperatures reach higher values, and the water column is more stratified later in the upwelling season when periods of wind relaxation are more frequent and more persistent. During winter, there is considerably less upwelling, water column temperatures are less variable, and the mixed layer deepens due to decreased insolation and increased mixing by winter storms. These data support the increased

incidence of HABs observed during the latter part of the upwelling season, assuming that dinoflagellate bloom formation is favoured by the development of increasingly stratified conditions.

Physical processes, in terms of current variability forced by changes in the local wind field, determine the transport and dispersion of phytoplankton blooms resulting in sequential changes in phytoplankton community composition, while variations in water column structure, associated with differing degrees of mixing and stratification, determine successional changes in phytoplankton community. A combination of these processes result in the observed variations in phytoplankton community composition at the mooring location. Fluctuations in biomass and community composition occur too rapidly at a single location to be explained by *in situ* growth and processes. Southward currents, associated with wind relaxation and reversal, are found to introduce phytoplankton populations to the nearshore area, as has been observed previously in the region (e.g. Pitcher & Nelson 2006); increasingly stratified conditions associated with these currents further favour the selection of flagellate species. Inertial oscillations affect the timing of the detection of blooms at the mooring location but do not appear to affect net transport. Further investigation is required to determine the effect of inertial oscillations on mixing and the appearance of nutrient pulses above the thermocline, as well as the impact of vertical shear induced by inertial oscillations on phytoplankton distribution.

Areas of potential impact by HABs are usually close inshore, and therefore predicting HABs in these areas may rely more on understanding the processes underlying the transport, concentration and dissipation of blooms than on algal dynamics in offshore waters (Pitcher & Weeks 2006). This study has characterised the dominant processes and time scales of variability in currents and water column structure at seasonal and event time scales for HABs. The close relationship observed between the currents, temperature and water column structure, and local winds allows for a degree of predictability of these parameters, based on wind observations and forecasts. In conjunction with real-time indications of biomass from the mooring it is then possible to suggest bloom transport pathways, which are of particular interest once a bloom reaches inshore locations. In this respect hydrodynamic models of the region may also be useful in predicting bloom introduction and transport associated with wind forced currents. The

availability of real-time temperature profile data from the mooring, along with an insight into how the water column structure is likely to develop based on observations and weather predictions, may enable some level of prediction of species succession and high biomass bloom development via a probabilistic "ecological window" or fuzzy logic model (Bernard *et al.* 2006).

Research in the region is ongoing; subsequent to this study a weather station has been installed in Lambert's Bay, and a number of satellite tracked drogues have been deployed off Lambert's Bay helping to resolve shelf scale circulation patterns and potential bloom transport pathways. Studies are taking place examining vertical structure and thin layers of phytoplankton, and internal waves, all of which require much higher frequency sampling (< 10 minute intervals, < 0.5m vertically) for their resolution. Further characterisation of the nature and scale of alongshore processes requires the use of multiple moorings distributed along the coast, or HF radar systems such as CODAR that can provide simultaneous spatial coverage of surface currents, enabling the phase propagation of alongshore current reversals to be determined and the forcing mechanisms inferred. Use of a towed undulating vehicle with an appropriate instrument package could provide synoptic mapping of vertical alongshore and across-shelf variability in temperature and biomass, providing further insight into physical forcing mechanisms. These systems are often used in process oriented studies off the coasts of Oregon and California (e.g. Austin & Barth 2002, Ryan *et al.* 2005) and one such vehicle is now available in South Africa. The installation of pressure sensors or tide gauges in locations north and south of Cape Columbine would enable the existence of alongshore pressure gradients to be established and their effect on alongshore currents to be investigated. A robust investigation of seasonal differences, as well as the examination of the coherence of signals over months and at periods longer than two weeks, requires longer term deployment of instruments or moorings, which do not have gaps in the data due to servicing.

7 References

Andrews, W. R. H. and Hutchings, L. 1980. Upwelling in the southern Benguela Current. *Prog.Oceanogr.* 9, 1-81.

Austin, J. A., and Barth J.A. 2002.Variation in the position of the upwelling front on the Oregon shelf *J. Geophys. Res.* 107(C11), 3180, doi:10.1029/2001JC000858,.

Bailey, G.W. and Chapman, P. 1991. Short-term variability during an anchor station study in the southern Benguela upwelling system: Chemical and physical oceanography. *Prog Oceanog.* 28, 9-37.

Bernard, S. 2004. Development of an Operational Capacity for Real-time Observations and Forecasting of Harmful Algal Blooms in the Benguela Current Large Marine Ecosystem Region: Detection of Harmful Algal Blooms through Deployment of Bio-optical Moorings. Progress Report 1: Buoy Construction and System Development. University of Cape Town, South Africa. pp.16.

Bernard, S. 2005. The bio-optical detection of harmful algal blooms. PhD thesis, Department of Oceanography, University of Cape Town, Private Bag, Rondebosch 7701, Cape Town, South Africa, pp. 232.

Bernard, S., Balt, C., Pitcher, G., Probyn, T., Fawcett, A. and Du Randt, A. 2005. The Use of MERIS for Harmful Algal Bloom Monitoring in the Southern Benguela. *Proceedings of the MERIS (A)ATSR Workshop 2005 (ESA SP-597).* 26 - 30 September 2005 ESRIN, Frascati, Italy. Editor: H. Lacoste. Published on CDROM., p.26.1

Bernard, S., Kudela, R., Franks, P., Fennel, W., Kemp, A., Fawcett, A., and Pitcher, G.C. 2006. The requirements for forecasting harmful algal blooms in the Benguela. In *The Benguela: Predicting a Large Marine Ecosystem* [eds.] Shannon, V., Hempel, G., Malanotte-Rizzoli, P., Moloney, C. and Woods J. Elsevier.

Brink, K.H. 1983. The near-surface dynamics of coastal upwelling. *Prog. Oceanog.* 12, 223-257.

Brown, O.B., Brown, J.W. and Evans, R.H. 1985. Calibration of advanced very high resolution radiometer infrared observations. *J. Geophys. Res.* 90, 11667-11678.

Brown, P.C., Painting, S.J. and Cochrane, K.L. 1991. Estimates of phytoplankton and bacterial biomass and production in the northern and southern Benguela ecosystems. *S. Afr. J. mar. Sci.* 11, 537-564

Byfield, V. and Boxall, S. 2002. The Volvo Ocean Adventure, *Ocean Challenge*, 11(3), 6-10.

Carpenter, E.B., Leonard, J.W. and Yim, S.C.S. 1995. Experimental and Numerical Investigations of Tethered Spar and Sphere Buoys in Irregular Waves. *International Journal of Ocean Engineering* 22(8), 765-784.

Chavez, F.P., Wright, D., Herlien, R., Kelley, M., Shane, F. and Strutton, P.G. 2000. A Device for Protecting Moored Spectroradiometers from Biofouling. *Journal of Atmospheric and Oceanic Technology* 17, 215-219

Cockcroft, A.C., Schoeman, D.S., Pitcher, G.C., Bailey, G.W. and Van Zyl, D.C. 2000 A mass stranding or "walkout" of west coast rock lobster *Jasus lalandii* in Elands Bay, South Africa: Causes, results and implications. In *The biodiversity crises and Crustacea* [eds.] Von Kaupel Klein, J.C. and Schram, F.R. *Crustac. Issues* 11: 362-688

Craig, P.D. 1989 A model of diurnally forced vertical current structure near 30° latitude. *Continental Shelf Research.* 9(11), 965-980.

Cullen, J.J., Ciotti, A.M., Davis, R.F. and Lewis, M.R. 1997. Optical detection and assessment of algal blooms. *Limnol. Oceanogr.*, 42(5), 1223-1239.

Cullen, J.J. and MacIntyre, J.G. 1998. Behaviour, physiology and the niche of depth-regulating phytoplankton. In *Physiological Ecology of Harmful Algal Blooms.* [eds.]

Anderson, D.M., Cembella, A.D. and Hallegraeff, G.M. Springer-Verlag, Berlin Heidelberg. pp. 559-579.

Demarcq, H., Barlow, R.G. and Shillington, F.A. 2003. Climatology and variability of sea surface temperature and surface chlorophyll in the Benguela and Agulhas ecosystems as observed by satellite imagery. *Afr. J. mar. Sci.* 25, 363–372

Demer, D.A., Needham, D.J. and Soule, M.A. 2003. Multi-instrumented Remotely Monitored Buoy Project In: *AMLR 2001-2002 Field Season Report* [Ed.] Lipsky, J.D. pp. 169-173

Detrick, R., Frye, D., Collins, J., Gobat, J., Grosenbaugh, M., Petitt, R., Plueddeman, A., von der Heydt, K., Wooding, F.B., Orcutt, J., Berger, J., Harriss, R., Vernon, F., Halkyard, J. and Horton E. 2000. DEOS Moored Buoy Observatory Design Study, Final Report, WHOI Report, pp.102.

Dickey, T.D. 1991. The emergence of concurrent high resolution physical and bio-optical measurements in the upper ocean and their applications. *Rev. Geophys.* 29, 383-413.

Dickey, T.D., R.H. Douglass, D. Manov, and Bogucki, D. 1993, An experiment in duplex communication with a multi-variable moored system in coastal waters, *J. Atmos. Ocean. Tech.* 10, 637-644.

Dickey, T.D. and Falkowski, P.G. 2002. Solar energy and its biological-physical interactions in the sea. In *The Sea* , Vol. 12, [eds.] Robinson, A.R., McCarthy, J.J. and Rothschild, B.J. Wiley, New York. pp. 401-440

Dickey, T., 2003, Emerging ocean observations for interdisciplinary data assimilation systems, *J. Mar. Syst.* 40-41, 5-48.

Duncan, C.P. and Nell, J.H. 1969. Surface currents off the Cape Coast. *Investl Rep. Div. Sea Fish. S. Afr.* 76, 1-19.

Fawcett, A., Bernard, S., Pitcher, G., Probyn, T. and du Randt, A. 2006. Real-time monitoring of harmful algal blooms in the southern Benguela. *African Journal of Marine Science* (special edition on harmful algal blooms). 28(2)

Franks, P.J.S., 1994. Thin layers of phytoplankton: a model of formation by near-inertial wave shear. *Deep Sea Res.* 42(1), 75-91.

Gan, J., and Allen, J.S. 2002a. A Modeling study of shelf circulation off Northern California in the region of the Coastal Ocean Dynamics Experiment. Part 1, response to relaxation of upwelling winds. *J. Geophys. Res.*, 107, 3123. doi: 10.1029/2000JC000768.

Gan, J., and Allen, J.S. 2002b. A Modeling study of shelf circulation off Northern California in the region of the Coastal Ocean Dynamics Experiment. Part 2, Simulations and comparisons with observations. *J. Geophys. Res.*, 107(C11), 3184. doi: 10.1029/2000JC001190.

Gentien, P., Donaghay, P., Yamazaki, H., Raine, R., Reguera, B. and Osborn, T. 2005. Harmful algal blooms in stratified environments. *Oceanography* 18(2), 172-183

GEOHAB, 2001. Global Ecology and Oceanography of Harmful Algal Blooms, *Science Plan.* [eds.] Glibert, P. and Pitcher, G. SCOR and IOC, Baltimore and Paris. pp. 87

Glenn, S.M., Dickey, T.D., Parker, B. and Boicourt, W. 2000. Long-term real-time coastal ocean observation networks. *Oceanography* 13, 24-34.

Grinsted, A., Jevrejeva, S. and Moore, J. 2004. Application of the cross wavelet transform and wavelet coherence to geophysical time series. *Nonlinear Proc. Geophys.*, 11, 561-566

Guastella, L.A-M. 1992. Sea surface heat exchange at St Helena bay and implications for the southern Benguela upwelling system. *S. Afr. J. mar. Sci.* 12, 61-70.

Hasle, G.R. 1978. The inverted-microscope method, p. 88-96. In *Phytoplankton manual.* [ed.] Sournia, A. UNESCO, Paris.

Hill, A.E., B.M Hickey, F.A. Shillington, P.T. Strub, K.H. Brink, E.D. Barton and A.C. Thomas, 1998. Eastern ocean boundaries: coastal segment (E). In *The Sea* 11 [Eds.] Robinson A.R. and Brink K.H. John Wiley & Sons. pp. 29–68.

Holden, C.J. 1985. Currents in St Helena Bay inferred from radio-tracked drifters. In *South African Ocean Colour and Upwelling Experiment.* [Ed.]. Shannon, L.V. Sea Fisheries Research Institute, Cape Town. pp. 97-109.

Holden, C.J. 1986. Spatial and temporal scales of the coastal currents in the St. Helena Bay. MSc thesis. Department of Oceanography, University of Cape Town, Private Bag, Rondebosch 7701, Cape Town, South Africa, pp. 133.

Holden, C.J. 1987. Observations of low-frequency currents and continental shelf waves along the west coast of South Africa. In *The Benguela and Comparable Ecosystems.* [Eds.] Payne, A.I.L., Gulland, J.A. and Brink, K.H. *S. Afr. J. mar. Sci.* 5, 197-208

Horstman, D.A. 1981. Reported red-water outbreaks and their effects on the fauna of the west and south coasts of South Africa. 1959-1980. *Fish. Bull. S. Afr.* 15, 71-88.

Hutchings, L. 1992. Fish harvesting in a variable, productive environment, *S. Afr. J. mar. Sci.* 12, 297-318

Hyder, P., Simpson, J.H. and Christopoulos, S. 2002. Sea-breeze forced diurnal surface currents in the Thermaikos Gulf, North-west Aegean. *Continental Shelf Research.* 22, 585-601.

Jackson, S.P. 1947 Air masses and the circulation over the plateau and coast of South Africa. *S. Afr. geogrl J.* 29, pp. 15

Jury, M. and G.B. Brundrit. 1992. Temporal organization of upwelling in the Southern Benguela Ecosystem by resonant coastal trapped waves in the ocean and atmosphere. *S. Afr. J. Mar. Sci.* 12, 219-224.

Jury, M. R., McArthur, C.I. and Brundrit, G.G. 1990a. Pulsing of the Benguela upwelling region: large-scale atmospheric controls, *S. Afr. J. mar. Sci. 9*, 27-41

Jury, M.R., MacArthur, C.I. and Brundrit, G.B. 1990b. Observations of trapped waves in the atmosphere and ocean along the coast of southern Africa. *S. Afr. geogrl J.* 72, 33-46
Kamstra, F. 1985. Environmental features of the southern Benguela with special reference to the wind stress, In *South African Ocean Colour Experiment* [Ed.] Shannon, L.V. Sea Fisheries Research Institute, Cape Town. pp. 13-27

Kashino, R., Ethier, T. and Phillips, R. 2005. TRIAXYS™ Acoustic Doppler Current Profiler Comparison Study. Nortek Technical Note No.:023, Nortek AS, Norway. pp. 21

Klein, P. and Coste, B. 1984. Effects of wind-stress variability on nutrient transport into the mixed layer. *Deep-Sea Res.* 31, 21-37.

Knight, P.J., Howarth, M.J. and Rippeth, T.P. 2002. Inertial currents in the northern North sea. *Journal of Sea Research*. 47, 269-284.

Kudela, R., Pitcher, G., Probyn, T., Figueiras, F., Moita, T. and Trainer, V. 2005. Harmful Algal Blooms in Coastal Upwelling Systems. *Oceanography*. 18(2), 184 -197.

Largier, J.L., Magnell, B.A. and Winant, C.D. 1993. Subtidal circulation over the northern California shelf, *J. Geophys. Res.* 98(C10), 18147-18180

Lentz, S.J. and Chapman, D. 1989. Seasonal differences in the current and temperature variability over the northern California shelf during the Coastal Ocean Dynamics Experiment. *J. Geophys. Res.* 94(C9), 12571-12592

Limeburner, R., (Ed) 1985 CODE-2: Moored array and large-scale data report. *WHOI Tech. Rep. 85-35*, Woods Hole Oceanographic Institution, Woods Hole, MA02543-1541. pp. 234

Lohrmann, A. 1998. Comparison of buoy mounted NDP current velocity data with upward looking ADCP data. Nortek Technical Note No.:001, Nortek AS, Norway. pp. 4

Lorenzen, C. J. 1966. A method for the continuous measurement of in-vivo chlorophyll concentration, *Deep-Sea Res.* 13, 223-227

Margalef, R. 1978 Life-forms of phytoplankton as survival alternatives in an unstable environment. *Oceanol. Acta.* 1, 493-509

Mélice, J.L., Coron, A. and Berger, A. 2001 Amplitude and frequency modulation of the Earth's obliquity for the last millions years. *J. Clim.* 14, 1043-1054

Minnett, P. J. 1991. Consequences of sea surface temperature variability on the validation and applications of satellite measurements. *J. Geophys. Res.* 96(C10). 18,475-18,489.

Morel, A. and Prieur, L., 1977. Analysis of variations in ocean colour. *Limnol. Oceanogr.* 22, 709-722

Mueller, J.L., Clark, D.K., Kuwahara, V.S., Lazin, G., Brown, S.W., Fargion, G.S., Yarbrough, M.A., Feinholz, M., Flora, S., Broenkow, W., Kim, Y.S., Johnson, B.C., Yuen, M., Strutton, P.G., Dickey, T.D., Abbott, M.R., Letelier, R.M., Lewis, M.R., McLean, S., Chavez, F.P., Barnard, A., Morrison, J.R., Subramaniam, A., Manov, D., Zheng, X., Harding Jr., L.W., Barnes, R.A., and Lykke, K.R. 2003a. Special Topics in Ocean Optics Protocols and Appendices. In *Ocean Optics Protocols for Satellite Ocean Color Sensor Validation, Revision 4, Volume VI* [Eds.]. Mueller, J.L., Fargion, G.S. and McClain C.R. NASA/TM-2003-211621/Rev4-Vol.VI. NASA Goddard Space Flight Center, Greenbelt, Maryland.

Mueller, J.L., C. Davis, R. Arnone, R. Frouin, K. Carder, Z.P. Lee, R.G. Steward, S. Hooker, C.D. Mobley, and McLean, S. 2003b. Above-Water Radiance and Remote Sensing Reflectance Measurement and Analysis Protocols In *Ocean Optics Protocols for Satellite Ocean Color Sensor Validation, Revision 4, Volume III:* Radiometric Measurements and Data Analysis Protocols [Eds.] Mueller, J.L., Fargion, G.S. and McClain C.R., NASA/TM-2003-211621/Rev4-Vol. III, NASA Goddard Space Flight Center, Greenbelt, Maryland. pp. 21-31.

Nelson, G. 1992. Equatorward wind and atmospheric pressure spectra as metrics for primary production in the Benguela system. *S. Afr. J. mar. Sci.* 12, 19-28

Nelson, G. and L. Hutchings. 1983. The Benguela upwelling area. *Prog. Oceanog.* 12, 333-356.

Penven, P., Roy, C., Colin de Verdière, A. and Largier, J. 2000. Simulation of a coastal jet retention process using a barotropic model. *Oceanologica Acta,* 23, 615-634.

Pitcher, G., J. Agenbag, D. Calder, D. Horstman, M. Jury and J. Taunton-Clark. 1995. Red tides in relation to the meteorology of the southern Benguela upwelling system. In *Harmful Marine Algal Blooms.* [Eds.] Lassus, P., Arzul, G., Erard, E., Gentien, P. and Marcaillou, C. Lavoisier, Intercept Ltd. pp. 657-662.

Pitcher, G.C. and Boyd, A.J. 1996. Across-shelf and alongshore dinoflagellate distributions and the mechanisms of red tide formation within the southern Benguela upwelling system In *Harmful and Toxic Algal Blooms.* [Eds.] Yasumoto, T., Oshima Y. and Fukuyo Y. Intergovernmental Oceanographic Commission of UNESCO pp. 243-246.

Pitcher, G.C., Boyd, A.J., Horstman, D.A. and Mitchell-Innes, B.A., 1998. Subsurface dinoflagellate populations, frontal blooms and the formation of red tide in the Southern Benguela upwelling system. *Marine Ecology Progress Series* 172, 253-264.

Pitcher, G.C., Brown, P.C. and Mitchell-Innes, B.A. 1992. Spatio-temporal variability of phytoplankton in the southern Benguela upwelling system. *S. Afr. J. mar. Sci.* 12, 439-456.

Pitcher, G.C. and Calder, D. 2000. Harmful algal blooms of the southern Benguela current: A review and appraisal of monitoring from 1989 to 1997. *S. Afr. J. mar. Sci.* 22, 255-271.

Pitcher, G.C. and Nelson, G. 2006. Characteristics of the surface boundary layer important to the development of red tide on the southern Namaqua shelf of Benguela upwelling system. *Limnol. Oceanogr.* 51(6), 2660-2674

Pitcher, G.C., Walker, D.R., Mitchell-Innes, B.A., and Moloney, C.L. 1991. Short term variability during an anchor station study in the southern Benguela upwelling system: Phytoplankton Dynamics. *Progress in Oceanography*, 28, 39-64

Pitcher, G.C. and Weeks, S.J. 2006. The variability and potential for prediction of harmful algal blooms in the southern Benguela ecosystem. In *The Benguela: Predicting a Large Marine Ecosystem* [eds.] Shannon, V., Hempel, G., Malanotte-Rizzoli, P., Moloney, C. and Woods, J. Elsevier

Pollard, R.T. and Millard, R.C. 1970. Comparison between observed and simulated wind-generated inertial oscillations. *Deep Sea Res.* 17, 813-821

Probyn, T.A., G.C. Pitcher, P.M.S. Monteiro, A.J. Boyd and G. Nelson. 2000. Physical processes contributing to harmful algal blooms in Saldanha Bay, South Africa. *S. Afr. J. mar. Sci.* 22, 285-297.

Rippeth, T.P., Simpson, J.H., Player, R.J. and Garcia, M. 2002. Current oscillations in the diurnal-inertial band on the Catalonian shelf in spring. *Continental Shelf Research* 22, 247-265.

Risien, C.M., Reason, C.J.C, and Shillington, F.A. 2004. Variability in satellite winds over the Benguela upwelling systems during 1999-2000. *J. Geophys. Res.* C109, C03010, doi:10.1029/2003JC001880.

Roesler, C.S., and M.J. Perry. 1995. In situ phytoplankton absorption, fluorescence emission, and particulate backscattering spectra determined from reflectance. *J. Geophys. Res.* C100: 13 279-13 294.

Ryan, J., Dierssen, H.M., Kudela, R., Scholin, C.A., Johnson, K.S., Sullivan, J.M., Fischer, A.M., Rienecker, E.V., McEnaney, P.R. and Chavez, F.P., 2005. Coastal ocean physics and red tides: An example from Monterey Bay, California. *Oceanography* 18(2), 246-255.

Schumann, E. H., and Brink, K.H., 1990. Coastal-trapped waves off the coast of South Africa: generation, propagation and current structures, *J. Phys. Oceanogr. 20*, 1206-1218

Sellner K.G., Doucette, G.J. and Kirkpatrick, G.J. 2003. Harmful algal blooms: causes, impacts and detection, *J. Ind. Microbiol. Biotechnol.* 30, 383–406.

Send, U., Beardsley, R.C. and Winant, C.D. 1987. Relaxation from upwelling in the Coastal Ocean Dynamics Experiment. *J. Geophys. Res.* 92(C2), 1683-1698.

Shannon, L. V. 1985. The Benguela ecosystem. 1. Evolution of the Benguela, physical features and processes. In *Oceanography and Marine Biology. An Annual Review* 23, 105-182.

Shanon, L. V. and Nelson, G. 1996 The Benguela : Large scale features and processes and system variability. In *The South Atlantic Past and Present Circulation.* [Eds.] Wefer, G., Berger, W. H., Siedler, G. and Webb D. J. Springer Verlag, Berlin, Heidelberg pp. 163-210.

Shillington, F.A. 1998. The Benguela upwelling system off southwestern Africa, In *The Sea*, Vol. 11 [Eds.] Brink, K.H. and Robinson, A.R. Wiley, New York. pp. 583-604

Simpson, J.H., Hyder, P. and Rippeth, T.P. 2002. Forced oscillations near the critical latitude for diurnal-inertial resonance. *J. Phys. Oceanogr. 32*, 177-187

Smayda, T.J. 1980. Phytoplankton species succession. In: *The physiological ecology of phytoplankton* [Ed.] Morris, I. Blackwell, Oxford. pp. 493-570

Smayda, T. J. (1997) Harmful algal blooms: their ecophysiology and general relevance to phytoplankton blooms in the sea. *Limnol. Oceanogr.* 42, 1137-1153.

Smayda, T.J. 2000. Ecological features of harmful algal blooms in coastal upwelling systems. *S. Afr. J. mar. Sci.* 22, 219-253

Sordo, I., Barton, E.D., Cotos, J.M. and Pazos, Y. 2001 An inshore poleward current in the NW of the Iberian Peninsula detected from satellite images, and its relation with *G. catenatum* and *D. acuminate* blooms in the Galician Rias. *Estuaries Coastal Shelf Sci.* 53, 787-799

Taunton-Clark, J. 1985. The formation, growth and decay of upwelling tongues in response to the mesoscale wind field during summer. In *South African Ocean Colour Experiment* [Ed.] Shannon, L.V. Sea Fisheries Research Institute, Cape Town. pp. 47-61

Torrence, C., and Compo, G.P. 1998 A practical guide to wavelet analysis, *Bull. Am. Meteorol. Soc.* 79, 61-78

Twardowski, M.J., M.R. Lewis, A. Barnard and Zaneveld, J.R.V. 2005. In-water instrumentation and platforms for ocean color remote sensing applications. In: *Remote sensing of Coastal Aquatic Environments, Remote Sensing and Digital Image Processing*, Vol. 7. [Eds.] Miller, R.L., del Castillo, C.E. and McKee, B.A. Springer, Dordrecht. pp. 347

van Haren, H., Howarth, M.J., Jones, K. and Essi, I. 2003. Autumnal reduction of stratification in the northern North Sea and its impact. *Continent. Shelf Res.* 23, 177-191

Waldron, H. N. and Probyn. T. A. 1992 - Nitrate supply and potential production in the Benguela upwelling system. In *Benguela Trophic Functioning* [Eds.] Payne, A. I. L., Brink, K. H., Mann, K. H. and Hilborn, R. *S. Afr. J. mar. Sci.* 12, 865-871.

Weeks, S.J., Pitcher, G.C. and Bernard, S. 2004. Satellite monitoring of the evolution of a coccolithophorid bloom in the southern Benguela ecosystem. *Oceanography* 17(1), 83-89

Winant, C. D., Beardsley, R.C. and Davis, R.E. 1987. Moored wind, temperature and current observations made during the Coastal Ocean Dynamics Experiments 1 and 2 over the northern California continental shelf and upper slope *J. Geophys Res.* 92 (C2), 1569-1604.

Zaneveld, J.R.V, 1995. A theoretical derivation of the dependence of the remotely sensed reflectance on the inherent optical properties. *J. Geophys Res.* 100 (C7), 13,135-13,142.

Appendix I: Flow charts outlining architecture of burst sampling software in Ocean-i unit

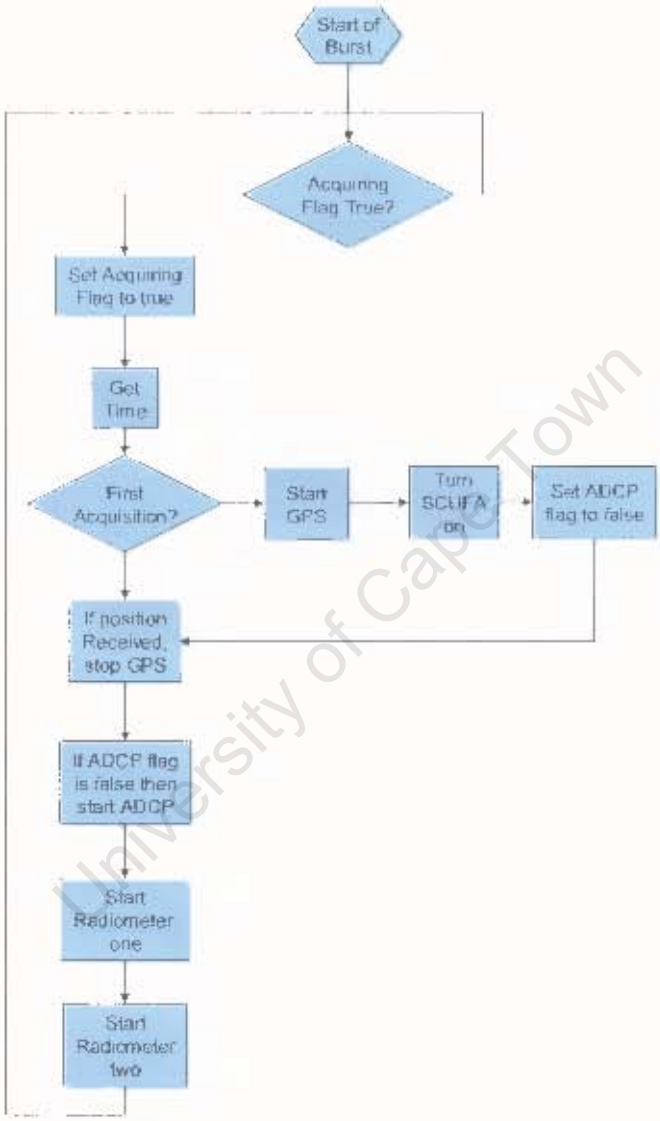

Figure I-1 Schematic of Start Acquisition process in Ocean-i unit software

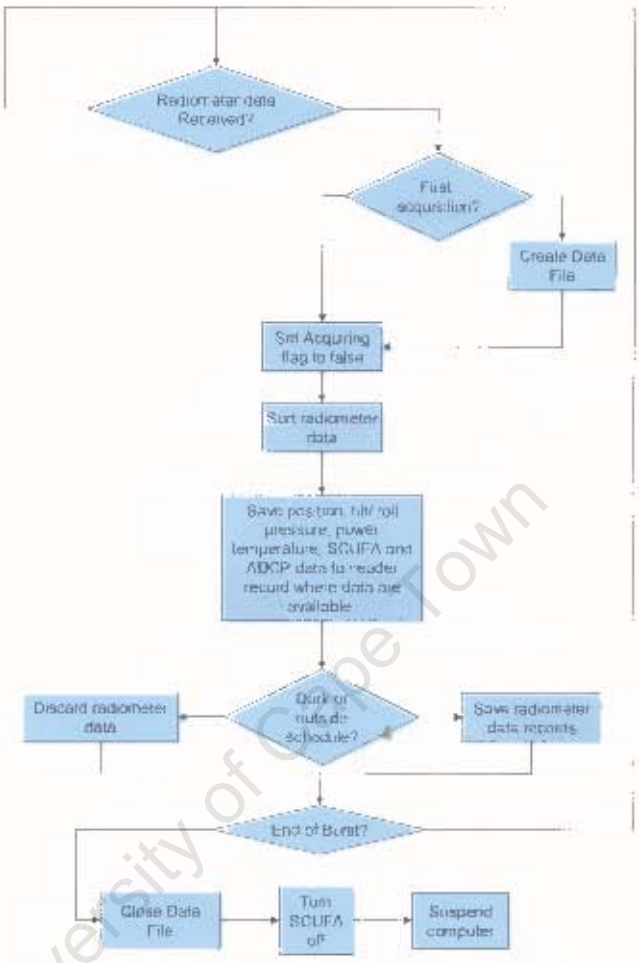

Figure I-2 Schematic of Update Files process in Ocean-i unit software

Appendix II: Data storage format for Ocean-i unit, Ver. CE/SA

For each acquisition of radiometer data there will be 3 records of 528 bytes, a header record, followed by a data record for each of the two radiometers. If radiometer data is not being collected (i.e. when it is dark) then there will only be 1 record, a header, for each acquisition.

Header Sector Format

Time	Position	Roll	Depth	Power	EEPROM1	EEPROM2	Thermistors	SCUFA	ADCP	Blank (FF)	Time
6 bytes	*20 Bytes*	*2 bytes*	*4 bytes*	*3Bytes*	*9 bytes*	*16 bytes*	*34 bytes*	*8 bytes*	*317 bytes*	*103 bytes*	*6 bytes*
12 chars	40 chars	4 chars	8 chars	6 chars	18 chars	32 chars	68 chars	16 chars	634 chars	206 chars	12 chars

Time : Time and Date as BCD *ssmmhhddmmyy*
Position : Position as ASCII *N/SddmmmmmE/Wdddmmmmmhhh* d = degrees, m= minutes/100, h = heading degrees
Roll: 1 byte Hex Pitch, 1 byte Hex Roll. To get the value for Pitch or Roll, convert to decimal and subtract the offset (supplied by TriOS)
Depth: Raw uncalibrated data as ASCII Hex
Power: Raw uncalibrated data as ASCII Hex

EEPROM1 Format

HW Version	Serial No	Econfig	Edn RID	Configured Sensors
2 bytes	*4 bytes*	*1 byte*	*1 byte*	*1 byte*
4 chars	8 chars	2 chars	2 chars	2 chars

HW Version : Not used, filled with FF
Serial No : Not used, filled with FF
Econfig : Not used, filled with FF
Edn RID : Lower 3 bits
The port number of the radiometer selected as Edn. If these bits > 0 the acquisition regime will pause at night
Configued Sensors : Not used, filled with FF

EEPROM2 Format

Sens Ser 1	Sens Ser 2	Sens Ser 3	Sens Ser 4	Sens Ser 5	Sens Ser 6	Sens Ser 7	Sens Ser 8
2 bytes	*2 bytes*	*2 bytes*	*2 bytes*	*2 bytes*	*2 bytes*	*2 bytes*	*2 bytes*
4 chars	4 chars	**4 chars**	**4 chars**	**4 chars**	**4 chars**	**4 chars**	**4 chars**

Sens Ser : In this version, only the serial numbers of the radiometers are saved here (not any of the other instruments) and they will always be in positions 1 and 2.

Thermistors Format

Therm 1	Therm 2	Therm 3	Therm 4	Therm 5	Therm 6	Therm 7	Therm 8	Therm 9	Therm 10	Therm 11	Therm 12	Therm 13	Therm 14	Therm 15	Therm 16	Therm 17
2 bytes	*2 bytes*	*2 bytes*	*2 bytes*	*2 bytes*	*2 bytes*	*2 bytes*	*2 bytes*	*2 bytes*	*2 bytes*	*2 bytes*	*2 bytes*	*2 bytes*	*2 bytes*	*2 bytes*	*2 bytes*	*2 bytes*
4 chars	4 chars	4 chars	4 chars	4 chars	4 chars	4 chars	4 chars	4 chars	4 chars	4 chars	4 chars	4 chars	4 chars	4 chars	4 chars	4 chars

Therm : Temperature for Thermistors 1 to 17 as BCD, degrees C x 100. (To get temperature, divide value for the relevant thermistor by 100)

SCUFA Format

Fluorescence	Turbidity
4 bytes	*4 bytes*
8 chars	8 chars

Fluorescence : Fluorescence as BCD x 1000. (To get Fluorescence, divide the value by 1000)
Turbidity : Turbidity as BCD x 1000. (To get Turbidity, divide the value by 1000)

ADCP Format

Header	Fixed Leader Data	Variable Leader Data	Velocity	Reserved & Checksum
12 bytes	*50 bytes*	*56 bytes*	*194 bytes*	*5 bytes*
24 chars	100 chars	112 chars	388 chars	8 chars

For a description of how the ADCP data is made up please refer to the ADCP manual.

Data Sector Format

Spectral Data	Blank (FF)	Serial No.
512 bytes	*14 bytes*	*2 bytes*
1024 chars	28 chars	4 chars

Spectral Data : Data for each of 255 wavelengths as 2 bytes (4 chars) Hex with the low byte first and then the high byte. (Data starts from the 3rd byte (5^{th} character).) The first byte (second character) of the spectral data is the integration time. The integration time in ms is 2^{n+1}, if n is the number in the first byte.

(modified and reproduced from data format documentation supplied by John Cheriton, Saturn Solutions Ltd.)

Appendix III: Deployment Logs for Moorings

Bokkom Log

Date	Time	Notes
28/02/04	11:30	Bokkom deployed on mooring
02/03/04		Bokkom turned upside down on mooring. Taken back to shore to repair. SCUFA removed from buoy.
06/03/04	10:25	Bokkom deployed on mooring
18/03/04	13:15	Bokkom retrieved from mooring
19/03/04	08:30	Bokkom deployed on mooring SCUFA now on buoy.
01/04/04	07:30	Bokkom upside down on mooring, retrieved and taken ashore.
02/04/04	09:10	Bokkom redeployed on mooring New weight configuration.
03/04/04		Dial in from Cape Town. Data logger often loses time and resets to 01/06/99 12:00 due to removal of damaged GPS
07/04/04	17:30	Bokkom retrieved from mooring Main mooring appears to be sinking, light only just visible above water surface.
21/04/04	10:45	Bokkom redeployed on mooring Divers clean fouling off main mooring which was causing it to sink.
23/04/04		Dial into buoy from Cape Town. No thermistor data.
17/05/04	16:00	Bokkom retrieved from mooring for routine servicing. Thermistor chain has gone, possibly became wrapped around main mooring line
18/05/04	14:20	Bokkom deployed on mooring
26/05/04	15:15	Bokkom retrieved from mooring
28/05/04	09:30	Bokkom redeployed on mooring
17/06/04		Bokkom suffered irreparable damage.

BOB Log

Date	Time	Notes
26.01.05	09:15	BOB deployed on mooring
14.02.05		Pressure sensor data reading incorrectly
16.02.05		SCUFA giving high readings relative to radiometer data – treat fluorescence data with caution
23.02.05	12:45	BOB retrieved from mooring for servicing
24.02.05	10:45	BOB deployed on mooring
15.03.05	11:00	BOB retrieved from mooring for servicing – no data collected since 14:30 07.03.05 due to battery failure.
17.03.05	10:00	BOB deployed on mooring

18.03.05	10:30	BOB retrieved from mooring – battery pack failed
19.03.05	10:25	BOB deployed on mooring
05.04.05	11:30	BOB retrieved from mooring – pressure sensor and GPS removed from BOB as not operational.
06.04.05	11:10	BOB deployed on mooring
11.04.05		Thermistor chain giving missing or incorrect values
04.05.05	08:45	BOB retrieved from mooring – thermistor chain caught on landward mooring line
05.05.05	12:35	BOB deployed on mooring. Temporary thermistor chain deployed with recording temperature sensors.
09.06.06	11:30	BOB retrieved from mooring Trawl floats either side of mooring sinking due to fouling. Battery voltage 6.4V – appears that solar panels cannot charge battery sufficiently during winter. Replace batteries
10.06.05	13:10	BOB deployed on mooring
13.06.05		Tilt and roll sensor appears to be stuck and giving continuously high readings
23.06.05		No data from ADCP
11.07.05		Time seems to have been resetting continuously and no data – suspect power problem
21.07.05	15:00	BOB retrieved from mooring ADCP battery voltage too low to power ADCP Radiometers removed for servicing and calibration Mooring needs attention as sinking due to fouling and not possible to service from small boat.
10.11.05	09:15	BOB deployed on new mooring. No pressure sensor. Temporary thermistor chain deployed with recording temperature sensors.
13.12.05	15:15	BOB retrieved from mooring. One solar panel damaged by water intrusion.
14.12.05	12:45	BOB deployed on mooring. Temporary thermistor chain.
19.12.05		Unable to download data – board failure
10.01.06	15:45	BOB retrieved from mooring. Replace damaged solar panel.
12.01.06	09:50	BOB deployed on mooring.
16.01.06		Unable to download data – board failure
19.01.06	09:50	BOB retrieved from mooring
20.01.06		BOB deployed on mooring with instruments in self-logging mode where possible.
07.03.06	11:00	BOB retrieved from mooring
	18:05	BOB redeployed on mooring – all instruments connected to Ocean-i with new board installed.
22.03.06	10:30	BOB retrieved from mooring.
23.03.06	10:15	BOB deployed on mooring.